MACHINING OF POWDER METAL TITANIUM

by

KEHINDE KOLAWOLE SOBIYI

Thesis presented in partial fulfilment of the requirements for the degree
Master of Science in Engineering at the
University of Stellenbosch

Supervisor: Dr. DEBORAH C BLAINE
Faculty of Engineering
Department of Mechanical and Mechatronic Engineering

March 2011

ABSTRACT

The purpose of this study is to investigate the machinability of commercially pure (CP) titanium, manufactured using the press-and-sinter PM process.

To this end, CP titanium powder (-200 mesh) was compacted and sintered in vacuum (10^{-4} torr) for two hours at 1200°C. Small cylindrical samples were compacted at pressures varying from 350 to 600 MPa in order to determine the compressibility of the powder. Following these tests, four larger stepped-cylinder samples were compacted at pressures close to 400 MPa and sintered under similar conditions. These samples had sintered densities varying between 3.82 and 4.41 g/cm^3. They were used to evaluate the machinability of the sintered titanium using face turning machining tests.

The samples were machined dry, using uncoated carbide (WC-Co) cutting tool. Cutting speeds between 60-150 m/min were evaluated while keeping the feed rate and depth of cut constant at 0.15 mm/rev and 0.5 mm, respectively. The final machined surface finish and the tool wear experienced during the face turning machining tests were monitored in order to evaluate PM titanium's machining performance.

This study showed that it is possible to use the press-and-sinter PM process with CP titanium powder, with a particle size of less than 75 µm (-200 mesh), to manufacture sintered titanium. However, particle shape influences the compressibility of the powder and pressing parts of larger volume, such as the machining test sample shape, is challenging when using such small particle size powder. Processing conditions, such as compaction pressure, sintering temperature and sintering time, influence the sintered density.

Results from the machinability tests show that tool wear increases with a decrease in the porosity of the sintered titanium. A more porous sintered material has both lower strength and thermal conductivity. As these factors have opposing effects on the machinability of materials, it is concluded that the strength of the sintered titanium has a stronger influence on its machinability than the thermal conductivity.

The cutting tool wear was uniform but showed indications of crater wear. The machined surface of the denser parts had minimal defects compared to less dense parts. Chip shape is long for the dense parts, and spiral for the less dense parts. The chips formed were all segmented, which is typical for titanium.

The machinability of the sintered CP titanium was compared to that of wrought titanium alloys. As expected, it was found that the machinability of the sintered titanium was poor in comparison.

OPSOMMING

Die doel van hierdie studie is om die masjineerbaarheid van kommersieel suiwer (KS) titaan, wat deur die pers-en-sinter poeiermetallurgie (PM) metode vervaardig word, te ondersoek.

Om hierdie doel te bereik, is KS titaan poeier (-200 ogiesdraad) gekompakteer en gesinter in ‘n vakuum (10^{-4} torr) teen 1200°C vir 2 ure. Klein silindriese monsters is tussen drukke van 350en 600 MPa gekompakteer om die samedrukbaarheid van die poeier te bepaal. Na aanleiding van hierdie toetse, is vier groter trapvormige-silinder monsters by drukke naby aan 400MPa gekompakteer en onder soortgelyke omstandighede gesinter. Hierdie monsters het gesinterde digthede tussen 3.82 en 4.41 g/cm^3 gehad. Hulle is gebruik om die masjineerbaarheid van die gesinterde titaan te ondersoek deur middel van vlak-draai masjineringstoetse.

Die monsters is sonder smeermiddel gemasjineer met onbedekte karbied (WC-Co) snygereedskap. Snysnelhede tussen 60 – 150 m/min is geëvalueer terwyl die voertempo en diepte van die snit konstant by 0.15 mm/rev en 0.5 mm, onderskeidelik, gehou is. Die finale gemasjineerde oppervlak afwerking en gereedskapsslytasie tydens die vlak-draai masjinering toets is van die faktore wat gemonitor is sodat PM titaan se optrede tydens masjinering geëvalueer kan word.

Hierdie studie wys dat diepers-en-sinter metode wel met KS titaan poeier, met ‘n partikel grootte van minder as 75 µm (-200 maas), gebruik kan word om gesinterde titaan te vervaardig. Die partikelgrootte beïnvloed wel die samedrukbaarheid van die poeier. Die samedrukking van parte met groter volume, soos bv die masjinerings toetsmonster, is uitdagend wanneer klein partikelgrootte poeier gebruik word. Proses omstandighede, soos kompaksie druk, sinteringstemperatuur en sinteringstyd, beïnvloed die gesinterde digtheid.

Resultate van die masjineerbaarheidstoetse wys dat beitelslytasie toeneem met ‘n afname in porositeit van die gesinterede titaan. ‘n Meer poreus gesinterde materiaal het beide laer sterkte en termiese geleidingsvermoë. Aangesien hierdie faktore teenoorgestelde uitwerkings op masjineerbaarheid het, word dit dan afgelei dat die sterkte van gesinterde titaan ‘n groter invloed het op sy masjineerbaarheid as die termiese geleidingsvermoë.

Die beitel se slytasie is hoofsaahlik, maar het tekens van kraterslytasie getoon. Die gemasjineerde oppervlak van die meer digte onderdele of toetsmonters het min gebreke gehad in vergelyking met die minder digte dele. Die vorm van die spaanders is lank vir digte parte, en spiraalvormig vir minder digte toetsmonsters. Die spaanders wat gevorm het, was almal gesegmenteerd, wat tipies is vir titaan.

Die masjineerbaarheid van die gesinterde KS titaan is met dié van gesmede titaanallooie vergelyk. Soos verwag is, is gevind dat die masjineerbaarheid van die gesinterde titaan in vergelyking swak is.

DECLARATION

By submitting this thesis/dissertation electronically, I declare that the entirety of the work contained therein is my own, original work, and that I have not previously in its entirety or in part submitted it for obtaining any qualification.

March 2011

ACKNOWLEDGEMENTS

I thank Almighty God for his grace and favours during my studies in South Africa. This research would have been impossible if not for the Lord being on my side.

I appreciate my parents Dr and Mrs Sobiyi for their encouragements and supports that made my stay a worthwhile.

To my family, Taiwo, Oluwakemi, Oluwatosin and Olumayowa for their prayers, emotional and financial supports. Thank you for being there for me.

I would like to express my sincere gratitude to Dr Deborah Blaine, my academic supervisor, for her support and encouragement throughout the duration of my studies towards my thesis. It was a privilege to have the opportunity to work with her and to share from her valuable expertise and knowledge.

I will like to thank the member of staff of Jerimet Pty South Africa, most especially Aubrey, for allowing me to use their press and other technical assistance provided.

I wish to thank, Shaheeda Peterson and Nicolas Clinning for their inputs and the opportunity to use University of Cape Town furnace for my sintering experiments.

Lastly, I wish to thank the project sponsor, TIA the former AMTS for their financial support.

TABLE OF CONTENTS

Page

ABSTRACT ..... **I**

OPSOMMING ..... **II**

DECLARATION ..... **III**

ACKNOWLEDGEMENTS ..... **IV**

TABLE OF CONTENTS ..... **V**

LIST OF FIGURES ..... **VIII**

LIST OF TABLES ..... **X**

LIST OF SYMBOLS AND ABBREVIATIONS ..... **XI**

CHAPTER 1: INTRODUCTION……1

1.0 INTRODUCTION **1**

1.1 OBJECTIVES **6**

1.2 MOTIVATION **6**

CHAPTER 2: LITERATURE REVIEW……..……..8

2.1 PROPERTIES OF TITANIUM **8**

2.2 TITANIUM POWDER METTALURGY **10**

2.2.1 POWDER METALLURGY 10
2.2.2 TITANIUM POWDERS 13
2.2.3 ADVANTAGES & CHALLENGES OF TITANIUM POWDER METALLURGY 16
2.2.4 PM TITANIUM ALLOY PRODUCTION 17
2.2.5 SINTERING KINETICS OF PM TITANIUM 19
2.2.6 TOOLING DESIGN 21

2.3 TITANIUM MACHINING **24**

2.3.1 IMPROVEMENTS IN TITANIUM MACHINABILITY 24
2.3.2 CUTTING SPEED 25
2.3.3 EFFECTS OF COOLANT 26
2.3.4 CUTTING TOOL GEOMETRY 27
2.3.5 CUTTING TOOL MATERIAL 28
2.3.6 CUTTING FORCES 29
2.3.7 SURFACE INTEGRITY 31

2.3.8 CUTTING TEMPERATURE 32
2.3.9 CHIP FORMATION 33

2.4 MACHINING OF PM METAL 34

2.5 FACTORS AFFECTING PM MACHINABILITY 36

2.6 IMPROVEMENTS OF PM MACHINABILITY 37

CHAPTER 3: METHODOLOGY 39

3.0 EXPERIMENTAL PROCEDURE 39

3.1 DESIGN OF TEST SPECIMEN SHAPE 39

3.2 POWDER CHARACTERISATION 40

3.3 POWDER COMPRESSIBILITY AND SINTERING 40

3.4 MACHINING TEST SPECIMEN PREPARATION 43

3.4.1 TOOLING DESIGN 43
3.4.2. COMPACTION AND SINTERING 44

3.5 METALLOGRAPHIC EXAMINATION 45

3.6 MACHINING SET–UP 46

3.6.1. MACHINING PARAMTERS 46
3.7.2. EVALUATING MACHINABILITY 48

CHAPTER 4: RESULTS AND DISCUSSION 49

4.1 POWDER CHARACTERISATION 49

4.2 COMPRESSIBILITY STUDIES 50

4.3 SINTERING 52

4.4 COMPACTION AND SINTERING OF MACHINING TEST SPECIMEN 55

4.5 MACHINING TRIAL: PILOT TEST (SAMPLES A AND B) 58

4.5.1 FLANK WEAR 58
4.5.2 INFLUENCE OF CUTTING SPEED 60
4.5.3 INFLUENCE OF POROSITY 60

4.6 MACHINABILITY TRIALS: FINAL TESTS (SAMPLE C AND D) 62

4.6.1 FLANK WEAR 63
4.6.2 INFLUENCE OF CUTTING SPEED 64
4.6.3 INFLUENCE OF POROSITY 65

4.7 EVALUATION OF SURFACE INTEGRITY 69

4.7.1 MACHINED SURFACE TEXTURE 70

4.7.2 LAY 72

4.7.3 DEFECTS/DAMAGES 73

4.8 HARDNESS 75

4.9 EVALUATION OF CHIP FORMATION 76

CHAPTER 5: CONCLUSION AND RECOMMENDATION……82

5.1 CONCLUSION 81

5.2 RECOMMENDATIONS 82

REFERENCES……84

APPENDIX A: TOOLING DESIGN 92

APENDIX B: G96 CODES 99

APPENDIX C: COMPRESSIBILITY AND SINTERING DATA 100

LIST OF FIGURES

Figure 1 Typical parts made from titanium alloy (Froes *et al.*, 2004) 1
Figure 2 Percentages of total cost of Titanium at processing stages (adapted from Seong and Goldsmith, 2009) 4
Figure 3 1971-2006 producer price index for titanium (Seong and Goldsmith, 2009) 5
Figure 4 Specific strengths at temperature of some metals including titanium and titanium alloys (Kobelco, [S.a.]) 8
Figure 5 Powder metallurgy production processes 11
Figure 6 Density gradient lines during single and double action pressing (German, 2005) 12
Figure 7 Emerging technologies of titanium part production, (adapted from Seong and Goldsmith, 2009) 18
Figure 8 Green and sintered density of CP titanium powder between compaction pressures of 200 - 800 MPa (Robertson and Shaffer, 2009) 20
Figure 9 Component forces acting on the single point cutting tool, (adapted from Awopetu *et al.*, 1995) 29
Figure 10 Effect of feed rate on component cutting forces (Sun *et al.*, 2009) 30
Figure 11 The effect of cutting conditions on the cutting temperature of titanium and selected alloys (Kikuchi, 2009) 32
Figure 12 Green part specifications in mm 39
Figure 13 Right cylinder sample preparations before compaction showing the preweighed powder (left), lower punch and die assembly (middle, bottom), die wall lubrication solution (middle, top) and upper punch (right). 41
Figure 14 Carver® 12-ton hand operated compaction press 42
Figure 15 Vertical tube furnace for vacuum sintering 43
Figure 16 Tooling set-up for powder compaction at fill position 44
Figure 17 Machined sample compaction set-up 45
Figure 18 Machining lathe set-up 46
Figure 19 Cumulative percentages of the titanium powder particles 49
Figure 20 SEM Image of CP titanium sponge fines powder at 500x and 1000x magnification 50
Figure 21 Compressibility of the green titanium compacts 51
Figure 22 Shape of the sintered titanium compact 52
Figure 23 Green and sintered density at different compaction pressures and sintering times 53
Figure 24 Light optical micrographs of sintered titanium microstructure at different compaction pressures (a) 400 MPa 100x (b) 400 MPa 500x (c) 600 MPa , 100x core of sample (d) 600 MPa, 500x core of sample and (e) 600 MPa, 100x, edge of sample. 55
Figure 25 Green specimen of the sample shape from powder titanium 56
Figure 26 Shapes of samples before machining, (a) sample C, (b) sample D 57
Figure 27 Light optical micrographs of the porosity of sample D observed at the (a) core and (b) inner edge. 58

Figure 28 Flank wear growth with material removal rates for sample B (cutting speed 60 m/min) 59
Figure 29 Tool flank wear after four passes at varying cutting speeds (Sample A) 60
Figure 30 Effect of porosity on tool flank wear on machinability of CP titanium at different cutting speeds 61
Figure 31 Wear observed on the cutting tool after machining titanium (a) sample A (more porous) (b) sample B (less porous) 62
Figure 32 Optical microscope images flank wear of the cutting tool for (a) sample C and (b) sample D, both at a cutting speed of 60 m/min, and (c) flank wear and (d) crater face wear of sample D at a cutting speed of 90 m/min. 64
Figure 33 Tool wear curves for machining Sample D at two cuttings speeds (60 m/min and 90 m/min). 65
Figure 34 Cutting tool flank wear vs number of cuts 67
Figure 35 Relationship between the tool wear and cutting time for samples with different porosity at cutting speed of 60 m/min 67
Figure 36 Average flank wear in relationship to the material removal rate at different porosity 68
Figure 37 Scanning electron micrograph of machined surfaces at different cutting speeds (a) sample A, 60m/min (b) sample A, 150 m/min, (c) sample B, 150 m/min (d) sample C, 60 m/min (e) sample D, 60 m/min (f) sample D, 90 m/min 71
Figure 38 Typical whitelayer on machined surface (sample C) 72
Figure 39 Micro chips, debris and tears produced by the cutting tool on sample C 74
Figure 40 Chip shapes formed during machining (a) sample D, 60 m/min (b) sample D, 90 m/min and (c) sample C, 60 m/min 77
Figure 41 Optical microscopy image (100x magnification) of serrated chip formed during machining 77
Figure 42 Chip obtained after machining the samples at different cutting speeds (a) sample A at 60 m/min, (b) sample A at 90 m/min, (c) sample A at 120 m/min, (d) sample A at 150 m/min, (e) sample C at 60 m/min, (f) sample D at 60 m/min, ... 78

LIST OF TABLES

Table 1 Comparative cost of titanium, aluminium and steel as of, 2007 (adapted from Froes *et al*., 2007) 3
Table 2 Composition and mechanical properties of some typical titanium alloys (Callister, 2003) 9
Table 3 Basic method of Titanium powder production (Naboychenko and Dowson, 2009) 14
Table 4 The effect of density variations on the properties of PM material 35
Table 5 Cutting Parameters for Machining Tests 47
Table 6 Particle size distribution at cumulative finer percentages 50
Table 7 Relative sintered density and densification ratio of CP titanium at varying compaction pressures 53
Table 8 Machined specimens at their relative green and sintered densities 55
Table 9 Hardness HV 10 of samples of sintered and machined surface at relative cutting speeds 75

LIST OF SYMBOLS AND ABBREVIATIONS

u	SPECIFIC CUTTING ENERGY
vol. %	PERCENTAGE VOLUME
wt	WEIGHT
α	ALPHA
β	BETA
ρ	DENSITY
AlTiN	ALUMINIUM TITANIUM NITRIDE
AMTS	ADVANCED MANUFACTURING TECHNOLOGY STRATEGY
ASTM	AMERICAN SOCIETY FOR TESTING AND MATERIALS
BE	BLENDED ELEMENTAL
BN	BORON NITRIDE
BTF	BUY-TO-FLY
BUS	BROKEN UP STRUCTURE
CaF_2	CALCIUM FLOURIDE
CBN	CUBIC BORON NITRIDE
CIP	COLD ISOSTATIC PRESSING
CR	COMPRESSIBILITY RATIO
CrN	CHROMIUM NITRIDE
CNC	COMPUTER NUMERICAL CONTROLLED
CP	COMMERCIALLY PURE
CVD	CHEMICAL VAPOUR DEPOSITION
EDS	ENERGY DISPERSIVE SPECTROSCOPY

EBM	ELECTRON BEAM MELTING
HDH	HYDRIDE-DE-HYDRIDE
HIP	HOT ISO-STATIC PRESSING
HSS	HIGH SPEED STEELS
ISO	INTERNATIONAL STANDARD ORGANISATION
MBW	MATERIAL BUY WEIGHT
MER	MER CORPORATION
MFW	MATERIAL FLY WEIGHT
$MgSiO_3$	MAGNESIUM SILICON OXIDE
MHR	METAL-HYDRIDE REDUCTION
MIM	METAL INJECTION MOULDING
MnS	MANGANESE SULPHIDE
MoS_2	MOLYBDENIUM DISULPHITE
PA	PRE ALLOYED
PAM	PLASMA ARC MELTING
PCBN	POLYCRYSTALLINE CUBIC BORON NITRIDE
PCD	POLYCRYSTALLINE DIAMOND
PIM	POWDER INJECTION MOULDING
PM	POWDER METALLURGY
S	SULPHUR
Se	SELENIUM
SEM	SCANNING ELECTRON MICROSCOPE
SiC	SILICON CARBIDE
SS	STAINLESS STEEL
Pb	LEAD

PbS	LEAD SULPHITE
PVD	PHYSICAL VAPOUR DEPOSITION
Ti	TITANIUM
TiAlN	TITANIUM ALUMINIUM NITRIDE
TiCN	TITANIUM CARBONITRIDE
TiN	TITANIUM NITRIDE
VAR	VACUUM ARC REMELTING
WC-Co	TUNGSTEN CARBIDE-COBALT
ZrN	ZIRCONIUM NITRIDE
Zn	ZINC

INTRODUCTION

1.0 INTRODUCTION

In the last 50 decades, after the emergence of titanium in commercial quantities in the early 1950's, there has been an ever increasing demand in titanium use as a substitute over many metals in the aerospace, automotive, petrochemical, chemical, oil and biomedical industries.

Titanium and its alloys play an important role in the aerospace industry in the construction of airframes and aero engines where weight, safety and fuel economy is highly prioritised. In automotive, chemical and biomedical industries, titanium is typically used to manufacture valves, valve springs, connecting rods, bolt fasteners and exhaust system of automobiles, heat exchangers, tanks, structural parts, process vessels and medical implants. Other areas of application are in spectacle frames, cameras, watches, and golf club heads. Some parts produced from powder metallurgy (PM) titanium are shown in Figure 1.

Figure 1 Typical parts made from titanium alloy (Froes *et al.*, 2004)

Properties that make titanium very useful and attractive in these industries are its high strength to density ratio, low thermal expansion rate, corrosion resistance and enhanced stiffness/wear resistance which can be improved with coatings and reinforcement (Deura *et al.*, 1998; Elyon *et al.*, 1998; Moll, 2000; Froes, 2000; Donachie, 2000; Froes *et al.*, 2007).

Commercially pure titanium is 45% lighter than low grade steel of the same strength, and about 60% more dense but twice as strong as a typical aluminium alloy (Barksdale, 1968). The tensile strength of titanium is three times more than that of aluminium which gives it the advantage of its high strength to weight ratio.

The combination of the low elastic modulus and its high strength make titanium very ductile. The thermal expansion of titanium is significantly less than that of many stainless steels, brass, copper- nickel alloys and ferrous alloys (Barksdale, 1968).

Titanium provides excellent resistance to corrosive media, such as chlorine compounds in aqueous solution, chlorine dioxides, neutral chloride solutions, chlorine chemicals, chlorine gas, bromide water, steam in excess of 315°C, sea water as high as 260°C, erosion of high velocity water, alkaline medium, gaseous oxygen, and organic media. It is non-toxic to marine organisms. It shows a relative resistance to reducing acids, such as hydrochloric, phosphoric and sulphuric, but notably corrodes as the temperature and concentration of those media increase. The corrosion resistance of titanium is due to its passivity; a strong oxide film forms on the metal surface which is relatively stable against most substances.

Titanium as a natural resource is found in rutile or ilmenite. South Africa is the second largest supplier of titanium ore in the world after Australia with 850,000 tonnes in 2003 alone (Cordellier and Didiot, 2004).

A number of stages are involved during the production of parts from titanium. Titanium must first be extracted from ore (typically rutile which is TiO_2 sand). The extraction process occurs by chlorinating the ores to produce titanium tetrachloride and then reducing the chloride using a magnesium or sodium reduction process to produce pure titanium. Generally, the magnesium reduction process, the Kroll process is commonly used for producing titanium sponge. The Hunter process is the less-used, sodium reduction process which also produces titanium sponge. The Armstrong process is a semi-continuous version of the Hunter process that has recently been commercialised by International Titanium Powder for producing titanium powder (International Titanium Powder homepage, [S.a.]).

Following the reduction process, the sponge is melted and formed into ingots. The melting and forming processes involve vacuum arc melting which is an expensive process. It takes up to 25 hours to melt the sponge, thus requiring a substantial amount of energy and expensive equipment for melting which makes it not only costly but also labour intensive (Seong and Goldsmith, 2009).

Billets are then formed from the ingots. A finished product of the desired shape, size and surface quality is then usually produced by machining wrought titanium billet. Up to 90% by volume of titanium ingot is wasted during machining (Capus, 2004; Tital Gmbh, 2010). Furthermore, machining titanium is a difficult, slow process. Overall, manufacturing a titanium product is tedious, energy intensive and expensive, thus making traditional titanium forming processes unattractive.

With all the advantageous properties titanium possesses, cost is still a major challenge. Titanium and its alloys are so expensive to produce that their use is

limited to areas with high performance requirements (Deura, 1998; Elyon *et al*., 1998; Froes, 2000b; Donachie, 2000). The high cost of a finished titanium component can be attributed to each of the process steps: extraction from ore, fabrication into preform and the final machining operations.

Table 1 shows the cost of titanium at different production stages compared to steel and aluminium. It is 30 times more expensive to manufacture 1 kg of titanium ingot compared to 1 kg of steel, and note that the ingot is only the preform to the billet from which the final part is then machined.

Table 1 Comparative cost of titanium, aluminium and steel as of, 2007 (adapted from Froes *et al*., 2007)

Production Stage	Steel	Aluminium	Titanium	
	Cost/weight	Factor to Steel	Factor to Steel	Factor to Aluminium
Ore Extraction	1	5	15	3
Metal Refining	1	6.8	20	2.9
Ingot forming	1	4.7	30	6.4
Sheet Forming	1-2	3.3-8.3	50-83	10-15

Several factors lead to the ever increasing price of titanium. The production stages involve the purchase of rutile, extraction, ingot casting and melting, and finally fabrication processes (which includes machining). Of all the processing stages, the relative costs of which are shown in Figure 2, the cost of fabrication is the most expensive. Fabrication alone contributes about 47% of the total production cost of the mill product (such as sheet, billets, plate and bars). Fabrication costs include forming and machining processes to produce the final product. Ingot melting (15%) is achieved using vacuum arc re-melting (VAR). The extraction process (33%) uses either the Kroll or Hunter process. The rutile ore (where South Africa obtains its share revenue) constitutes only 4% of the total cost.

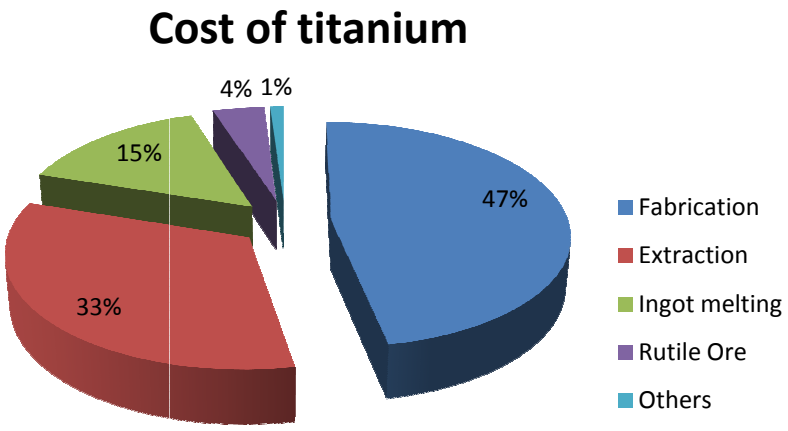

Figure 2 Percentages of total cost of Titanium at processing stages (adapted from Seong and Goldsmith, 2009)

The two main contributors to the high fabrication cost are the slow machining and high Buy-to-Fly (BTF) ratio. BTF ratio is the ratio of the weight of material that is purchased to machine a part to the weight of the finished part, thus making the useful component almost minute compared to the starting material. Slow machining, is necessary due to the high hardness, high chemical reactivity at elevated temperatures and low thermal conductivity of titanium. This requires machining of titanium to take place at slow cutting speeds to reduce the thermal load and low depth of cut to reduce the mechanical load, making machining difficult and time consuming. Consequently, the BTF ratio is usually very high for titanium. For instance, the BTF ratio of titanium parts from plate to sheet can be as high as 20:1 (Seong and Goldsmith, 2009).

There is a significant amount of titanium used in aircraft manufacturing. The percentage of an aircraft's body weight that is constituted of a certain material is called the material fly weight (MFW). For titanium, the actual amount of material necessary for the production of the aircraft (material buy weight, MBW) is many times more than the titanium MFW. For instance, titanium's MFW for the F-22A raptor fighter plane is about 39% (Seong and Goldsmith, 2009).

A study conducted by Seong and Goldsmith (2009) on the price index of titanium between the years of 1971 to 2006 showed a consistent increase in the price of titanium. As can be seen from Figure 3, there was a sharp increase in the price of titanium in 2003 and from this point, it kept on progressing rapidly.

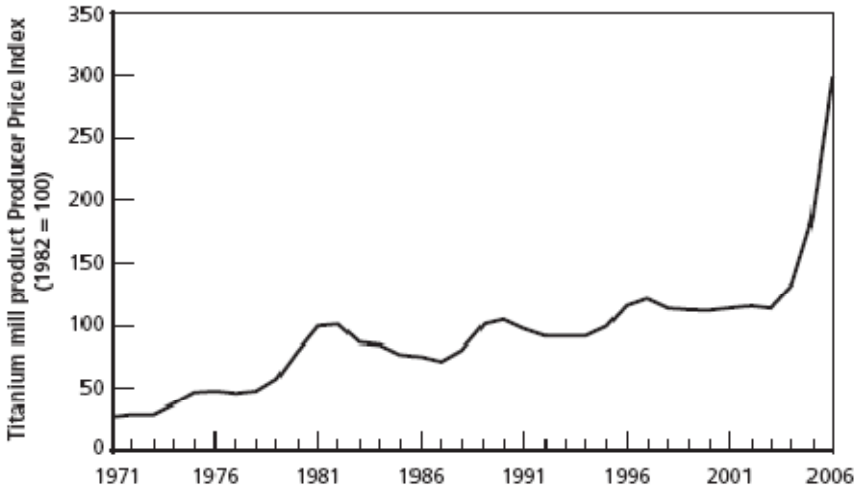

Figure 3 1971-2006 producer price index for titanium (Seong and Goldsmith, 2009)

Several analysts claimed that the peak in the demand of titanium in 2004 led to the sharp increase in the price in 2005 - 2006 (Seong and Goldsmith, 2009). Whenever there is an increase in demand of a product and the supply of such product cannot meet this demand, there is always a strong tendency for an increase in the price.

However, the sharp increase in the titanium demand in 2004 was not the only reason for the subsequent increase. The extreme shortage in the supply of scrap and titanium sponge over these years also contributed to the increase in price Furthermore, increase in the percentage of titanium used for aircraft parts increased as aircraft orders increased during this time. The Western countries industrial demand and the Chinese continual heavy consumption of titanium kept pushing the price up.

Titanium sponge itself is supplied in varying grades that is used to produce engine parts, air frame parts and golf club heads. Titanium manufacturing plants are, as of yet, unable to cope with the increase in the demand of titanium sponge production because of the limited supply of scrap, enormous capital investments and long lead time for building titanium production plants.

These major cost and supply challenges encouraged a shift to exploring titanium powder metallurgy (PM), a near net shape technology (products can be manufactured close to their final shape) by offering a solution to these problems. Compacts can be produced at 50 - 60% the cost of wrought titanium (Barksdale, 1968) because of the reduced cost of producing powder compared to ingot, as well as cost savings due to near net shape capability which avoids high material waste associated with wrought machining. Secondary processing and machining costs are also minimised (Norgate and Wellwood, 2006).

Many researchers and companies have successfully manufactured titanium parts using powder metallurgy; however, the manufacturing cost has still remained too high for this technology to become mainstream. The high costs relate to powder price as well as secondary operations, such as hot isostatic pressing, required to form materials with sufficient quality to be of use to the primary titanium consumers, the aerospace industry. Recent efforts in titanium powder metallurgy have been focused on lowering the cost of powder production and improving the quality of the sintered material; however, little research has been conducted on machining of PM titanium. Typically, as PM is a netshape manufacturing technology, machining of the material is not a major consideration. However, most PM parts require some level of finish machining, either to comply with dimensional tolerance requirements or to add features which are not possible to form using typical PM forming processes. Furthermore, due to the fact that the PM route for manufacturing titanium material cuts out many of the expensive, time-consuming processes (for instance, VAR and forming to billet) of conventional manufacturing, there has also been interest in exploring the possibilities of manufacturing mill product (sheet, billet) directly from powder. In this case, rough as well as finish machining would constitute a significant aspect of the manufacturing process. Accordingly, this thesis will look into issues associated with machining PM titanium.

1.1 OBJECTIVES

The aim of this project is to investigate the machinability of commercially pure (CP) titanium produced through PM techniques. The titanium will be produced, with a density greater than 90% of the theoretical density. The machinability of PM titanium will be investigated by face turning machining tests. Factors such as the final machined surface finish and tool wear are monitored in order to evaluate machining performance.

This thesis forms part of the TIA (the former AMTS) Light Metals Program Project: High Performance Machining of Titanium and its alloys. The objective of the project is improving the usage of high performance cutting techniques in machining integral parts of titanium alloys in the South African industry.

1.2 MOTIVATION

A large amount of research has been published on PM titanium and its alloys; however, no research efforts have been focused on the machinability of PM titanium. Some particular shapes cannot be produced ordinarily without machining the PM parts. The machinability of PM materials generally differs from the machinability of their wrought equivalent. Wrought titanium is notorious for long machining times, large tool consumptions and poor surface finish when

machined at high speed. These factors lead to an increase in the manufacturing costs of titanium, thus limiting the range of use.

By developing PM processing for titanium, its usage in high-tech and custom-made applications can be increased. However, the machinability of PM titanium must be understood and optimised for this to happen.

LITERATURE REVIEW

2.1 PROPERTIES OF TITANIUM

Titanium is categorised as a transition element. It is a light metal in its pure form, with a relatively low density of 4.506 g/cm^3. Other physical and chemical properties titanium possesses are its high melting point of 1668°C, a relatively a low elastic modulus of 107 GPa and high ductility (Timet, 1997).

Titanium has good corrosion resistance and good creep resistance above 500°C. It maintains its excellent strength properties at elevated temperatures, as shown in Figure 4. However, it is highly reactive with other metals at temperatures above 400°C. It is relatively stable in air and industrial environments (Astana *et al*., 2006; Joubert, 2008).

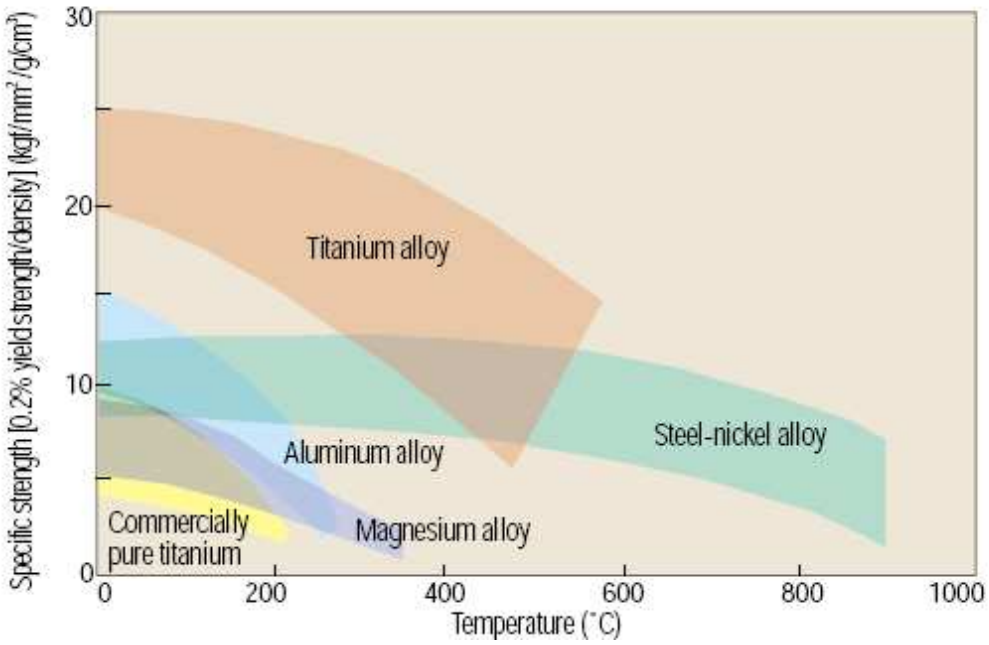

Figure 4 Specific strengths at temperature of some metals including titanium and titanium alloys (Kobelco, [S.a.])

The high specific modulus (elastic modulus/density) of titanium alloys has encouraged its use in the aerospace industry. A typical application is compressor blades in gas turbines, which operate at varying pressures and at extremely high peripheral speeds.

When comparing titanium properties to steel and nickel-based alloys, titanium possesses (Moll, 2000; Timet, 1997);

- Lower density
- Higher melting point
- Good ductility
- Easily contaminated during welding operations
- Lower modulus of elasticity

The differences in the properties can however be compensated for, thus allowing it to be fabricated using techniques that are similar to both stainless steels and nickel based alloys.

Titanium alloys are categorised into four major classes: α-alloys, near α-alloys, α-β alloys and β alloys. Compositions and mechanical properties of typical titanium alloys are shown in the Table 2.

Table 2 Composition and mechanical properties of some typical titanium alloys (Callister, 2003)

Alloy	Common Name	Condition	Tensile Strength (MPa)	Yield Strength (MPa)	Ductility (% EL in 50mm)
CP	Unalloyed (99.1 Ti)	Annealed	484	414	25
α	Ti-5Al-2.5Sn	Annealed	826	784	16
Near α	Ti-8Al-1Mo-1V	Annealed (duplex)	950	890	15
α-β	Ti-6Al-4V	Annealed	947	877	14
β	Ti-10V-2Fe-3Al	Solution + aging	1223	1150	10

Titanium has an α-phase allotrope which has a hexagonal close-packed structure (hcp) and this transforms to a β-phase allotrope with a body centre-cubic (bcc) structure at temperatures above 882°C (Barksdale, 1968; Joubert, 2008). The α-alloy is more ductile than the β-alloys and can be easily formed while β-alloys are relatively brittle and hard.

Commercially pure grades of titanium are unalloyed α-phase allotrope but, sometimes have traces of impurities, such as oxygen and iron. Titanium has a tendency of deflecting up to twice that of steel under the same load due to its elastic modulus which is 30-50% lower than that of steel at values between 100 - 125 GPa (Laubscher and Van Trotsenburg, 2010). The high strength (170-480 MPa) and excellent corrosion resistance makes its application favourable in cryogenic applications and they have good weld-ability (Laubscher and Van Trotsenburg, 2010).

In Table 2, the α/β-alloys, for example Ti-6Al-4V, contain a mixture of α and β phases at ambient temperatures and can be applied at temperatures of 315-400°C with characteristics of good corrosion resistance, high strength, low weldability, high hardenability and good responsiveness to heat treatments. They are responsible for the largest percentage of titanium alloy in application (up to 60% of titanium used). The aerospace industry is the highest consumer of this alloy (Joubert, 2008).

The α + β phase zone can be stabilized by the addition of different metalloid and metallic elements. The properties of titanium can be altered by inclusions of some elements during the alloying process and by heat treatments. Titanium can be alloyed or heat treated to improve its strength, but this is usually at cost to its ductility.

2.2 TITANIUM POWDER METTALURGY

2.2.1 POWDER METALLURGY

Modern powder metallurgy technology commenced in the 1920's with the production of tungsten carbides and porous bronze bushes for bearings. Between the 1930's and 1960's, there was steady growth into the developments in ferrous and non-ferrous materials. Since then, the industry had grown more rapidly than conventional processes because of its potential to manufacture products with unique properties, near net shape ability to manufacture complex shapes, and economics in material utilization (Rajiv *et al*., 2006).

PM is a near net shaping technology, where high material waste is reduced, and close proximity of final dimensions and elimination/minimisation of machining processes are achieved. In addition, the final properties of a sintered PM material can be easily controlled to suit some applications, for example in biomedical applications where the density is controlled in order to produce porous material into which bone can grow.

Manufacturing of complex parts that are challenging and expensive using conventional methods, can be achieved with relative ease using PM. Impurities on grain boundaries can also be controlled and up to 97% of the full properties of the wrought form are achievable (Froes *et al*., 2007).

Powder metallurgy (PM) processes typically use metal powders that are formed into final shape. The most common PM process is press-and-sinter where the powders are pressed into shape under high pressures and then the compacted shape is sintered in a protective atmosphere.

Four main steps are involved in fabricating press-and-sinter PM metal parts: powder production, mixing and blending, powder compaction and lastly, sintering. The process chart is shown in Figure 5. In many cases, parts are re-sized or machined after sintering to improve their dimensional accuracy and to produce small features that are difficult or impossible (perpendicular to pressing direction) to press.

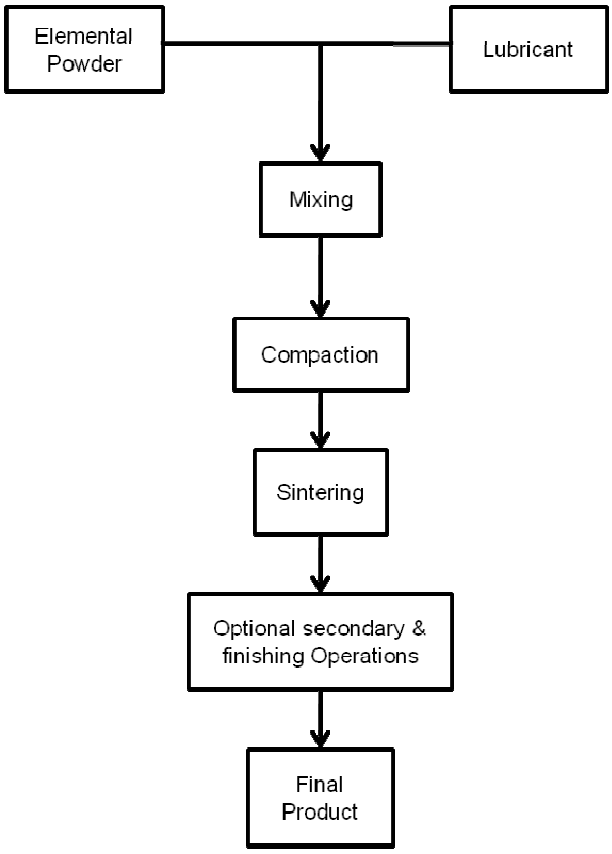

Figure 5 Powder metallurgy production processes

There are a number of ways for producing metal powders: atomisation, electrodeposition, chemical synthesis, crushing and milling, to name a few. Powders ranging in size between 0.1-200 µm can be manufactured by these methods (Naboychenko and Dowson, 2009). These methods are useful for producing powders with varying shape and surface texture.

In powder mixing, different powders are blended, sometimes with the addition of lubricants. In many cases, alloys are blended by combining of two or more different elemental powders. Powder lubricants are mixed in with the metal powders to assist in ejection of the part after compaction and to help prevent tool wear. Zinc stearate and paraffin wax are common lubricants used in traditional

powder metallurgy. Mixing is necessary in order to remove segregation, facilitate compaction and aid sintering (Astana *et al.*, 2006).

Compaction is a process where the loose, mixed powders are pressed into a part shape, after which the compacts are usually called 'green'. The powders undergo plastic deformation under the external pressure or load. Traditional powder metallurgy uses uniaxial compaction to press powders. This can be done by a single action and double action compaction method (Astana *et al*., 2006). The compaction method depends on the specific powder's size, shape and the desired component shape. Double action is usually preferred as it produces the lowest density gradients in the compacted part. The green density gradients for single and double action compaction in a typical ferrous alloy part are shown in Figure 6. Note that the density varies from 4.7 to 5.5 g/cm^3 for single action compaction, while the density variance is much less, from 5.1 to 5.5 g/cm^3, for double action compaction. The density gradients in the green part cause it to warp during sintering due to anisotropic shrinkage (German, 2005). To achieve uniformity in compacts, powders can be pressed using isostatic compaction, but the shape complexity of the part is limited.

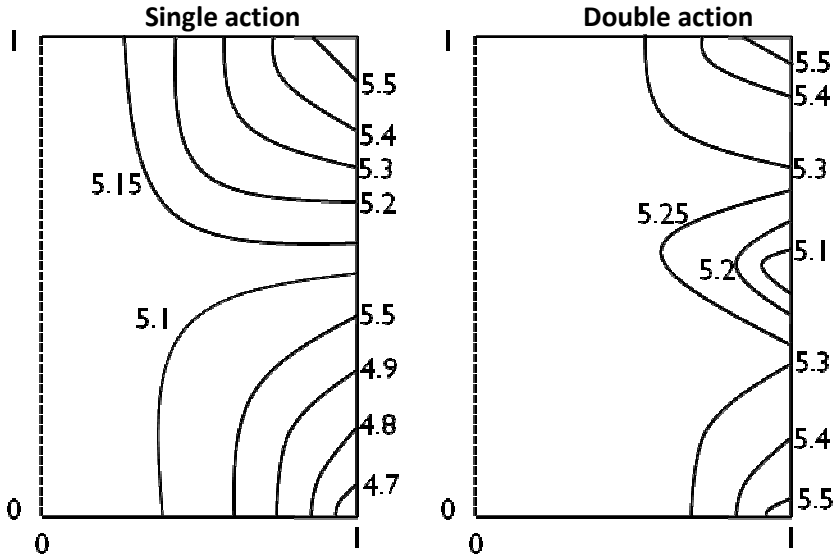

Figure 6 Density gradient lines during single and double action pressing (German, 2005)

Metal injection moulding (MIM) is another common PM technique. It was developed from the injection moulding of plastics as an alternative approach to part manufacturing. The metal powder is mixed with a polymer binder into a thermoplastic paste. The paste is injection moulded, under pressure and heat, into the desired shape. The injection moulded part is then heated so that the binder is burnt off before sintering takes place. MIM is most successfully used to make high volumes of small, highly complex parts (German, 2005; Astana *et al*., 2006).

Sintering is a process where powder particles that are in contact bond together at high temperature. The temperature which sintering takes place is usually below the melting point of the material. Sintering occurs as a result of the diffusion of atoms at a high temperature, driven by a reduction in the free surface energies of the small powder particles. Accordingly, small powder particles usually sinter very quickly because of the high specific area and energy (German, 2005). Green PM compacts are typically sintered in controlled atmosphere continuous furnaces, at a temperature below the melting point of the powder and are allowed to cool slowly in a controlled atmosphere (Froes *et al*., 2004).

The evidence of bonding between particles during sintering on microstructural scale is seen as neck growth, where small neck grow at the sinter bonds between particles. The particle bonding is associated with an elimination of pores, evident in the final density, densification, sinter bond neck size, and shrinkage of the compact. Powder compacts normally change in dimensions during sintering as they densify. With the increase in density, there is also an increase in hardness, thermal conductivity, strength, and elastic modulus.

2.2.2 TITANIUM POWDERS

Various methods are commercially available for the production of titanium powder. Powders of sizes ranging from nanometers to a few millimetres are produced by following methods: mechanical milling, atomisation, reduction of metal oxides, thermal precipitation and chemical precipitation from liquid.
Different methods for producing titanium powders are shown in Table 3, along with the characteristics of the powder particles, including the typical sizes and shapes of the powders.

Table 3 Basic method of Titanium powder production (Naboychenko and Dowson, 2009)

Method of production	Process character	Characteristics of powder particles	
		Size (μm)	Shape
Mechanical Milling	Self grinding, mills rolls and ball mills	20 - 10^4	Irregular, scaly
Atomization (gas, centrifugal, liquid and water)	Stream of liquid material broken by impinging gas or liquid, rotating electrode process	5 - 800	Spherical, irregular, angular
Reduction of metal oxide (chemical and electrolytic method)	Precipitation from solution, Hydrogenation Metallothermy[1]	nano-size, 100 20 - 200 20 - 300	Irregular, angular, granular briquettes
Chemical precipitation from liquid	Injection into molten sodium	10 nm – 20	Irregular or cubic, sponge like
Thermal decomposition	Vapour decomposition and condensation	0.2 – 20	Irregular, rounded, chain shape
Electrolysis (physical and chemical method)	Electrolysis from melt	10 - 400	Dendritic
Gas phase precipitation	Evaporation and condensation	Ultrafine nano-size	Agglomerated particle clusters

The basic characteristics of the metal powder, such as the particle size distribution, particle shape, size and surface, are very important in the performance of the material during pressing and sintering, affecting the economy of the manufacturing process (Schwarzkopf, 1947).

The particle size distribution can be determined by different methods such as

[1] reduction of metal oxide by another metal

- ✓ Sieving, where the particle diameter is measured by a set of standard screens and thus a minimum diameter of the sample is measured. This method is limited to about 50 µm particles (Allen, 1990).
- ✓ Optical microscopy, used for counting and sizing from 0.5 to 100 µm (Schwarzkopf, 1947). This is a very time consuming method when used to determine a statistically significant particle size distribution. However, it is useful when used in conjunction with other methods to get a quick indication of the average particle size.
- ✓ Laser diffraction method, used for particle size analysis over a broad range of particle sizes finer than 200 µm based on the Mie theory (Allen, 1990). The device for measuring consists of a laser, particle dispersion and delivery system, a detector to measure the light scattering by the specimen and a computer to control the system and analyze the data. This method is easy to use define the particle size distribution.
- ✓ Sedimentation method, where powders are classified in accordance to their settling rate under gravity. It can be used for powders of different compositions but difficult to visualize particles that are irregular in shape.
- ✓ X-ray technique, used for measuring sizes of very small particles based on Scherre formula (Schwarzkopf, 1947). This technique is ideal for particles in the 50 nm size range.
- ✓ The Scanning electron microscopy (SEM) is a computer-based quantitative imaging analysis method using an electron beam and magnetic lenses to examine the particles with resolution ranging from 10 to 100 000 magnifications. Images are captured, digitalized and quantified. This allows the observation of grain boundaries, particle shape, size and chemical composition gradients of the powder by using energy dispersive spectrometry (EDS) (Naboychenko and Dowson, 2009). SEM is one of the best tools for observing the discrete characteristics of a powder.

Commercially available sponge fines of titanium powders are produced from titanium sponge. The titanium sponge is the final product of the Hunter and Kroll extraction processes, where a spongy porous cake of titanium is produced from the reduction of titanium dioxide by magnesium or sodium, respectively (Hayes *et al*., 1984). The sponge obtained from these processes is hydrogenated to make it brittle. It is then crushed and sieved to produce fines. The hydrogenated powder is then dehydrogenated to yield pure titanium powder. This process is known as hydrogenation-dehydrogenation and the powder is called HDH powder. The final sponge fines are graded in accordance to their particle size distribution and typically contain 0.12-0.15 wt % chlorine (Vladimir *et al*., 2000). The sponge fines are angular and irregular in shape and are relatively cheap compared to other processes of titanium powder production, such as gas atomization (spherical), electrolytic (dentritic) or mechanical milling of solids (irregular and scaly) (Oled *et al*., 1998). The sponge fines are best suited for die compaction because of its

shape. The HDH process is used to produce milled powder from titanium sponge, scrap titanium or Ti-6Al-4V and wrought titanium or Ti-6Al-4V.

In recent years, gas atomization has developed considerably in order to produce high quality prealloyed titanium powder. But these powders are not suitable for die compaction as they are spherical. They are typically used for powder injection moulding or mixed with HDH powder for compaction.

The developments of the hydrogenation-dehydrogenation (HDH), Armstrong (ITP) and metal hydride reduction (MHR) processes for powder production has helped in further reducing the cost of titanium powder and improves the mechanical properties of products (Lutjering and James, 2003; Froes *et al*., 2004).

2.2.3 ADVANTAGES AND CHALLENGES OF TITANIUM POWDER METALLURGY

Powder metallurgy can be described as a process where parts are made starting from elemental powder. This technology greatly limits material waste, especially compared to traditional titanium part manufacturing processes.

Using PM, parts are easily formed into the desired shape and have higher yields. Up to 97% of wrought physical and mechanical properties are obtainable using PM processing (Froes *et al*., 2007; Klar and Prasan, 2007). The near net shape capability (parts can be formed close to the desired dimensional requirements) provides a means of reducing waste that is associated with traditional titanium part fabrication, such as machining. In some cases of traditional titanium part manufacturing, up to 90% of the wrought material is removed so only 10% of the original material gets to the final stage of the production process. In comparison, little or no machining is required for PM parts (Watson *et al.*, 2007). With improvements of the yield over several steps of production, there is a considerable reduction of starting raw materials required to make the final part. However, even with the current advances in cost savings, PM is still insufficiently more cost effective for a major technology change in the production of titanium parts.

With titanium PM, there are several technical factors that make widespread use of this technology a challenge for high-tech applications, such as for aerospace. One of the major challenges is contamination control of the microstructure. In this case, the processing of the parts must be done in a very clean environment to avoid inclusions and impurities on the grain boundaries. Strict control of the oxygen level in the final microstructure is also required. The presence of hard particle phases observed in sintered titanium alloys leads to insufficient strength of the material. This can also be due to inhomogeneity of the microstructure because the powder in mixture is not of the same size (Alman and Hawk, 1999).

Moreover, the size of parts produced from PM is usually small (< 50 cm major dimension). Large parts are not economically viable. Usually titanium parts that

are used for aircraft are significantly large structural parts. So PM does not immediately fit into general aerospace part replacement.
Lastly, titanium powder is difficult to handle in large quantity because of the highly reactive, explosive nature of the powder (Klar and Prasan, 2007).

2.2.4 PM TITANIUM ALLOY PRODUCTION

Parts are produced from CP titanium powder by various consolidation and forming processes, including press-and-sinter, powder injection moulding (PIM), hot isostatic pressing (HIP), cold isostatic pressing (CIP) and powder rolling.

The press-and-sinter method is the most widely used PM manufacturing process and the most economical production technique for mass production of parts of desired density, strength and dimensional accuracy. It is not suitable for complex-shaped parts. PIM is used for the production of high volumes of small, complex-shaped metal parts. CIP is an economical, low volume production path for complex-shaped, highly uniform density compacts. It has the advantage of the short production times coupled with the ability to produce long and slender parts. The compacts must be sintered to bond the particles together after CIPping. HIP is similar to CIP except that it involves the simultaneous application of pressure and heat. HIP is used for powders that are difficult to sinter and parts that require excellent properties. Currently, most titanium parts that are commercially manufactured require HIPping to obtain the material properties required. Powder rolling is a method where powders are rolled to produce coherent strips. Parts with fine grains, high mechanical strength and close to theoretical density can be produce with this method (Angelo and Subramanian, 2008). Titanium powder rolling is one of the PM successes for this material.

Titanium alloy powder metallurgy fabrication methods are divided into two major categories based on the initial powder mixtures: blended elemental (BE) and pre-alloyed (PA) powders.

In the BE technique, different (for example, titanium, aluminium and vanadium) powders are blended together, consolidated and sintered to produce the alloyed material. Sponge fines used in this technique contains 0.12- 0.15 wt. % chloride which prevents full density being reached, resulting to inferior mechanical properties (Elyon *et al*., 1998). This approach produces titanium PM at a lower cost; however, parts produced by this method are limited in size and complexity. BE material can be improved by undergoing a secondary process of hot forging to increase its density.

For pre-alloyed (PA) titanium, titanium alloy powders are made from their molten state. The wrought form of the material, for instance wrought Ti6Al4V, is vacuum melted and atomised using gas. High purity, spherical powders are produced from this method due to the purity level of the starting raw materials. The powders are also consolidated and sintered to produce titanium alloys. These powders are not

suitable for die compaction unless mixed with sponge fines due to their spherical shape. They are suitable for PIM and laser sintering or direct metal deposition. The PA powders produced by gas atomisation and plasma rotating methods undergo hot isostatic pressing (HIP) to produce more fully dense compacts. PA titanium have superior properties as compared to BE produced parts but are much more costly. They are more in demand in aerospace industry because of their mechanical properties (Elyon *et al*., 1998; Lutjering and James, 2003; Froes *et al.*, 2004).

Figure 7, shows various methods for producing titanium powder and parts. From all the methods of producing titanium powders, the Armstrong, hydride-dehydride (HDH) and MER processes have been more widely adopted as promising methods of titanium metal powder production in an attempt to reduce the cost of the final part product (Seong and Goldsmith, 2009). The Armstrong process is a continuous, low temperature reduction of titanium tetrachloride based on the Hunter process, the MER process produces titanium powder using direct electrolytic reduction, while the HDH process directly produces titanium powder from sponge, scrap, turnings and other titanium waste products. Titanium sponge is mostly produced using the Kroll process. The Cambridge process is a newly developed process for extracting titanium, however, even after years of research and investment in scaling this process up to commercial levels, no real commercial success has been realised using this technique to date.

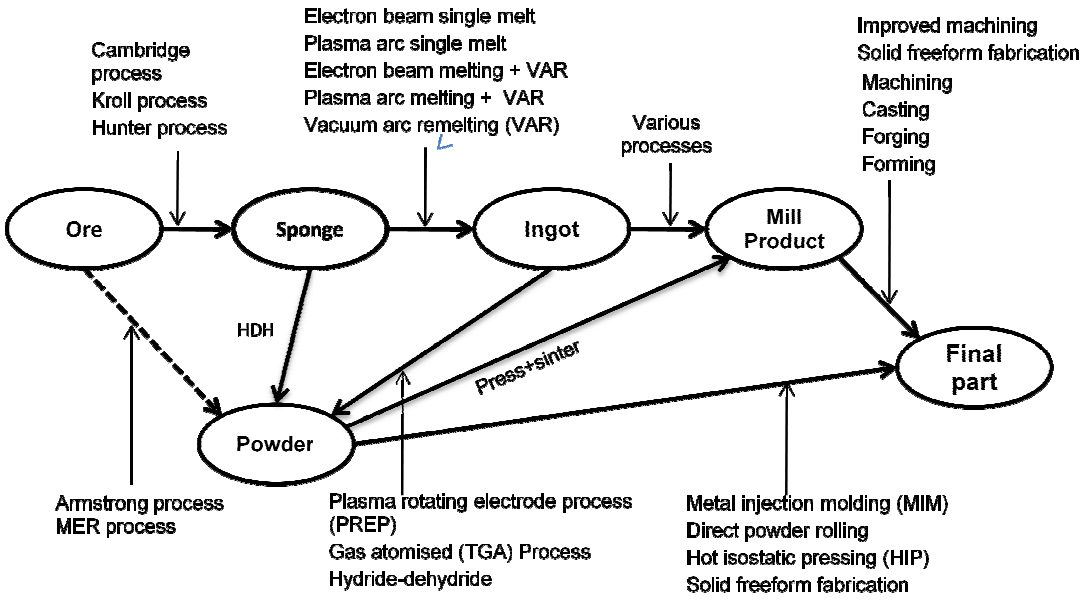

Figure 7 Emerging technologies of titanium part production, (adapted from Seong and Goldsmith, 2009)

The HDH, Armstrong and MER processes do not only reduce cost but also cut the energy use, requiring less capital and in most cases using continuous production to reduce the amount of labour needed. Many of the steps used for ingot production (VAR, EBM or PAM) are also eliminated.

Titanium alloys are often subjected to post compaction treatments after sintering (e.g. for Ti-6Al- 4V, broken-up structure (BUS) heat treatment) to improve the tensile and fatigue strength, and also to increase the uniformity of the microstructure. However, this further increases the cost of the final product (Donachie, 2000).

The developments of titanium and its alloys have been undergoing research in the area of mechanical alloying, powder injection moulding (PIM), rapid solidification, spray forming and vapour deposition to further lower the cost or enhance the properties (Elyon *et al.,* 1998; Froes *et al.,* 2004; Lutjering and James, 2003).

2.2.5 SINTERING KINETICS OF PM TITANIUM

Sintering of powders that have been consolidated (green parts) is performed at temperatures below the melting point of the metal. Sintering provides a means of fusing the molecules of the powders together to achieve more dense parts. Titanium is typically sintered between 1200-1400ºC, which is about 72-84 % (K) of its melting point, 1668ºC.

Titanium is usually sintered in a vacuum atmosphere because of its reactivity with gaseous substances at a temperature higher than 400° C, most especially with oxygen (Hooven III *et al.*, 1993) which can deteriorate the properties of PM titanium obtained. High vacuum ($>10^{-6}$ torr) is achieved by the use of a diffusion pump system in addition to a mechanical pump. This helps in removing gases trapped in the structure and increases the rate of sintering; in this case, a near full density product is obtained.

The factors that usually affect the final properties of the sintered products arise from powder types and sizes, compaction pressures, and sintering atmosphere, temperature, and time.

In the study conducted by Panigrahi *et al.* (2005), it was observed that the sintered density increases steadily with an increasing sintering temperature for parts starting with the same initial green density. A relative sintered density of 85% was achieved after sintering of green parts of about 68% relative density at 1250°C. Relative density is the density relative to the theoretically full density which for pure titanium is 4.51 g/cm^3.

In another study by Panigrahi *et al.* (2005), on the factors that affect dimensional change during sintering, the authors found that adjustments in compacting pressure, sintering temperature, and sintering time can cause noticeable change.

The effect of sintering temperature can be observed on the shrinkage (axial, radial and anisotropy) pattern on the compact. Larger dimensional changes (shrinkage) occur as the sintering temperature increases (Panigrahi *et al*., 2005).

Dabhade *et al.* (2007) investigated the sintering of die compacted micron-sized (12 μm mean particle size) and nano-sized CP titanium powder (40 nm mean particle size). Attrition milling was used to produce the nano-sized powder from the micron-sized powder. Constant heating rate sintering experiments, heating at 10°C/min up to 1250°C, were conducted in vacuum. The linear shrinkages of the two powders were studied in order to determine the dominant sintering mechanism (diffusional path) during the sintering of titanium. The sintering onset temperature for CP titanium was found to be 606°C. The nano-sized powder showed lower grain boundary and volume diffusion activation energy than the micron-sized powder. The dominant sintering mechanisms were found to be a mixture of volume and grain boundary diffusion.

Robertson and Schaffer (2009) examined the effect of the particle sizes and compaction pressures of both commercially pure titanium and Ti-6Al-4V on both green and sintered densities, as shown in Figure 8. They compacted samples between 200 – 800 MPa and sintered them at 1200°C for 2hrs in vacuum. Results showed that a slight increase in the green density results from increasing the mean particle size. They compared sieved HDH and gas atomised powders from different suppliers. Better results were obtained after further sieving the powder to specific particle size ranges. The powders with lower oxygen content had a higher green density than the ones with higher oxygen content. The apparent density was higher for gas atomised powder which was attributed to the particle shape or internal porosity of the powder. Higher apparent density plus better packed particles usually lead to slightly higher green density. The green density obtained increased with increase in compaction pressure.

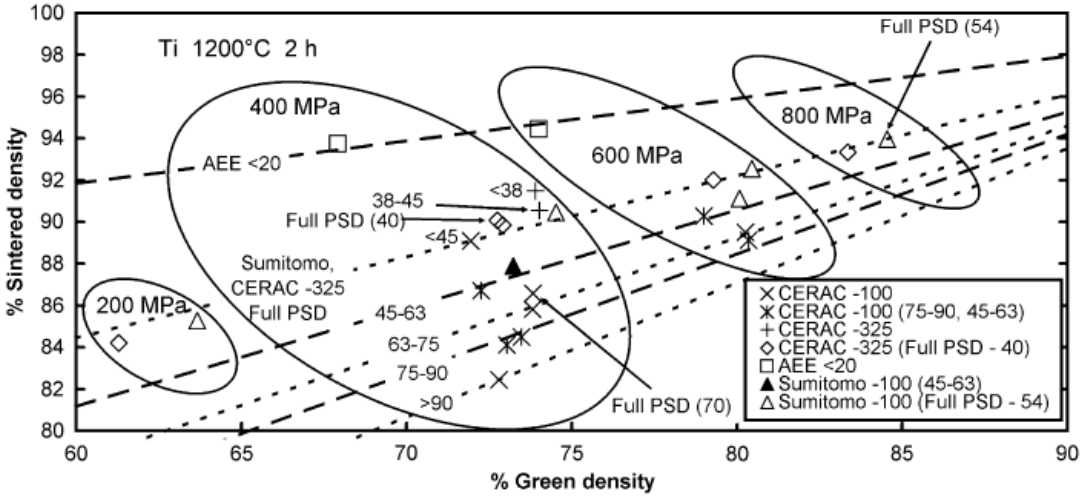

Figure 8 Green and sintered density of CP titanium powder between compaction pressures of 200 - 800 MPa (Robertson and Shaffer, 2009)

For sintered density, reduced mean particle size generally gives rise to an increasing sintered density (Panigrahi *et al*., 2005). This is due to the sintering rate being inversely proportional to the curvature of the particle (German, 2005). However, particle shape can also have a significant influence on sintering. For instance, irregularly shaped powder particles compact well, delivering a higher green density than spherical powders of the same mean size. Therefore when sintered, they deliver a higher sintered density. However, if a spherical powder is compacted to the same green density, its potential to sinter is higher than that of an irregularly shape particle. This again is due to the curvature of the particle. Oxides present on the surface of the powder can also affect the rate of sintering. The effect of oxides is more pronounced at lower temperatures compare to higher temperatures (Robertson and Shaffer, 2009).

Increase in green density reduces dimensional changes during sintering. A lower green density leads to a greater change in density during sintering, but not necessarily a higher sintered density. Problems of poor powder flow rate, variations in apparent density can lead to variations in the part to part sintering dimensions.

Sintering temperature, time and atmosphere also affect the dimensional changes; sintering temperature is usually the sensitive process parameter. A change in sintering temperature as little as 15°C can result in a shift in dimensional change (Panigrahi *et al.*, 2005).

2.2.6 TOOLING DESIGN

Tooling design is an integral part of fabrication processes in powder metallurgy. Tooling enables the powder metallurgist to be able to form powders into the required shapes by the application of pressure during the die compaction process. In manufacturing, where mass production of parts is involved, thousands of parts can be produced with a consistent dimensional accuracy. Basically there are several shapes that can be formed using the various methods of powder consolidation processes. The tooling requirements for these processes differ slightly from each other most.

Most die compacted PM parts are in sizes which range between 80 mm^2- 16 000 mm^2 and are 1-150 mm long (Cubberly and Bakerjian, 1989). Shapes that are more appropriate for die compaction have uniform dimensions in the pressing direction, typically square, rectangular, simple cylindrical and some multilevel variations of these shapes (with contours as a plane at right angles to the pressing direction).

Materials used for die compaction tooling are typically made from hard and wear resistant steels, and cemented carbides (Klar and Prasan, 2007). These tools can

be used to manufacture up to 1 million parts (this is dependent on the powder material used and, the part shape).

For the tooling material selection, mechanical properties and the length of service of the materials are of importance. The tooling material requirements are high toughness, high strength and, resistance to thermal softening at elevated temperature (German, 2005). All these qualities can, however, be attained by proper heat treatment of steels. The tooling is first machined close to the final finishing dimensions, heat treated and finally grinding and lapping is carried out on the moving interfaces between the respective tooling parts to ensure high precision.

Tool steels are typically hardened by heat treatment followed by air quenching. Air is preferable for tool steels because of the tendency of distortions of the tooling when quenched in water. The hardeneability of each steel differs from each other and the heat treatment process is specific to each steel. Tooling made from steel usually has a surface roughness of 0.2 μm and hardness of at least 30 HRC (Klar and Prasan, 2007).

Tooling must be designed to produce an oversized part in order to accommodate large shrinkage during sintering (Cubberly and Bakerjian, 1989). Different powders behave differently during sintering, so this behaviour must be determined before the tooling is designed. Shrinkage is usually anisotropic (differing in the radial and axial directions to compaction), so this must also be taken into account.

When designing tooling for PM parts, it is important to consider the following points:

- Powders do not flow or pack well into corners or small grooves. The uniform distribution of powder in the die is important in creating a uniform density in the compact. The shape of the part must be designed to avoid sharp corners, thin walls or narrow splines. Sufficient length should be provided for thin walled or high aspect ratio parts. Therefore, corners and edges are preferably provided with 45° chamfers or large radii.
- During compaction, pressure perpendicular to the pressing direction causes the compact to stick in the die due to friction with the die wall. The tooling must be designed with features, such as tapers on diameters, to aid ejection from the die after compaction. Ejection forces can cause cracking and delamination of the compact. Parts that have flanges are sometimes given flange taper that is approximately 0.8% of the flange thickness to aid part ejection.
- Because of the difficulties in the uniform distribution of powders in the die, large, rapid changes in the height should be avoided. Design should accommodate the fewest possible changes in the sections.
- Tooling design must be as simple as possible and strong enough to manufacture high volumes of identical parts. The part shape should permit strong and durable design of tooling.

Some of these limitations can be overcome by using complex, multilevel tooling. However, this drives the costs of compaction up and can make the process uneconomical.

The compaction procedure is divided into three stages: filling, compaction, and ejection. Typical tooling consists of a die with a die cavity, forming the negative of the shape to be compacted; an upper and lower punch that fit into the die cavity and are used to apply the uniaxial pressure to compact the powder; and, if the part has a through-hole in the axial direction, a core rod that fits inside the punches. During filling, the lower punch inserted into the die cavity from the underside and remains a fixed position. The powder is poured into the die cavity, filling it from the upper surface of the lower punch. During compaction, the top punch is inserted into the top of die cavity so that when pressure is applied to the top and bottom punches simultaneously, the powder in the die cavity is then compacted between the two punches. For a floating die assembly, the die is kept in position by the friction of the powder with die wall and moves down with the upper punch, creating a more uniform density gradient in the green part (see Figure 6 for double action compaction).

During ejection, either the lower punch is raised, ejecting the compact from of the die, or the die is pushed down to eject the compact.

An important parameter for tooling design is the compressibility ratio (CR). The compressible ratio is the ratio of green density, ρ_g to the apparent density, ρ_{app} at a specified compaction pressure. Considering that the apparent density relates to the fill position and green density to the compaction position, and noting that the mass and cross-sectional area remain constant from filling to compaction, this relationship can be extended to relate the fill height, h_{fill}, (height of powder in die cavity before compaction) to the green height, h_g, (height of compact after compaction) as shown in equation (1).

$$CR = \frac{\rho_g}{\rho_{app}} = \frac{h_{fill}}{h_g} \quad (1)$$

The total height of the die is usually designed to be between 10 -15 % longer than the maximum fill height to allow for stable insertion of the punches in the die before compaction. The die wall thickness must be sufficient to withstand the circumferential and radial forces exerted during compaction. The lower entrance of the die cavity is preferably chamfered at an angle of 45º for easy entry of the lower punch, likewise the lower punch for core rod entry.

The total lengths of the upper and lower punches must long enough to compact the sample while allowing a minimum clearance between the foot of the lower punch and the bottom surface of the die over all the stages of compaction. The

core rod must be longer than the lower punch with sufficient lapped surfaces for easy removal before ejection.

2.3 TITANIUM MACHINING

Machinability is the ability of a material to be machined, or the ease or difficulty for metal removal. The machinability of a material is termed 'good' if, during machining, the cutting tool has a long life and low tool wear, low cutting forces are experienced, continuous chips form and are easily removed, and an acceptable surface finish is achieved (Kikuchi *et al.,* 2003). Titanium has been characterised as difficult to cut material and has poor machinability (Machado and Wallbank, 1990, Rahman *et al.,* 2006).

2.3.1 IMPROVEMENTS IN TITANIUM MACHINABILITY

Machining of wrought titanium has been studied extensively in the past. Machado and Wallbank (1990), Ezugwu and Wang (1997), Yang and Liu (1999), and Rahman *et al.* (2003) have all reviewed technologies and difficulties associated with titanium machining.

Titanium alloys are described as the next most difficult materials to cut after nickel alloys (Lutjering and James, 2003). This is largely due to the low thermal conductivity and low modulus of elasticity of the material, high cutting stresses during machining, and high chemical reactivity of the workpiece with the cutting tool. All these factors result in high tool vibration, high cutting temperature and short tool life (Capus, 2005; Machado and Wallbank, 1990).

The two major factors described by these authors are the high temperature concentration in a small area at the tool tip promoting tool diffusion wear and the segmented chip formation with adiabatic shear band due to thermal-mechanical instability, both factors that limit the machinability of titanium.

Recent research in wrought titanium machining concentrates on studying the effect of the machining process on fatigue life (Jones and Elyon, 1999; Yang *et al.,* 2002), understanding the adiabatic shear band formation (Sheikh-Ahmad and Balley, 1997; Chivpuri, 2002; Molinari *et al.,* 2002; Baker, 2003), investigating cryogenic machining (Hong *et al.,* 2001), high-speed machining (Gente and Hoffmeister, 2001; Norihiko, 2002), and wear of new tool materials (Balkrishna, 2002).

Different grades of titanium (commercially pure and various alloys) do not have identical machining characteristics, unlike the aluminium and steels that usually have identical characteristics for their alloys. The low thermal conductivity of titanium slows down the dissipation of heat from the workpiece; this makes cooling important for titanium machining. The use of the appropriate coolant,

sharp and correct cutting tools, rigid machine set-ups, heavy feeds and slower feeds ensure a general good tool life and work quality (ASM Metals Handbook, 1985). The milling of titanium is usually a more difficult operation compared to turning, whereby both CP titanium and titanium alloys can be cut with little difficulty. In the cutter mills, part of the chip tends to adhere to the teeth of the cutter during the revolution of the cutting tool. There is no cutting taking place at this instance. During the next contact of the cutting tool with the workpiece, the chip is knocked off, thus that tooth becomes damaged.

The use of a sharp cutting tool is recommended for machining titanium because a dull tool builds up heat quickly, which can cause seizing and galling leading to a premature tool failure (ASM handbook, 1985; Grzesik *et al.*, 2005).

Improvement in machining can be affected by the right combination of cutting tools, cutting conditions and machine tools that provide high speed machining. These factors work to improve the surface integrity, surface finish and cost of machining.

2.3.2 CUTTING SPEED

The cutting speed for machining wrought titanium until recently was generally low, in the range 18 to 30 m/min (Chandler, 1998) with a chip load of 0.05 to 0.25 mm (Barnett-Ritcey, 2004). Recently, there has been improvement with higher cutting speeds attainable (Sandvik Coromant, 2008; Kuttolamadom, 2010).. Most of the improvements focused on cooling strategies and enhanced cutting tool materials in order to machine titanium at higher cutting speeds.

For turning operations, the general recommendations by Sandvik coromant (2008) for use of uncoated carbide cutting tools for both roughing and finishing cuts are, cutting speeds of 30-60 m/min for feed rate of 0.3-0.4 mm/rev and depth of cut up to 10 mm, cutting speeds of 80-120 m/min for feed rate of 0.1-0.3 mm/rev and depth of cut of 0.25-1 mm respectively.

The cutting conditions applied for machining titanium limits the use of high cutting speeds and thus lowers productivity. The effect of increasing the cutting speed is generally detrimental to tool wear for machining titanium. The cutting speed has the highest influence on the cutting tool life (Ezugwu and`Wang, 1997). For dry machining, low cutting speeds are usually employed, but with the use of a better cutting tool material and cutting fluids, the cutting speeds for machining titanium have greatly increased. Recent research has been focused on the high speed machining of titanium alloys for better productivity (Kitagawa *et al.*, 1997; Barnett-Ritcey, 2004; Ginting and Nouari, 2009; Daymi *et al.*, 2009).

In studies conducted by Abele and Frohlich (2008) and Daymi *et al.* (2009) on the effect of cutting speed on cutting forces at speeds between 100 - 600 m/min (extreme tool life experimentation), it was observed that the cutting force decreases with an increase in cutting speed. The chips formed at a cutting speed of

100 m/min and above show saw-type serrated or shear localised chips while below this speed there is a flow chip with a non-oscillatory material flow (Daymi *et al*., 2009). The non-oscillatory material flow of the chip indicates a better tool life than the saw-type serrated chip. The segmentations of the chips at higher cutting speed results from the ductility and the high heat flow into the chip (Daymi *et al*., 2009).

2.3.3 EFFECTS OF COOLANT

Cutting fluids assist in lubrication, cooling and chip flow during machining. They are divided into three categories: neat cutting oils, water-soluble fluids, and gases. The water-soluble fluids are more commonly used for machining at high cutting speeds and low cutting tool pressure while the neat cutting oils are utilised for higher tool cutting pressures.

The use of coolant during machining of titanium alloys has proved to significantly improve its machinability. The objective of the application of coolant is to reduce the cutting temperature generated at the chip-tool and workpiece-tool interface, minimise friction, lowering the cutting forces, improve the chip formation and increase the cutting tool life (Ezugwu, 2004).

The type of cutting fluid used for machining titanium alloys is very important. The application of coolants as concentrates, emulsions, in spray cooling, or as solutions in mineral oil, or of mineral oil or synthetic coolants causes more wear than when dry face milling of titanium. With both HSS and carbide tools, water-based fluids are more efficient than oils (Ezugwu and Wang, 1997).

Flood cooling is the most common cooling method used for machining titanium alloys. This method is most effective when machining at relatively low cutting speeds where low cutting temperatures are generated. This method is still not satisfactory for high speed cutting because of the coolant's tendency to vapourise at the high cutting temperatures generated at high speed cutting conditions (Ezugwu, 2004). Flood cooling applied at 60 m/min, 120 m/min and 150 m/min with coolant flow rate of 4.9 l/min reportedly resulted in tool lifes of 18 min 48 s, 4 min 56 s and 56 s, respectively (Hong *et al*., 2001). With high pressure cooling, titanium has been machined at cutting speeds as high as 250 m/min (Ezugwu, 2005). Because of the setbacks associated with the flood cooling methods, high pressure cooling (coolant supplies of over 200 bars is applied in some cases) and minimum quantity lubrication methods have been developed to enhance the machining of titanium alloys at high cutting speeds (Ezugwu, 2004). From the study conducted by Ezugwu (2005) 150% increase in tool life was observed when Ti-6Al-4V was subjected to face milling at a conventional coolant flow pressure of 30 MPa using cemented carbide tools.

Cryogenic machining is a novel cooling techniques recently been used for the machining of titanium alloys. Cryogenic machining is based on the use of gases

as a coolant during machining. Liquid nitrogen is commonly used as a coolant applied to the cutting tool rake and flank (Hong *et al*., 2001; Ezugwu, 2004). The main reason for the application of this state-of-the-art cooling technique to titanium machining is to reduce the high temperature at the chip-tool interface. In addition, the environmental issues surrounding the use of conventional cutting fluids prompted the use of cryogenic cooling (Hong *et al.*, 2001). During a study of cryogenic cooling, the maximum temperature generated at the cutting interface was much lower at 829°C compared to the temperature of 1153°C during dry machining (Ezugwu, 2004). Different techniques of applying cryogenic coolant have been explored, including indirect cooling, pre-cooling, flooding, enclosed bath and, recently, the application of two nozzle cooling at both the flank and rake of the tool (Hong *et al.*, 2001).

Of the cryogenic cooling techniques studied, most methods have not been very effective except for flood cooling, however, this technique involves a lot of liquid waste of nitrogen. Furthermore, the coolant can get to areas where it is not required and can cause pre-cooling of the workpiece material. The cryogenic cooling approach is characterised for its economy; however, practically, it is still difficult to replace conventional cooling techniques. Accelerated tool failure while cutting titanium alloys is inevitable since temperatures reaches 1000°C easily. Even with cryogenic cooling, titanium alloys maintain their toughness and ductility, but experience a rapid increase in the hardness as temperature decreases (Hong *et al*., 2001). The effect of the liquid nitrogen as coolant on the cutting edge surface of the material improves the hardness of the tool, thus increasing tool life. Sun *et al.* (2009) showed that the hardness of the material increases under cryogenic temperatures.

An innovative cryogenic cooling approach was evaluated by Hong *et al.* (2001) to minimise the nitrogen coolant waste. The fluid was only applied to the tip of the cutting tool, at the heat generating interface (cutting fluid flow rate proportional to the heat generated), thus preventing distortion from extreme heating or cooling. There was an introduction of micro nozzle in between the tool face and chip breaker as an economiser and convenient tooling design. They compared this new technique with flood cooling at speeds of 90 - 150 m/min. Results showed the tool life when the two nozzles were used for general flood cooling with optimised chip breaker; a tool life of 4 minutes 56 seconds was achieved at a cutting speed of 150 m/min compared to 56 seconds when conventional emulsion was applied as coolant.

2.3.4 CUTTING TOOL GEOMETRY

For end milling, the most commonly used tool geometry is a round insert with a cutting rake angle of -6°, axial angle of -6° and radial rake angle of -2°. This is a common cutting tool employed in machining turbine blades (Ginting and Nouari, 2009).

For finishing operations, a positive cutting tool angle and small nose radius is recommended (Smith, 1998). The small tool nose radius is required to prevent vibration problems but fretting behaviour is very common with the use of a small tool nose radius especially along shorter cutting length.

In a study on tool parameters such as the rake angle, helix angle, back rake angle and the back clearance angle on the tool life when machining titanium, the side clearance angle was observed as the most influential (Ten Haaf *et al.*, 2008).

2.3.5 CUTTING TOOL MATERIAL

Titanium usually reacts with the cutting tool material and chips weld to the substrate as they slide down the rake face of the insert, tearing out the carbide particles in carbide tools. The cutting tools usually have a short tool life (Ibrahim *et al.,* 2009). Several cutting tool materials have been developed for machining titanium to improve its machinability. These tools include coated carbides, uncoated carbides, ceramics and diamond tools.

Materials commonly used for machining titanium are uncoated tungsten carbide and high speed steel (HSS). For continuous cutting operations, tungsten carbide is regarded as the best tool, whereas HSS tools are recommended for interrupted cutting. HSS tools cannot withstand high cutting temperatures.

For turning and face milling operations, straight WC-Co cutting tools (C-2 grades) performed best during machining of engines and aero-frames, and are recommended for dry machining of titanium (Grzesik *et al*., 2005; Ginting *et al*., 2009). During drilling of Ti-6Al-4V, carbides tools, H13A (S15-S25) grade inserts are recommended (Grzesik *et al.,* 2005). Diamond and cubic boron nitride (CBN) tools are sometimes used for turning of Ti-6Al-4V but straight cemented carbide tools are more suitable (Che Haron and Jawaid, 2005). Ceramics and CBN/polycrystalline cubic boron nitride (PCBN) tools are not suitable for machining of titanium alloys due to excessive wear rates and because they react with titanium (Nabham, 2001; Machado and Wallbank, 1990). Using CBN tools for machining titanium resulted into low performance with increased notch wear with an increasing CBN content (Ezugwu *et al.,* 2005).

Different opinions exist on the use of surface coatings. Ginting and Nouari (2009) claimed that some of the coatings are removed early in the cutting process and thus lose their effectiveness. The coatings used for their experiments on carbide tools peeled off usually after the first pass of the cutting (the coating layer is completely removed when the tool reaches its initial flank wear at the end of the first cut). Ten Haaf *et al.* (2008) studied the effect of coatings on the tool life of the carbide cutting tool when milling Ti-6Al-4V alloys. The coatings investigated were CrN, TiAlN, TiNAl, AlTiN and ZrN. These were compared to an uncoated carbide tool. Their study showed that the uncoated carbide performed better than all the coated carbides in terms of improved cutting tool life. In contrast, Ezugwu

et al. (2004) showed that flank and crater wear can be significantly reduced by coating cemented carbide with TiN and TiCN layers. They theorised that thin coating layer reduces friction between the cutting edge work and work piece materials, yielding a smooth surface finish in titanium alloy with less surface damage.

2.3.6 CUTTING FORCES

The cutting force is at times is used as an indication of the machinability of a metal. A higher cutting force usually indicates a poorer machinability. The schematic diagram in Figure 9 shows the component forces acting on the tip of a single point cutting tool. The orientations of the forces are oriented perpendicular to one another, combined they act on the tool as a resultant force. The component forces acting are the longitudinal feed or axial force, F_x, the radial force, F_y, and the tangential force, F_z. F_x is created by the operating conditions. Tooling selections produce a resistance to the longitudinal feed of the cutting tool. F_x consumes power but is relatively small compared to the component force F_z. There is no power consumption associated with F_y, but its acts as if it is pushing the cutting tool out of the workpiece. F_z is the main power consumption force, associated with the cutting speed. It is also generated by the same conditions as the F_x but in resistance to the rotation of the workpiece.

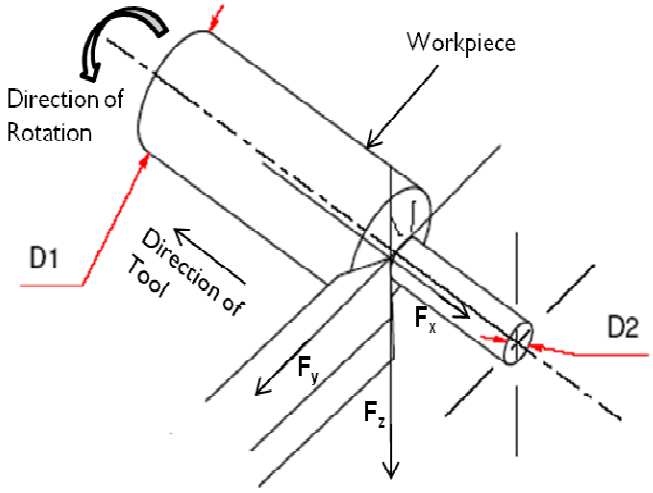

Figure 9 Component forces acting on the single point cutting tool, (adapted from Awopetu *et al.*, 1995)

Ezugwu (2005) compared the cutting forces generated when machining titanium alloys using uncoated carbide and CBN cutting tools at a cutting speed of

150 m/min with the application of a cutting fluid. In the study, it was observed that CBN generated a lower cutting force compared to uncoated carbide.

To understand the effect of cutting force at different feed rates, Sun *et al.* (2009) showed that at lower feeds, as observed in Figure 10, there is severe vibration of the cutting tool, particularly at feeds less than 0.122 mm. They also found that the cutting forces increase with an increase in feed, but only drop with feeds within the 0.122-0.148 mm range. This is mainly due to the tool vibration at lower feeds. The low feed rates and high cutting speed give rise to the force oscillation which is attributed to the small cross-sectional area of material removed and the low modulus of elasticity of titanium. They found the cutting force (F_z) to be 4 times larger than both the feed force (F_x) and the thrust force (F_y) which makes it the dominant force.

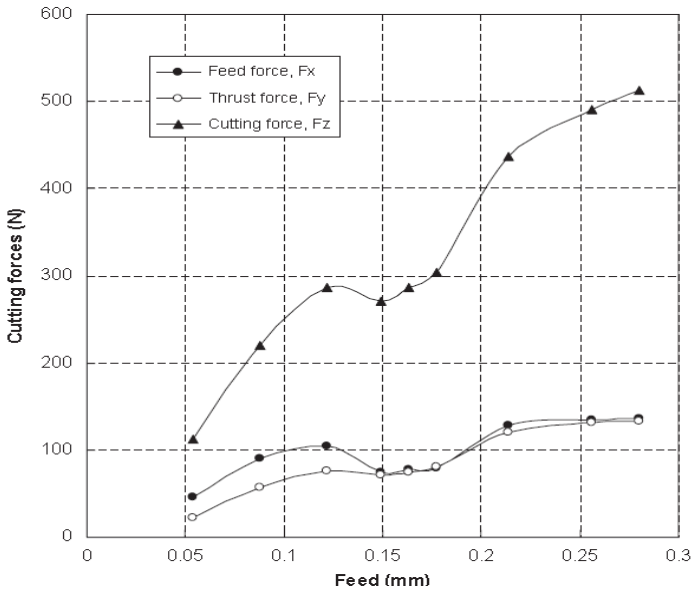

Figure 10 Effect of feed rate on component cutting forces (Sun *et al.*, 2009)

Furthermore, they found the cutting force variation increased from initial speed up to cutting speed of 21 m/min as a result of strain hardening and started to reduce considerably between speeds of 21 m/min and 57 m/min as a result in the increase in temperature causing thermal softening. The cutting force increased slightly from 57 to 75 m/min (both increase in the force is this is due to the strain hardening characteristics of titanium alloy) and became constant between 75-113 m/min and later decrease gradually beyond this point. The cutting speeds greater than 75 m/min induced lower amplitude of variation of the cyclic force which increased the cutting temperature.

2.3.7 SURFACE INTEGRITY

The surface integrity is based on many conditions, including surface roughness, microstructure, residual stress, plastic deformation of machined surface, surface defects and surface hardness. Surfaces are easily damaged during machining operations (Ginting and Nouari, 2009).

The machined surface integrity of titanium is affected by its difficulty in machining and the high temperature generated during machining (Ginting and Nouari, 2009; Ibrahim *et al*., 2009).

The surface defects associated with the machining of titanium alloys are the deformation of feed marks, re-deposition of the molten chip on the machined surface, microchip or debris deposited onto the machined surface, and tearing of the surface (Ginting and Nouari, 2009; Ibrahim *et al.*, 2009). According to Ibrahim *et al*. (2009), the major surface damage to Ti-6Al-4V using a coated cemented carbide tool is the re-deposition of the chip onto the machined surface and the deformation of the feed marks. Microchip defects do not occur when machining at low cutting speeds compared to machining at high cutting speeds. This is due to the high heat generation at high speeds. Feed marks are as a result of plastic flow of the material on the machined surface while the cutting operation is carried out; this results in high residual stress levels and surface roughness. And finally, the re-deposition of the material on the machined surfaceFeed marks are a common defect observed on all machined surfaces of titanium alloys (Ezugwu, 2007; Ginting and Nouari, 2009; Ibrahim *et al*., 2009). They are produced in a perpendicular direction to the direction of the feed of the cutting tool.

Tearing was observed by Ginting and Nouari (2009) during dry machining of titanium alloy. This phenomenon is as a result of the built up edge. A small part of the cutting tool is peeled off and deposited on the machined surface, producing cracks. This defect is not evident when using coated cemented carbide as cutting tool for machining Ti-6Al-4V alloy. Ibrahim *et al.* (2009) observed that while aggressively cutting titanium alloy, plastic deformation of the sub-surface of the material can occur due to the shearing force action of the tool during finishing operation.

Surface roughness of titanium usually increases with an increase in cutting speed (this usually deteriorate as the tool wear) when machining with CBN tools at a feed rate of 0.05 mm/rev and depth of cut of 0.5 mm with application of coolant. The roughness is minimal when using an uncoated carbide tool (Ezugwu *et al*., 2005).The increase in feed rate increases the surface roughness as well. However, at high cutting speeds and with low feed rates, the surface roughness is low (Ginting and Nouari, 2009). Comparing an uncoated carbide tool and a multilayer chemical vapour deposition (CVD) tool, the CVD coating is found to be ineffective since it produced a rougher surface during dry machining. The rough surface is largely due to the fact that the coating peels off at the first pass of the tool (Ginting and Nouari, 2009).

The surface roughness observed during cutting is found to be better towards the end of the tool life. Bhattacharta (1998) explained that it is caused by the changes in the nose radius which, when worn out, becomes bigger, thus producing a smoother surface. Furthermore, the wear is higher at the clearance face than the flank. In short, at the end of the tool life the surface roughness is better than when the tool is new.

2.3.8 CUTTING TEMPERATURE

The cutting temperature can be used at times as an indicator of the machinability of a material. The cutting temperature can be used at times as an indicator of the machinability of a material. The cutting temperature can be difficult to measure in some instance when the workpiece is small.

About 80% of the heat generated when machining titanium alloys, most especially Ti-6Al-4V, is absorbed in the cutting tool compared to the 50% absorbed when machining steel. This high temperature effect is the principal reason for rapid tool wear during machining of titanium alloys (Ezugwu and Wang, 1997).

In a study by Kikuchi (2009), the cutting temperature of CP titanium was compared to brass and to other titanium alloys cut at various cutting conditions to demonstrate the effect of increase in cutting speed, feed and depth of cut on the cutting temperatures. Figure 11 shows the results from this study. In all cases, the cutting temperatures of titanium alloys are significantly higher than CP titanium.

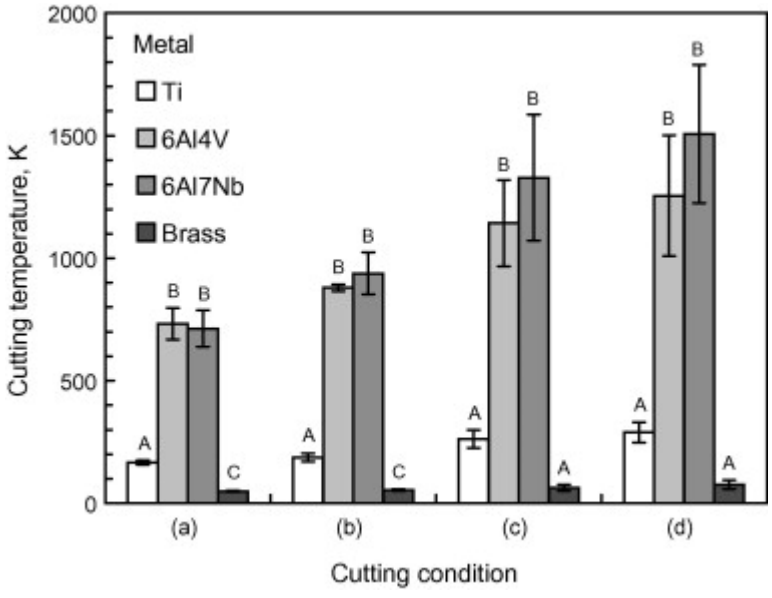

Figure 11 The effect of cutting conditions on the cutting temperature of titanium and selected alloys (Kikuchi, 2009)

The increase in the cutting force and low thermal conductivity of titanium implies a high cutting temperature. The tool life and surface finish of the workpiece is affected by the high cutting temperature which can lead to low accuracy of the cut due to the thermal expansion of the cutting tool and the workpiece. Titanium is also notorious for a very high chemical reactivity at elevated temperature, which also adds to the problem. There is also a significant increase in the cutting temperature when the feed and depth of cut or cutting speed is increased (Kikuchi, 2009).

It had been established that the mean cutting tool temperature on the rake face is proportional to $\sqrt[u]{Vf\ (k\rho C)}$, where f is the feed rate, V is cutting speed, u is the specific cutting energy, and k, C and ρ are the thermal conductivity, specific heat and the density of the workpiece, respectively (Kitagawa *et al.*, 1997).

The temperature of the tool face when machining titanium can often reach a value of 1000°C or more, even at a moderate cutting speed. Various types of tool wear can be promoted with these high temperatures such as the adhesive, abrasive and diffusive wear, leading to a poor tool life. When machining titanium alloys, most of the types of tool wear (abrasive, adhesive and diffusive) are as a result of the heat generation while cutting. The generated heat results from friction on the tool–chip interface and shearing on the primary shear plane, which considerably increase the temperature (Hong and Ding, 2001).

For better machinability, a lower cutting temperature is desired.

2.3.9 CHIP FORMATION

Studies into the mechanisms of the chip formation during the machining of titanium and its alloys have been conducted in the past. Machining of titanium usually produces a segmented chip; this can be as a result of the growth of cracks from the chip outer surface or adiabatic shear formation (Sun *et al.*, 2009). The segmented chip formed is as a result of localised shearing in association with the cyclic forces and acoustic emission generated.

Common factors that can affect the chip formation are the feed rate and the cutting speed, which can in turn lead to vibration of the tool.

The feed rate affects the thickness of chips formed during machining. The average chip thickness reported was 0.13 mm at feed rate of 0,122 mm. The chip is thicker at lower feed rates because of the vibration of the tool at low feed rates. The vibration produces chips with thinness that varies, thus making the machined surface rough (Trent, 1991; Sun *et al.*, 2009).

With an increase in feed rate, the length of chips produced increases linearly. Chips of uniform segmentation were observed with feed rate of 0.280 mm.

The effect of speed is shown with a shorter chip length produced at cutting speed of 57 m/min and below, while a longer chip length is produced at speeds of 75 m/min and above (Sun *et al.*, 2009).

Observation of the chip produced during machining shows coexistence of both continuous and segmented chips during one pass. The continuous chip shows a periodic and a-periodic sharp saw-tooth like shape. Chips are much thicker at the continuous part of the chip and thinner at the segmented part of the chip.

The amplitude of the cyclic cutting force becomes more pronounced when there is an increase in the segmented proportion of the chip. With a relative increase in the cutting speed from 16 m/min up to 75 m/min, chip segmentation increased by 10% (Poulachon, 2000; Sun *et al.*, 2009).

2.4 MACHINING OF PM METAL

Different machining operations are carried out to determine the optimal cutting conditions, tools and geometry for PM materials.

The metal removal rate for machining PM materials is very low since the amount of material removed in terms of chips (10-15 vol% maximum) is very small when compared to the production of components using conventional machining of wrought materials (up to 90 vol%). Most of the shapes that require machining of PM materials are undercuts, slots, blind holes, threads and holes that are perpendicular to the pressing direction. These features are typically machined as it is not possible or feasible to produce them using die compaction. Secondary finishing operations are very common for PM materials with approximately 40-50% of the products undergoing secondary finishing operations (Alizadeh, 2008).

PM materials have been described as more difficult cut due to the porosity (Causton and Cimino, 1998) and this can make it very expensive (Salak *et al.*, 2005). Machining is generally described to be poor when compared to wrought material equivalents, as tool life is usually shorter (Alizadeh, 2008). Due to the problems associated with machining of PM materials, it is regarded to be more expensive in practice compared to machining of wrought metal.

The feeds and speeds recommended for PM materials with greater than 92% relative density is similar to those of the wrought metals, while parts with lower density can use adjusted machining conditions to achieve best results (P/M design guide book, 1995). In practice, secondary machining operations performed on PM parts uses conditions (feeds and speeds) of approximately 20- 25% lower than that used for wrought materials similar in composition due to the abrasive nature of the machining process (Smith, 1998).

Some of the recommended cutting conditions for machining PM materials (usually ferrous alloys) are (P/M design guide book, 1995):

- ✓ For turning operations, sharp pointed carbide tools are recommended. Cutting speeds of 48 to 96 m/min and feeds of 0.05 to 0.10 mm are normally used.
- ✓ For milling, cutters of high-speed steel (HSS), cobalt steels and carbide are recommended. Helical cutters with axial rake are preferred so that the chips are sheared on an angle. Speeds recommended are 21.6 m/min for high-speed steels and up to 91.2 m/min for carbide tools. Feeds should be 0.05-0.13 mm per tooth for roughing and 0.03-0.05 mm per tooth for finishing.
- ✓ Drilling of PM parts is usually conducted at speeds lower (about 80-85%) than wrought of the same composition.

No published data is currently available for titanium PM machining, but there is published research on the machinability of sintered stainless steels. Reports on the effect of porosity on machinability of PM stainless steels (SS) showed contradicting results.

In a study done by Abduljabbar (1982) on drilling of sintered SS (relative density 70-98%), it was observed that the machinability increases as the porosity increases as a result of a lower cutting force when drilling a more porous part. In another study, investigating the machinability of a similar material and cutting conditions, the opposite result was observed (Agapiou *et al*., 1989).

The differences in machinability reported can be attributed to the balance between weakening of the material and decreasing the thermal conductivity as porosity increases. The tool life when machining PM parts is highest when the porosity is either too high or too low. At an intermediate density, there is more tool wear compared to the extreme low or high (German, 2005).

The properties of the PM materials, such as the thermal conductivity, fatigue strength and hardness or strength, play an important role in the tool life of the cutting tool, as shown in Table 4. When the density of the material is high, there is elimination of pores, thus its thermal conductivity is high and the fatigue on the tool is low, leading to improvement in the tool life. Conversely, there is a high tool life at a low density because associated low strength of the material means lower cutting forces are needed.

Table 4 The effect of density variations on the properties of PM material

	Low Density	High Density
Thermal conductivity	-	+
Tool Fatigue	+	-
Material hardness/strength	-	+

This thesis looks closely to stainless steel since it is the material that is closer to titanium as a difficult to cut material, though nickel-based alloys are more difficult to cut in comparison to titanium (Rahman *et al.*, 2006). The only major difference with titanium alloys is their reactivity with the cutting tool material.

2.5 FACTORS AFFECTING PM MACHINABILITY

Basically, several factors are responsible for the poor machinability of products from PM materials. This has been widely investigated with stainless steel. Apart from the general characteristics of PM materials that makes them more difficult to machine compared to their wrought metal equivalents, namely porosity, density variations within the compacts, and inhomogeneity of the powder mixture (in alloy production) which leads to inhomogeneity of the microstructure, other factors related to processing of PM compacts are, however, more influential on the difficulty and also improvement of the machinability (Salak *et al*., 2006; Robert-Perron *et al*., 2005, 2007a, 2007b; Alizadeh, 2008).

The effect of the powders and mixtures used, contribute to the final properties of the sintered stainless steel PM product. The powders used are normally sponge, water-atomised and, pre-alloyed powders. The type of powder production process affects the final properties of the PM product.

Alizadeh (2008) compared PM steel, sintered from atomised and sponge iron powder, during turning and drilling operations. He described the machinability of PM steel made from sponge iron powder as better when compared to that made from atomised iron powder during turning operations; while the response is reversed during drilling.

The final material properties are responsible for the machinability characteristics of the PM compacts. Factors such as the contents of the mixture (alloying elements, lubricants, base powder), can cause the heterogeneity of the microstructure of the PM material after it had been sintered and thus influence the machinability.

During compaction, compaction pressures, the method of lubrication, and method of carrying out the compaction influence the green density distribution in the compact. This in turn affects the final as-sintered density distribution and so the machinability. Porosity is the main deteriorating factor when machining PM compacts.

Sintering conditions, such as atmosphere, sintering temperature, time of sintering, gas flow rate, and cooling rate can also affect the final properties and machinability of the compacts. Sintering atmosphere for most PM materials also affect it dimensional tolerances and microhardness. The effects of variations in the microhardness of the sintered product usually affect the machinability of the PM product, due to variations in the wear rate of the cutting tool. The hardness is normally higher in the direction perpendicular to the pressing direction, and this is

the area that is mostly subjected to machining. The hardness is as a result of the surface being fully exposed to the flowing atmosphere during sintering

Different alloying elements have been investigated for stainless steel (Salak *et al.*, 2006; Alizadeh, 2008); both authors concluded that differences in the machinability between PM and wrought steel relate to the alloying elements.

2.6 IMPROVEMENTS OF PM MACHINABILITY

Several attempts have been proposed for a cost effective and easier approach to machining of PM materials. The methods are explained as follows:

- ✓ Green machining (machining of compacts before sintering): this implies that the PM compact is machined in its green state. At this stage, the hard phases and strong bonds that are associated with sintered products have not yet been formed. This method generates less heat during machining, resulting in less tool wear and longer tool replacement time because of the low cutting forces and temperatures within the cutting zone. This is, however, associated with a lower green strength that leads to a poor surface finish. Chipped edges and broken parts are inevitable when PM parts are machined in their green state (German, 1994; Capus, 2004). These adverse effects can be improved by binder technologies to improve their green strength (Cimino and Luk, 1995; St-Laurent and Chagnon, 1997) and warm compaction. Warm compaction entails die compaction of a preheated powder at temperatures ranging between 90 – 150°C (Benner and Beiss, 2000; Ramstedt, 2001; Capus, 2004; Robert-Perron *et al*., 2005, 2007a). The green strength obtained is doubled compared to cold compaction (Andersson and Benner, 2001). These PM products have to be sintered after machining to obtain the needed mechanical properties.

  Polymeric binder/lubricant systems: PM steel machinability has been inproved using the binders and machining additives such as MnS, MoS_2, but they decrease the toughness and fatigue resistance of the sintered compacts (Robert-Perron *et al.*, 2007b). Machining additives are advantageous for enhancing the machinability of PM parts, especially when applied to PM steels. The advantages include promoting the chip factor, preventing welding of the chip to the tool and preventing a built up edge. They act as a machining lubricant, leading to a decrease in the cutting forces and temperatures in the cutting zones by reducing the chip friction. They also improve the machined surface finish (Alizadeh, 2008) and help in separating the chips from the workpiece and enhancing the cutting tool edge lubrication (Robert-Perron *et al.*, 2007a). While MnS particles in the microstructure act as machining lubricants and increase the tool life and surface finish, they also act as a stress raisers by aiding shearing of the workpiece materials. Common machining aids are S, MnS (low or high purity or coated), MoS_2, BN, $MgSiO_3$, MnX, PbS, Pb, Se, Bi, Te, BN, CaF_2, and some “new” agent or “KSX” containing

complex calcium oxide. The various additives each have their own advantages and disadvantages over each other. MnS is commonly used (Alizadet, 2008) because of its low cost and capability of increasing the tool life at higher feed (Capus, 2004).

For the improvements in wrought forms of CP Ti and Ti-6Al-4V machinabilty, there have been some machining additives developed to aid the machinability of titanium alloys. The new alloys developed were the free-machining pure titanium (DT2F) and free machining Ti-6Al-4V (DAT5F, DAT52F). The additives included in both CP Ti and Ti-6Al-4V are sulphur and rare earth metals that produce globular sulphide inclusions but in varying combinations. The machinability of the new alloys with the additives was significantly improved (Kikuchi *et al.*, 2003).

- ✓ Post-sintering treatments: Impregnation with materials such as linseed oil, bees wax, varnish, sodium silicates, have the capability of improving the tool life up to 5 times (Graham, 1998).

- ✓ Infiltration: Infiltration of porous PM materials using metallic fillers is another good method for improving machinability. The most common and effective method is copper infiltration. Copper seals the pores within the sintered compact and also enhances the PM strength of ferrous alloys (Graham, 1998).

- ✓ Cryogenic machining: This involves injection of liquid nitrogen to the rake face of cutting tool insert while machining, but the nitrogen jet is prevented from having direct contact with the workpiece so that the workpiece does not freeze. The liquid nitrogen has a low boiling point (-196 °C), the nitrogen in contact with the tool vapourises to a non-toxic, inert gas. It is cost effective and safe. (Chilli factor prolongs cutting tool life in sinter-hard working, 2008)

The use of machining additives, copper infiltration and impregnation are difficult to remove and contaminate the PM product (Tremblay *et al*., 2002; ASM Metals handbook, 1985).

METHODOLOGY

3.0 EXPERIMENTAL PROCEDURE

For the purposes of this study, face turning machining is the method chosen to evaluate the machinability of PM titanium. Facing methods are a common test method applied in testing the machinability of sintered powder metals steels (Salak *et al.*, 2006). This test method can be easily applied to smaller diameter test pieces, making it particularly suitable to PM where parts are usually small (< 200 mm largest dimension). This method offers cost effective means for testing PM material machinability.

Other advantages are that it can predict modern production more accurately by simulating a short series of mixed cutting cycles and operations. Interrupted cutting, which involves a number of short cutting and non-cutting cycles, is more predominant in the modern production process (Salak *et al*., 2006).

3.1 DESIGN OF TEST SPECIMEN SHAPE

The machining test specimen shape chosen was a stepped cylindrical bushing, as shown in Figure 12. The bushing was compacted from CP titanium powder. The green shape was designed with an outer diameter of 36 mm that steps up to 42 mm after 10 mm length. It has an inner diameter of 20 mm and an overall length of 25 mm. The green compact shrinks during sintering. The level of shrinkage was calculated according to the powder behaviour which was determined as specified in section 3.3. The first section of the bushing (green outer diameter 36 mm) was designed to fit into the chunk of the CNC lathe (Leadwell T7, Fanuc controller) that was used for the machining test. This allowed for it to be held in easily and ensured that there was rigidity of the workpiece during machining. The test specimen was designed for the larger diameter section to be machined.

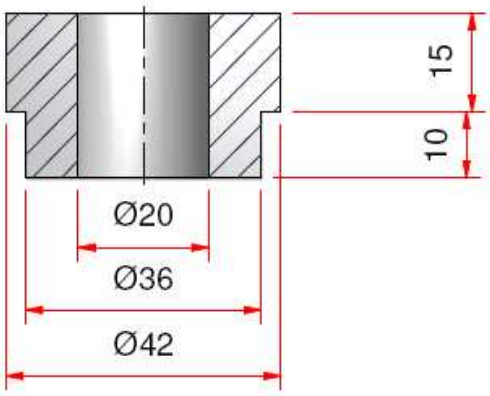

Figure 12 Green part specifications in mm

3.2 POWDER CHARACTERISATION

The metal powder used to compact the test specimens was -200 mesh, 99.5% purity titanium sponge fines (supplier: Alfa Aesar, Germany). A laser diffraction particle size analyzer (Micromeritics Saturn Digisizer 5200 V1.0 S/N 216 was used to determine the particle size distribution of the powder. A small sample of titanium was suspended in isopropyl alcohol and sonicated for 60 sec at a flow rate of 12.0 l/m and intensity of 60% before it was passed through the particle size analyser. Three tests were carried out with an obscuration rate of 15.4% for accuracy purpose.

Scanning electron microscopy (Leo® 1430VP) was used to observe the particle shape. A small sample of titanium was spread on a polymer tape before being carefully mounted on the SEM rotating holder for observation.

The apparent density and flow rate was measured using a Hall flowmeter, in accordance to ASTM standard B212-99 and B213-03, respectively.

3.3 POWDER COMPRESSIBILITY AND SINTERING

Before the machined samples were produced, the compressibility of the powder was determined by compacting right cylinders, 10 mm in diameter and 10 mm high. This test was performed according to ASTM standard B331-95 with an adjusted shape as given above.

The powder was pressed at pressures ranging from 350 - 600 MPa using a manual hydraulic press (CARVER 12 ton Model C) shown in Figure 14. Die wall lubricant was used during compaction. This limits contamination of the powder later during sintering, while still aiding compaction/ejection and protecting the tooling from wear due to friction. A mixture of 100 g zinc stearate in methyl alcohol was used for the die wall lubricant. The mixed lubricant was applied to the walls of the die and the mating surfaces of the upper and lower steel punches, excess lubricant was drained away and the solution adhering to the walls was allowed to dry. This takes a few minutes leaving a thin layer of lubricant on the die wall.

Three samples were compacted at each compaction pressure. The powder samples were weighed using a scale to accuracy level of 0.01 grams with the mass being adjusted at each pressure to achieve a height of 10 mm to an accuracy of $\pm$ 0.1 mm. The preparation of the samples is shown in Figure 13.

Figure 13 Right cylinder sample preparations before compaction showing the preweighed powder (left), lower punch and die assembly (middle, bottom), die wall lubrication solution (middle, top) and upper punch (right).

The lower punch was inserted into the die cavity, with a spacer inserted between the die and lower punch to position the lower punch so that the required fill height is achieved in the die cavity. The weighed powder samples were poured into the die cavity after assembling the tool set. The outer sides of the die wall were tapped to level the powder in the die cavity before the upper punch was inserted.

The tooling set (lower punch, die, upper punch and spacer) is positioned centrally in the hydraulic press and an initial pressure of 35 MPa was applied. The initial low pressure is released and the spacers are then removed from the lower end of the die. The initial low pressure application is in order to hold the die in place without the support of spacers, due to the friction of the powder with the die wall. Following the removal of the spacer, the final pressure is applied, effectively creating a floating die assembly in order to improve the green density distribution in the compact. The pressure is immediately released after maximum pressure is reached to accurately measure the compressibility of the powder, as suggested by the ASTM standard.

The compacts were deburred with a fine emery paper. The mass of the sample were weighted after deburring. The green density was calculated from the mass and dimensions of each specimen. The green density (at each compaction pressure) was used to determine the compressibility ratio (see section 2.2.6).

Figure 14 Carver® 12-ton hand operated compaction press

The compacts were sintered in a vertical tube furnace, as shown in Figure 15 under of 10^{-4} mbar vacuum at a sintering temperature 1200°C. A heating and cooling rate of 5 °C/min was used. Samples were sintered for 1 hr and 2 hrs. The furnace was flushed with argon before the vacuum was pulled and backfilled with argon after sintering was completed. The compacts were held in fused silica crucibles, suspended in a molybdenum wire basket in the hot zone of the furnace. The sintered density (ρ_s) was measured by Archimedes principle.

Archimedes principle is a phenomenon useful for density measurement. A body immersed in a fluid undergoes an apparent loss in weight equal to the weight of the fluid it displaces. The density of the solid, ρ_s is then determined according to the weight of the specimen in air, A and the difference in its weight when immersed in the liquid *(A-B)* as

$$\rho_s = \frac{A}{A-B} \times \rho_o \qquad (2)$$

where ρ_o is the density of the liquid. The liquid used for the density measurement is distilled water at room temperature.

The shrinkage of the samples in both the axial and radial direction during sintering was recorded as

$$\text{Shrinkage} = \frac{\Delta L}{L_o} \qquad (3)$$

where ΔL is the change in compact length or radius and L_o is the initial length or radius, respectively.

Figure 15 Vertical tube furnace for vacuum sintering

3.4 MACHINING TEST SPECIMEN PREPARATION

3.4.1 TOOLING DESIGN

Tooling was designed to compact the shape of the machining test specimen, shown in Figure 12. The compressibility ratio (CR) was used to calculate the fill height, according to equation (1), for the tooling. The CR of the titanium powder was determined from the powder compressibility study (section 3.3).

The machining test specimen shape is formed by a tooling set comprised of a die, an upper and lower punch, and a core rod. Additionally, spacers are used to position each piece of tooling to ensure accurate compaction and safe ejection of the part.

The tooling is machined oversize on outer diameters of the punches and core rod, and undersize on the inner diameters of the die and punches. Following hardening, the punches were ground and lapped in the die, and the core rod in the punches. The assembly of the tooling in the fill position is shown in Figure 16.

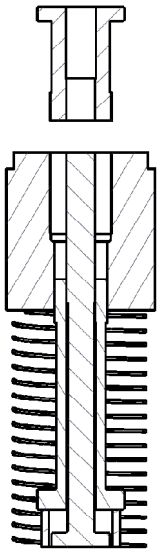

Figure 16 Tooling set-up for powder compaction at fill position

3.4.2. COMPACTION AND SINTERING

The machining test specimen was pressed in a 200 ton hydraulic press (custom-made press, Jerimet (Pty.) Ltd., Atlantis, South Africa) because the force requirement to produce the shape at the specified compaction pressure is high. The machined sample compaction set-up is shown in Figure 17.

The machining test specimens were produced at two compaction pressures, 280 MPa and 480 MPa using zinc stearate as die wall lubrication. The compaction pressures were adopted in order to investigate the effect of increase in porosity in machinability of titanium PM. The samples were sintered using the same sintering conditions used for the compressibility samples (see section 3.3) except that the sintering holding time in this case was 2 hrs.

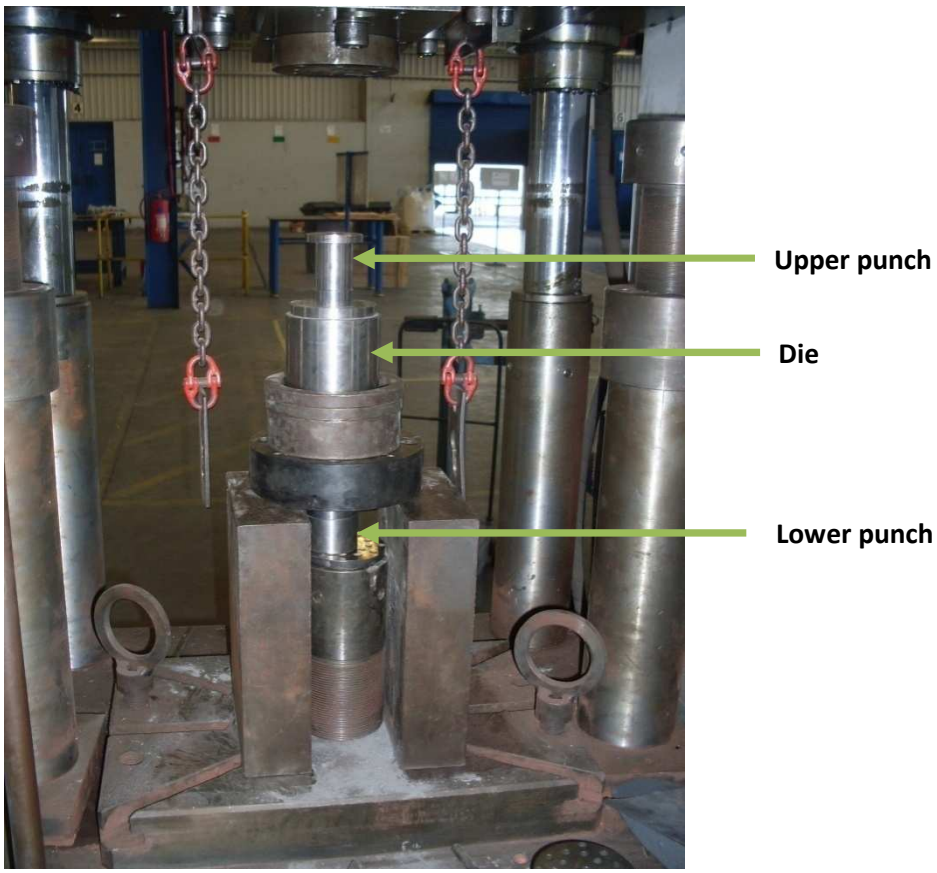

Figure 17 Machined sample compaction set-up

3.5 METALLOGRAPHIC EXAMINATION

The sintered microstructure was observed using typical metallographic techniques for light optical microscopy of PM titanium. The sintered cylinders (samples used for compressibility studies) were cut into two equal halves along their height using a low speed diamond cut-off saw (Buehler Isomet®). The sintered machining test specimens were similarly sectioned, in the same direction as the sintered cylinders, but only small section was cut-off. The speed of the saw was kept low in order to ensure that the line of cutting was straight. The sliced specimens were cold mounted in epoxy.

An automatic grinder/polisher (Struers: LaboPol-1 with LaboForce-3) was used to prepare the specimens for metallographic examination. Initially, the metallographic mounts were ground using 320 grit SiC paper with water until the surface was planar. Then the samples were grounded using 9 µm diamond paste on a grinding disc (Struers: DiaPro on MD Allegro disc,). The samples were rinsed using a jet of water and ultrasonically cleaned in ethanol between each step.

The samples were then polished using a colloidal silica solution (Struers: OPS suspension) mixed with hydrogen peroxide (30 vol.%) in the ratio 9:1. The

solution was dropped on the polishing cloth (Struers: MD NAP) during polishing. The grinder/polisher operates at speed of 250 rpm. A force of 30 N per sample was used during the grinding and 35 N during the polishing steps. At each step of the grinding/polishing, the specimen was viewed to see if the pores were revealed. If the pores appeared to be smeared, the process was repeated again.

3.6 MACHINING SET–UP

A 3-axis CNC lathe was used for the investigation of the machinability of the sintered specimen. The lathe is equipped with a clamping system that is used to fasten the work-piece material very securely to its chuck headstock. The machining set–up is shown in Figure 18.

In order to obtain repeatable results, the machining tests specimens were produced under similar conditions. The machining tests were all conducted dry (no lubrication). Typically, titanium is not machined dry, but the condition allows a worst case scenario benchmark to be established. Furthermore, this allows the tests to be compared with data from literature.

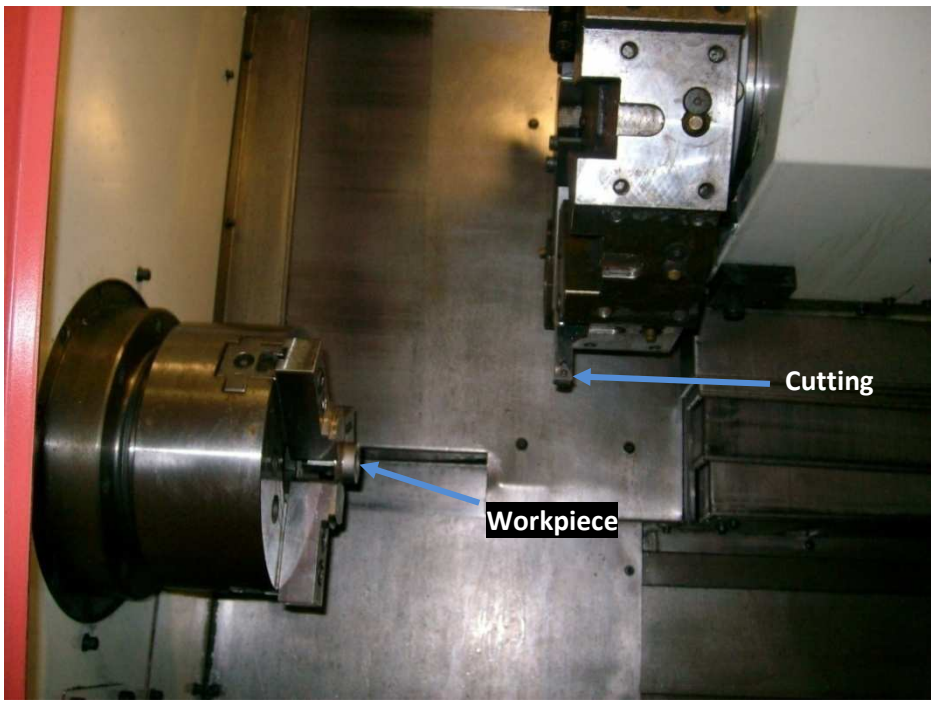

Figure 18 Machining lathe set-up

3.6.1. MACHINING PARAMETERS

A triangular uncoated carbide (K 20 grade, supplier: Sandvik Coromant, ISO tool designation: CNMX H13A with a nose radius of 0.8 mm) cutting tool was used

for all the tests. This is a typical grade for cutting wrought titanium. The tool geometry has rake angle of 0°, end relief angle of 7°, side relief angle of 7° and an approach angle of 90°.

For all the experiments conducted, a new insert was used for each pass at a specific feed rate and cutting speed. In the preliminary experiments, the feed rate as well as the depth of cut was kept constant at 0.15 mm/rev and 0.5 mm, respectively. Table 5 shows the cutting parameters investigated for the samples (A, B, C and D) evaluated. The cutting speed was varied from 60 m/min to 150 m/min.

Table 5 Cutting Parameters for Machining Tests

Sample	Sample Density (g/cm^3)	Cutting Speed (m/min)				Feed Rate (mm/rev)	Axial depth of cut (mm)
A	4.41	60	90	120	150	0.15	0.5
B	4.20	60	90	120	150	0.15	0.5
C	3.82	60				0.15	0.5
D	4.29	60	90			0.15	0.5

For the face turning method, cutting begins from the outer edge of the sample and proceeds to the centre hole, with the workpiece turning at a constant speed as the tool moves from the outside diameter (D_o) to the inside diameter (D_i). Under normal conditions, the cutting speed would then increase from the workpiece center outwards. To avoid variations in cutting speed, the lathe is programmed so that the cutting speed at the centre and the outside edge of the workpiece is constant. This is achieved by varying the speed with which the cutting tool is moved across the workpiece face.

To ensure a constant surface speed for the machined samples, a G-Code was written to machine the samples. The G-code is a numerical control programming language that instructs the machine tool on the type of action to perform. The code positions the tool and controls the cutting operation. The FANUC controller of the lathe uses the code to control the surface speed of the workpiece. Code G-96, given in the appendix, enables a constant surface speed.

The spindle speed, *N*, was calculated using the equation

$$N = \frac{v}{\pi \times D_i} \tag{4}$$

where v is the cutting speed and D_i is the inside diameter.

3.7.2. EVALUATING MACHINABILITY

The tool life is measured as the number of passes of the tool (from D_o to D_i) to reach the tool life criteria, defined as 0.3 mm flank wear for these tests. The tool wear is measured using a high resolution optical microscope (Olympus GX50) at each pass to evaluate the flank wear. This microscopic inspection enabled the determination of the average and maximum flank wear in accordance to ISO 3685 (1993) standard. In determination of the average flank wear of the cutting tool, an average of six different measurements, taken at a magnification of 100x, was calculated. A stop watch (measurement resolution of 1 msec) was used in measuring the time taken for each pass during cutting. For confirmation of the results, the tests were repeated where applicable.

The volume of material removed, *V*, per pass was calculated as

$$V = \pi \left(\frac{D_o^2 - D_i^2}{4} \right) \times t \qquad (5)$$

Where *t* is the change in length of the sample after one pass of the cutting tool. For these experiments, the change in length of the sample after 14 passes of the cutting tool was 1 mm, yielding a value of t = 0.07 mm, used for the calculations.

Taylor's relationship (Taylor, 1962), the relationship between the cutting tool-life, T, and the cutting speed, v, is determined using the face turning test method. This relationship is given as

$$T = Av^k \qquad (6)$$

where A and k are empirical constants, with k depends mainly on the tool material.

In order to view the segmented chip obtained after machining, the chips were cold mounted in epoxy resin on their edge so as to view the cross-sections after polishing the mounted across its length.

The criteria that are used to evaluate the machinability of the sintered titanium sample were the tool life, the difference in microhardness of the sample after sintering and after machining, surface roughness after machining, surface defects acquired during machining and chip formation. The effect of increasing cutting speed and feed, and the effect of different levels of porosity were evaluated using these criteria.

RESULTS AND DISCUSSION

4.1 POWDER CHARACTERISATION

Titanium powder exhibits a variety of particles shapes depending on the method of production as indicated in Table 3. The shapes can be angular (reduction of oxides), spherical (gas atomized), dendritic (electrolytic) and scaly (mechanical milling). This greatly influences the performance of the material during processing and the final PM product. A particle size analyzer using the laser diffraction method was used to determine the particle size distribution and a scanning electron microscopy was used to determine the particle shape of the CP titanium powder used in this research.

Figure 19 shows the particle size distribution of the titanium powder given as a volume frequency versus diameter (largest dimension) plot. Three tests were carried out and all showed a high level of correlation with single peak value. The shape of the distribution is a typical log normal distribution with a mean particle size of 32 µm. 90% of the powder size distribution (D_{90}) falls below the 54 µm size. The D_{10}, D_{50} and D_{90} particles sizes are given in Table 6. These data correlate with the powder supplier specification of -200 mesh, indicating a maximum particle size of 75 µm.

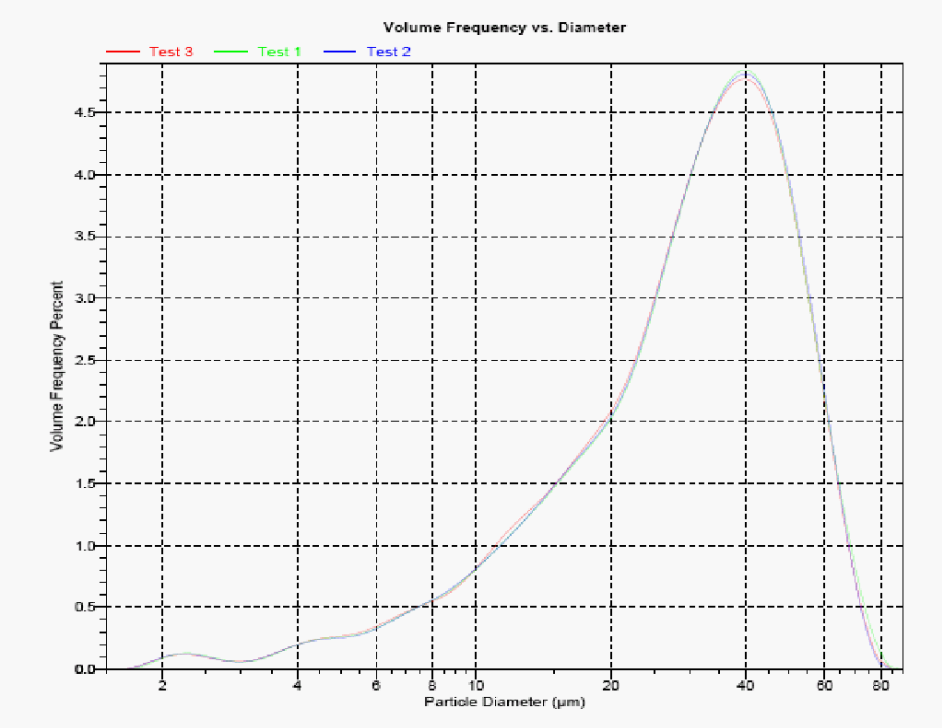

Figure 19 Cumulative percentages of the titanium powder particles

Table 6 Particle size distribution at cumulative finer percentages

D_{10}	11.30 μm
D_{50}	31.82 μm
D_{90}	53.60 μm

SEM images of the powder, shown in Figure 20, show that the particles are angular in shape. This is typical of titanium sponge fine particles, as the sponge is embrittled through hydrogenisation, then crushed to form powder, and then finally dehydrogenised. The image confirms that particles are approximately less than 75 μm in size in their longest dimension.

The apparent density of the powder was measured as 1.07 g/cm^3 by the Hall flowmeter. The powder does not flow freely.

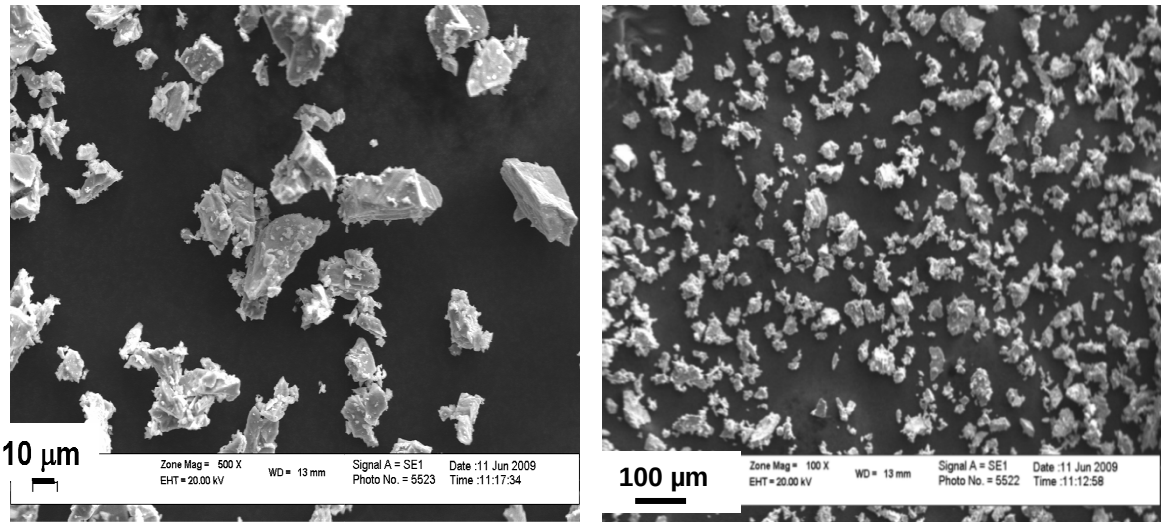

Figure 20 SEM Image of CP titanium sponge fines powder at 500x and 1000x magnification

4.2 COMPRESSIBILITY STUDIES

The compressibility curve, given in Figure 21 showing compaction pressure plotted against green density, is constructed from the data collected from the 10mm diameter cylinders. Each data point is the average green density of three samples compacted at a specific compaction pressure. The curve shows an increase in green density, from 3.05 g/cm^3 (about 68% relative density) at 350 MPa compaction pressure to 3.45 g/cm^3 (about 75% relative density) at 600

MPa. Data from literature shows that similar titanium sponge fines powder compacts at a relative green density of about 78% at 600 MPa (Robertson and Schaffer, 2009). These data translate to compressibility ratios (ratio between the green and apparent density) ranging from 2.99 to 3.17 over the range of compaction pressures measured.

Particle shape can greatly influence the compressibility of the powder, with a log normal particle size distribution yielding improved compressibility as compared to a monosized particle distribution. Irregular shaped particles are usually better suited to compaction than spherical powders, giving better compressibility and green strength (German, 2005).

The relationship between green density and compaction pressure is modelled using the Jones equation (German and Park, 2008).

$$\rho_g = 1 - (1 - \rho_A) exp(B - \theta P) \quad (5)$$

where ρ_g is the relative green density, ρ_A is the relative apparent density, P is compaction pressure (MPa) and θ is the powder compressibility factor (1/MPa). Using the results shown in Figure 21, this model is fit to the data. The results obtained showed a good correlation between the mathematical model and the experimental result. The r-squared value of the fit is 0.997, B was determined as 0.4291 and θ as 0.013.

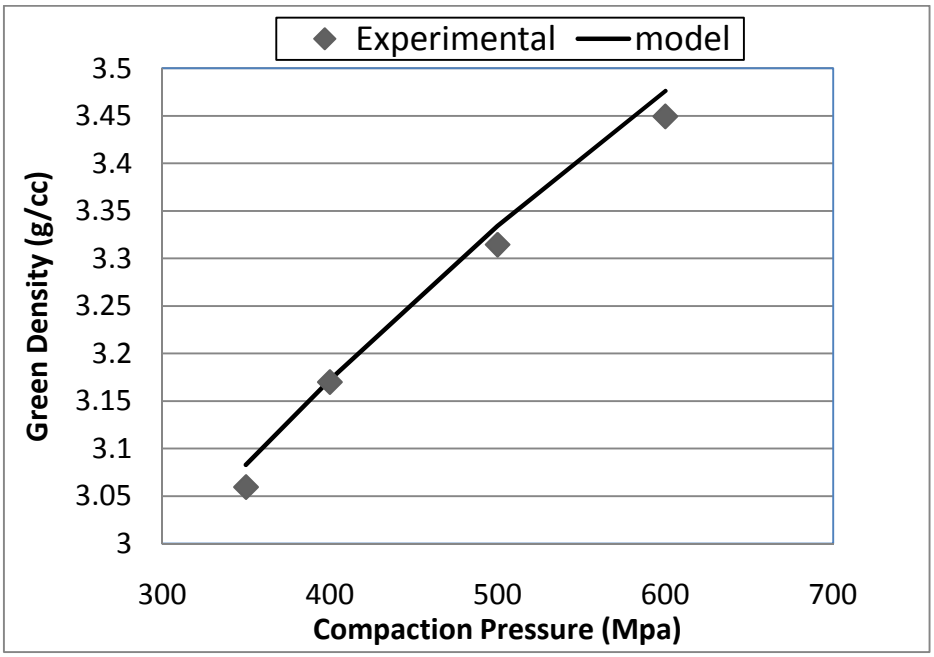

Figure 21 Compressibility of the green titanium compacts

4.3 SINTERING

The samples distorted during sintering, resulting in an hour-glass shape for the final part as shown in Figure 22.

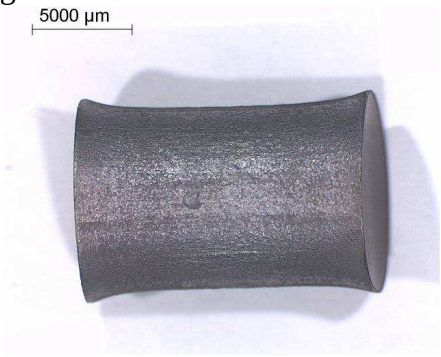

Figure 22 Shape of the sintered titanium compact

The distortion is due to green density gradients in the part that result in differences in shrinkage during sintering. The green density gradients are caused by interparticle and die-wall friction during compaction (German, 2005). Due to the floating die tooling setup during compaction of the samples, the density in the middle of the sample is lower than that at the top or bottom, as per Figure 6. This causes the hour-glass sintered shape seen above.

Figure 23 shows the effect of compaction pressure and sintering time on sintered density. There is a corresponding increase in the sintered density as the green density increases. This is typical of PM material behaviour (German, 2005; Klar and Prasan, 2007; Robertson and Schaffer, 2009).

Increasing sintering time from 1 hr to 2 hrs results in a small increase in densification, as shown in Table 7. The increase in sintered density with increase in sinter time is due to the increased amount of time available for particle bonding and pore shrinkage to take place (Panigrahi *et al.*, 2005).

Although the sintered density of samples compacted at 600 MPa is higher than that of samples compacted at lower compaction pressures, the shrinkage (or densification) during sintering is less. The radial shrinkage of the samples is more at the middle and less at the top and bottom of the samples; at the same time, there is axial shrinkage in the sample (see appendix for sample measurements). The shrinkage in both the axial and radial direction (at all locations) is greater in samples that are compacted at lower pressure. The effect of green density variation in the compacts constitute to variations in the axial and radial shrinkages.

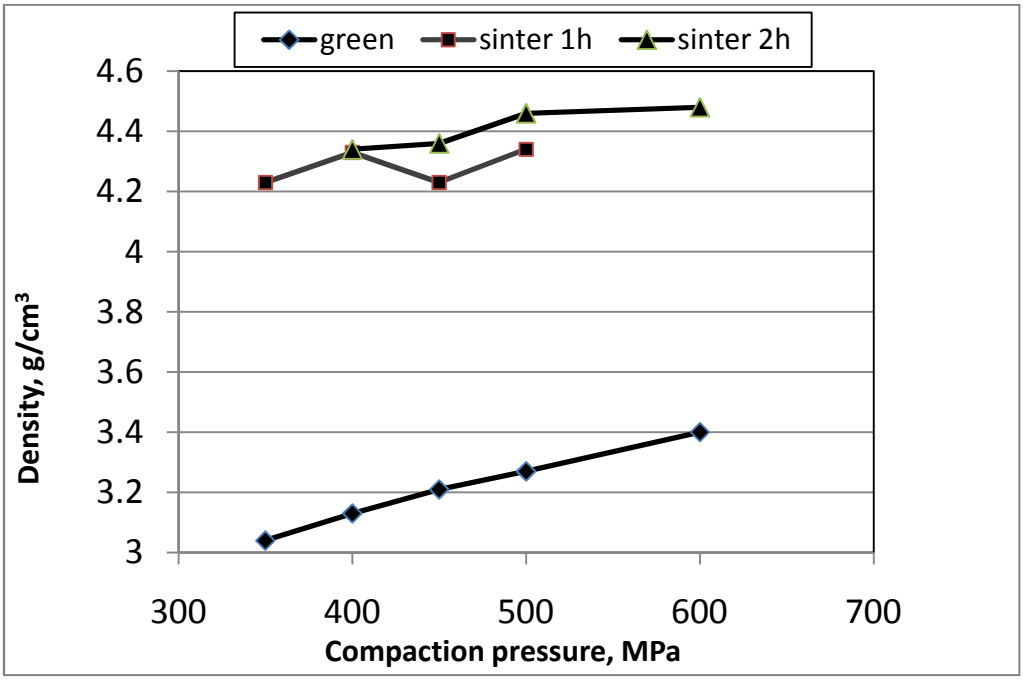

Figure 23 Green and sintered density at different compaction pressures and sintering times

Table 7 Relative sintered density and densification ratio of CP titanium at varying compaction pressures

Compaction pressure (MPa)	Relative Sintered density		Densification ratio	
	Sintering time		Sintering time	
	1 hr	2 hrs	1 hr	2 hrs
400	95%	96%	72%	72%
450	93%	96%	74%	75%
500	96%	98%	74%	75%
600	-	99%	-	76%

The densification can be measured as the ratio of the sintered to green density, as given in Table 7 by the densification ratio (in percent). The reason for less densification (for similar sintering conditions) when starting with a higher green density is due to the particles being more closely packed at higher compaction pressures. This results in more interparticle contacts with smaller pores between the particles. Thus, a higher green density, acquired by compacting at a higher pressure, results in less dimensional change during sintering as less densification is needed to reach a high sintered density.

Figure 24 shows the microstructure of the sintered titanium samples observed under the light optical microscope. Figure 24 (a) and (b) show the sintered (1200°C for 2 hrs) microstructure of samples compacted at 400MPa at magnifications of 100x and 500x, respectively. Figure 24 (c), (d) and (e) show the sintered (again, 1200°C for 2 hrs) microstructure of samples compacted at 600 MPa, also at 100x and 500x magnifications as indicated. The microstructures of the samples compacted at both pressures show that the material is well sintered (bonding between particles is solid and prior particle boundaries are not segregated). Few pores remain for the part compacted at 600 MPa, while more pores are visible for sample compacted at 400 MPa. The effect of higher green density, obtained from higher compaction pressures, can be clearly seen in the percentage of porosity remaining after sintering (compare Figure 24 (a) and (c)).

For both sintered materials, the pores that remain are small and on grain boundaries indicating that the material has reached the final stage of sintering. They are mostly rounded and elongated. The shape of the pores can also be seen more clearly at a higher magnification (Figure 24 (b) and (c)). It is observed that all the sintered microstructures showed porosity gradients from the outer edge of the sample, where there were few pores, to the core where there were more and larger pores. This is illustrated in Figure 24 (c) and (e).

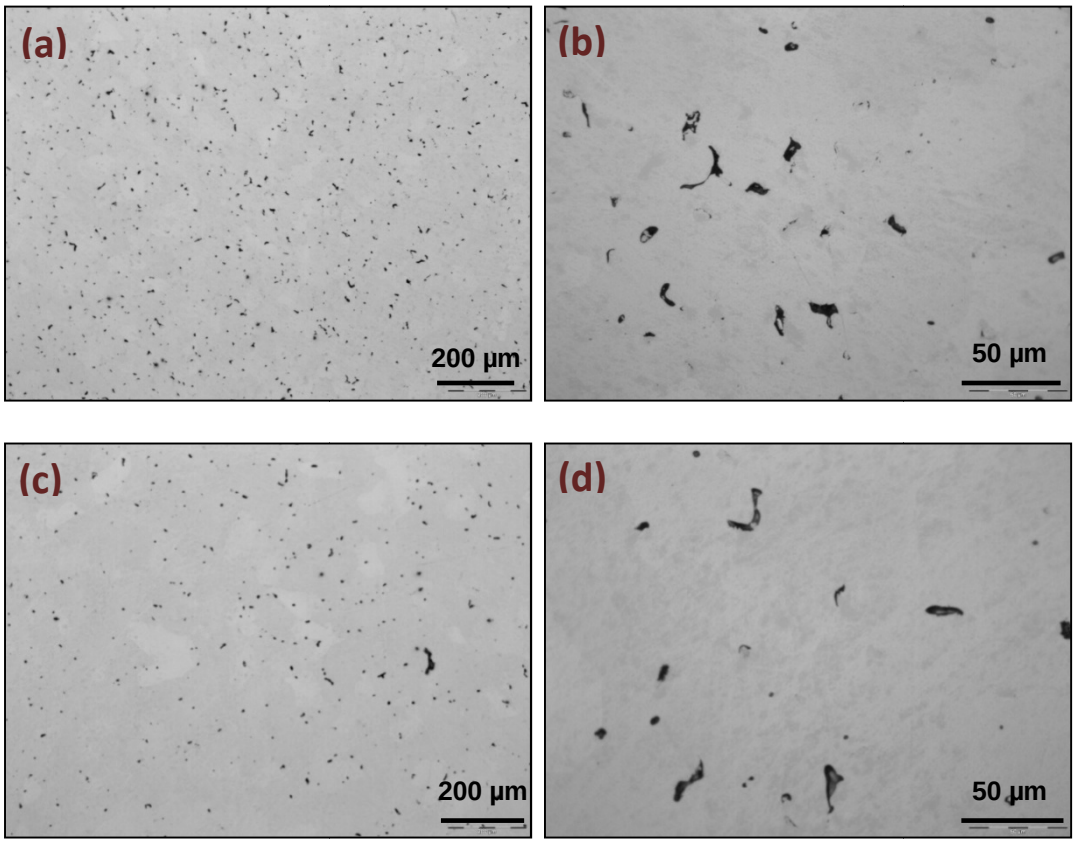

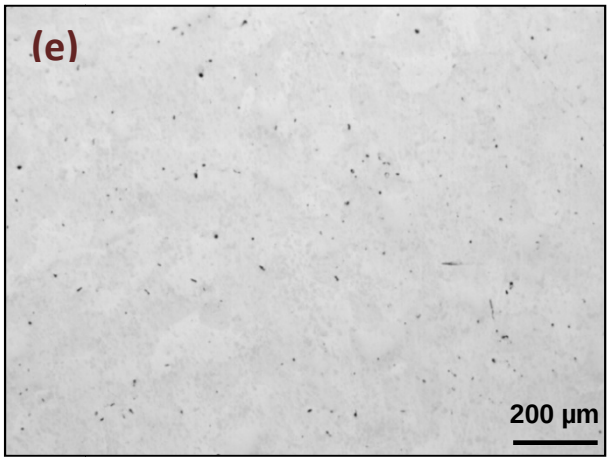

Figure 24 Light optical micrographs of sintered titanium microstructure at different compaction pressures (a) 400 MPa 100x (b) 400 MPa 500x (c) 600 MPa , 100x core of sample (d) 600 MPa, 500x core of sample and (e) 600 MPa, 100x, edge of sample.

4.4 COMPACTION AND SINTERING OF MACHINING TEST SPECIMEN

According to the compressibility results, a compressibility ratio of 3.04 (corresponding to a compaction pressure of 400 MPa) was used to design tooling for the machining test specimens. Two specimens (A and B) were compacted with the originally designed machining test specimen tooling at 400 MPa and 480 MPa, respectively. A further two specimens (C and D) were compacted with the redesigned tooling at 300 MPa and 450 MPa, respectively. The machining test specimens and their relative densities are given in Table 8.

Table 8 Machined specimens at their relative green and sintered densities

Specimen	Compaction pressure (MPa)	Green density (%)	Sintered density (%)	Notes
A	400	68	93	Delamination on ejection and crumbling of sharp corners
B	480	73	96	
C	320	Not measured	85	Reduced delamination
D	450	72	95	

Initial compaction trials using the original tooling setup resulted in the green density being lower (about 68% relative density for sample A) than what was expected from the compressibility study (about 71%). This is most likely due to the increased shape volume. For the compressibility study, 10 mm diameter x 10 mm height cylinders with a volume of 785 mm^2 were compacted compared to the test sample with a volume of 7 713 mm^2. The increased volume results in increased interparticle friction and eventually lower green density. Poor powder flow to sharp corners resulted in areas of very low green density that crumbled after ejection. The poor compaction is also attributed to the size of the powder particles. Typically, die compaction powders range from 45 µm to 150 µm (for iron powders). Here, 90 vol.% of the titanium powder used is mostly less than 54 µm (D_{90}). A smaller particle size implies a higher particle surface area. This translates to increased interparticle friction which lowers the green density.

To counteract these issues, the flow of powder was improved by some tooling design and process changes. In particular, the sharp corner in the die cavity was redesigned with a taper and radius to improve powder flow and lubricant (Zn stearate) was mixed with the powder before compaction to improve interparticle friction during fill and compaction. This removed the need for die-wall lubrication, but the contamination effect of lubricant on the sintered microstructure must be monitored.

A typical solution for improving the powder flow to sharp corners is to introduce a taper (2.5º) coming into the sharp corner area and to add generous radii to the inner corners (R1). These design changes, however, made little improvement to the compacted shape. Other methods for improving the compaction of the samples were to tap the sides of the die to settle the powder in the die before compaction. This method improved the compaction by greatly reducing delamination during ejection. Samples C and D were produced using the redesigned tooling, putting these measures of improving the powder flow in place. Figure 25 shows sample D green part produced.

Figure 25 Green specimen of the sample shape from powder titanium

The green specimens (A, B, C and D), showed an increase in the density when sintered in vacuum. Sample B had the highest sintered density and sample C the lowest. This corresponds to the sample with the highest green density yielding the highest sintered density, similar to the result obtained for the compressibility and sintering study (Sections 4.2 and 4.3). The effect of compaction pressure is clearly seen in the sintered density of all the samples.

The shapes of the sintered samples (C and D) before machining are shown in Figure 26. The outer edge as well as the core of the specimen, as indicated in Figure 27, were observed for variations in porosity. Figure 28 shows the porosity observed at both locations for sample D. The inner edge is observed to be slightly denser than the core of the sample. This correlates to typical green density distributions in compacted parts (see figure 6). A similar density distribution was found at the top and bottom surfaces (higher density) as compared to the middle of the sample (see figure 27 for locations).

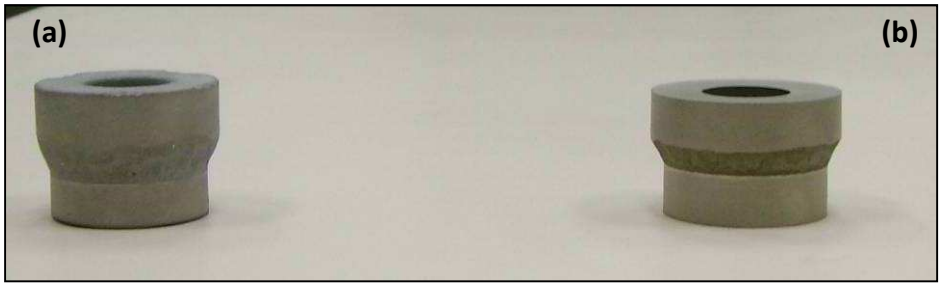

Figure 26 Shapes of samples before machining, (a) sample C, (b) sample D

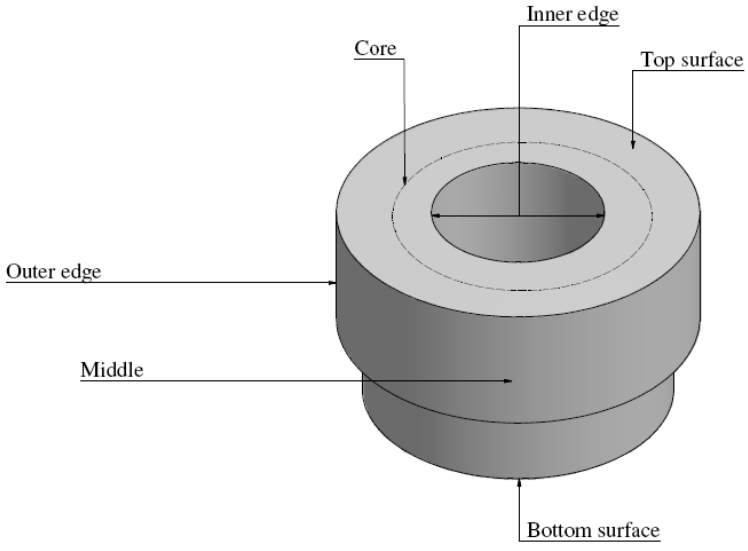

Figure 27 Density distribituions at different points on the machined sample

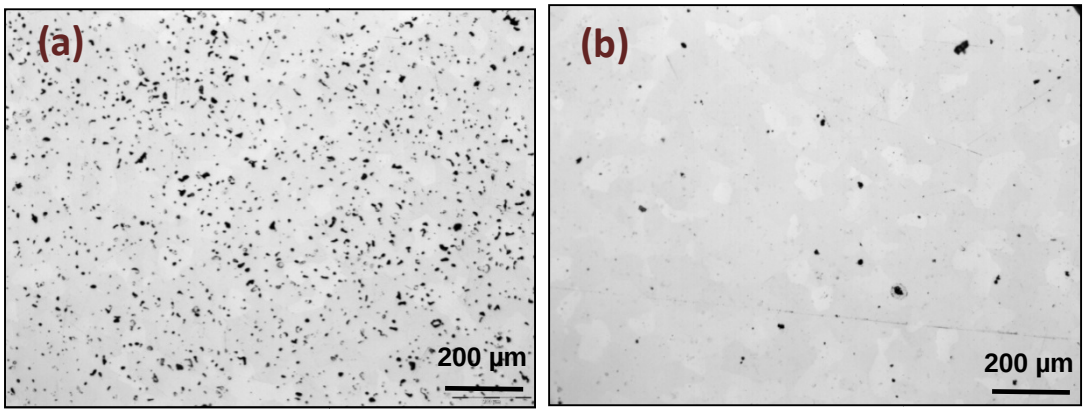

Figure 28 Light optical micrographs of the porosity of sample D observed at the (a) core and (b) inner edge.

4.5 MACHINING TRIAL: PILOT TEST (SAMPLES A and B)

Before the actual machining trials experiments were conducted, a pilot test was performed on similarly sintered CP titanium in order to determine the feasible cutting conditions for the final machining trials. The specimens used were sample A (density 4.41 g/cm^3) and sample B (density 4.20 g/cm^3). The variations in the density of the samples allowed the effect of porosity on the machinability of sintered titanium to be investigated. Similar machining parameters as those used for wrought titanium were used, as specified in Chapter 3.6.1.

The specimens were subjected to dry machining (without the use of lubrication) as a benchmark to evaluate its machinability. The machining procedure simulates interrupted cutting so it was expected that the tool wear may be higher when compared to normal continuous cutting results. Due to the problems associated with the forming process of the part, the lower 10 mm section of the part was machined.

4.5.1 FLANK WEAR

The tool wear at both the flank and crater edges was characterized at specific cutting intervals. However, initially about 0.5 mm of the surface was removed before the test was conducted in order to remove any microstructural contaminants from sintering and to ensure trueness of the workpiece in the head stock.

Four cutting speeds (60, 90, 120 and 150 m/min) were investigated, with four passes machined at the first three speeds and only two passes at the highest speed.

The volume of material removed at the end of the four passes was calculated using equation (5) as 209 mm^3. The tool flank wear was observed under the optical microscope and measured after each pass of the cutting tool across the work piece. The average flank wear experienced while machining the more porous sample (B) at a cutting speed of 60 m/min is plotted against the volume of material removed in Figure 29, with each data point indicating a single pass. This shows the wear progression of the cutting tool under dry cutting conditions.

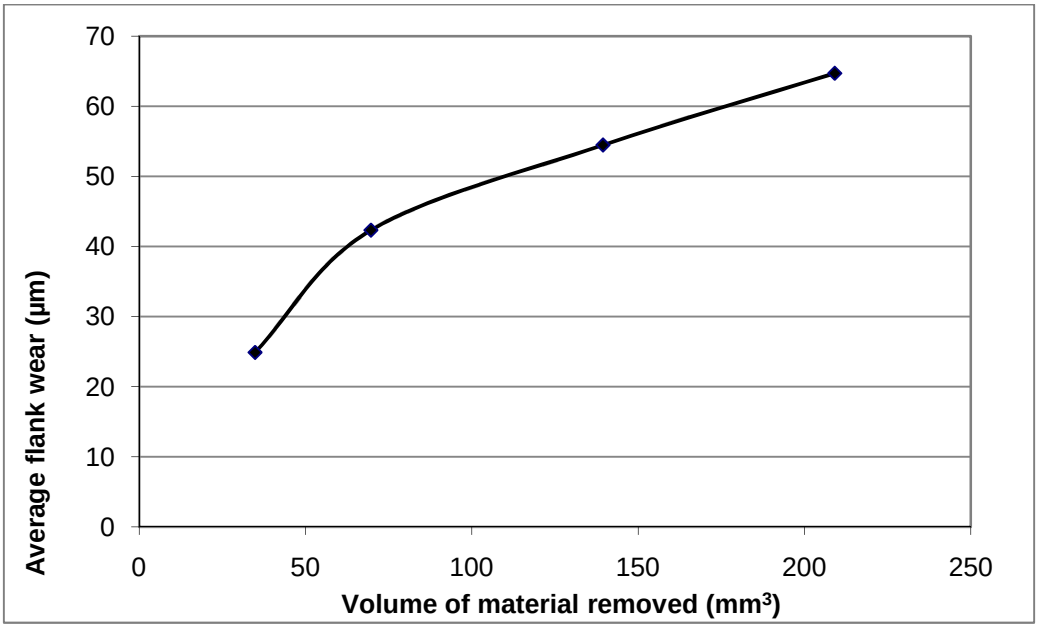

Figure 29 Flank wear growth with material removal rates for sample B (cutting speed 60 m/min)

There is rapid tool wear during the initial two cutting passes, with more uniform tool wear as cutting progresses. The cutting tool experienced predominantly uniform flank wear before tool failure. There is evidence of crater wear of the tool material and heavy adhesion of the chips on the cutting tool in some instances. Tool life of titanium is usually terminated by flank wear or/and tool deformation (Trent, 1991).

The tungsten carbide/cobalt (WC-Co) cutting tool showed a slow rate of tool wear. This is not a surprising result as studies have reported its resistance to diffusion wear and deformation at high temperatures, though the cutting tool material was not compared to others (Trent, 1991; Ezugwu *et al*., 2005). Because of the interrupted cuttings involved in the machining process, it is found that there is chipping associated with the tool wear at some intervals. This was common during the first few cuts and towards the end of the tool life. The high heat generation at the chip-tool interface is responsible for the adhesion (chemical

welding) of the workpiece material to the cutting face of the tool. This is a common phenomenon when machining titanium (Trent, 1991; Hong *et al*., 2001; Ibrahim *et al.,* 2009).

4.5.2 INFLUENCE OF CUTTING SPEED

In general, cutting speed has a pronounced influence on the cutting tool wear while machining titanium alloys. The cutting tool wear in relationship to the cutting speed for the machining tests performed on the less porous sample (A) is shown in Figure 30. The flank wear was measured after four passes at each cutting speed (60, 90 and 120 m/min).

As cutting speed increased, there was rapid deformation at the tool edge, mostly concentrated at the nose radius of the cutting tool. Sparks were observed as the cutting tool connected with the workpiece and during the cutting action. Sparking increased at higher cutting speeds. There was more rapid tool wear at high cutting speeds. After only four passes, the tool flank wear at a cutting speed of 120 m/min had already exceeded the 0.3 mm critical value. This supports the observation that dry cutting conditions for PM titanium are not desirable at high cutting speeds.

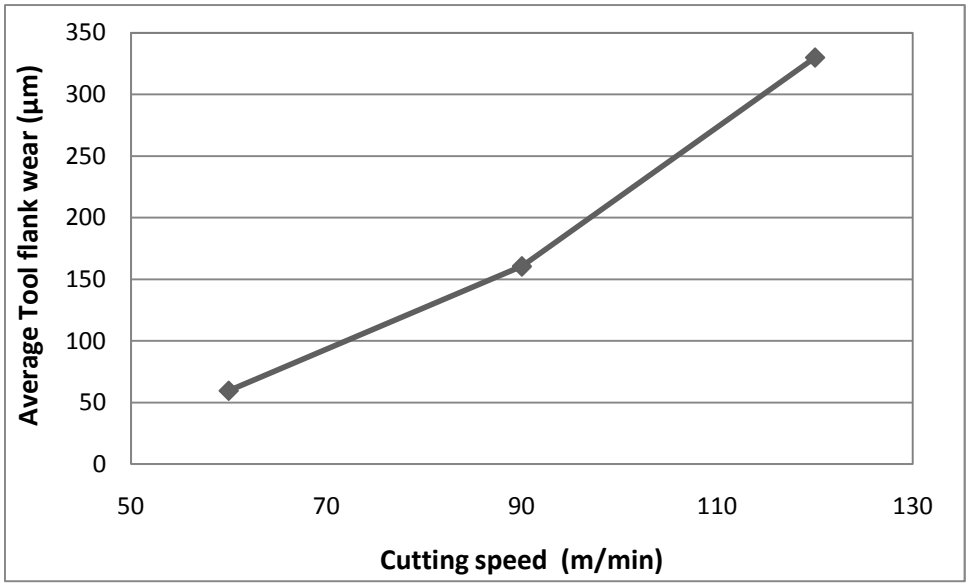

Figure 30 Tool flank wear after four passes at varying cutting speeds (Sample A)

4.5.3 INFLUENCE OF POROSITY

The effect of porosity on the machinability of PM titanium was investigated during the pilot test to determine its relationship to tool wear. The tool wear rate

for the less porous sample (A) during the initial cuts (to remove contamination and obtain a true surface) was higher than the less porous sample (B). After taking four cuts at a cutting speed of 60 m/min, the tool wear rate for the less porous sample (A) was lower than for the more porous sample (B). However, once the cutting speed was increased to 90, 120 and 150 m/min, the tool wear rate for the less porous sample (A) was higher than that for the more porous sample (B) at each of the reported cutting speeds. Note that the tool wear was measured after four passes for 90 and 120 m/min cutting speed, but only after two passes for 150 m/min. In summary, when the cutting speed was increased, tool wear rates for the less porous sample (A) showed more aggressive tool wear compared to more porous sample (B), as shown in Figure 31. This behaviour was not fully understood at first as typically, parts with less porosity should show improved machinability. Another set of machining trials was performed to confirm these results. The tests are reported in Chapter 4.6.

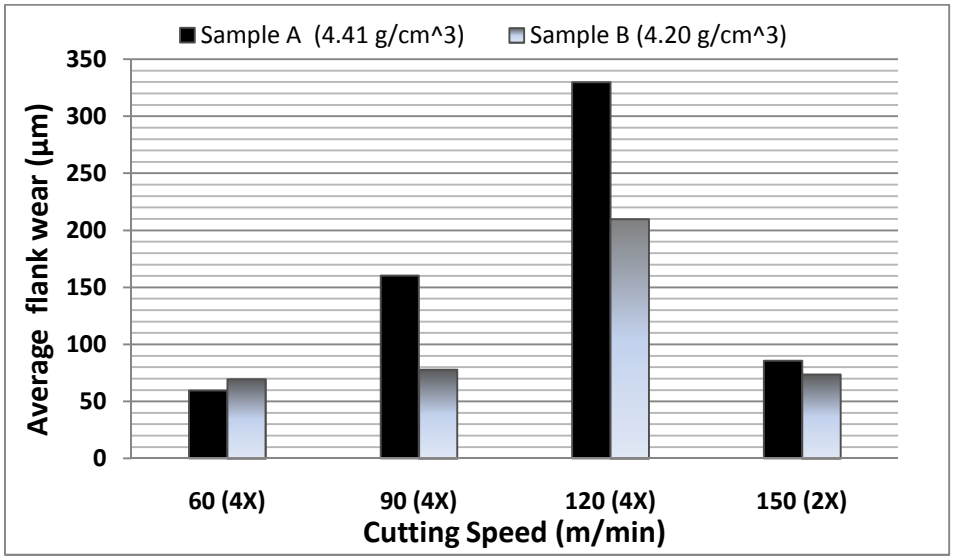

Figure 31 Effect of porosity on tool flank wear on machinability of CP titanium at different cutting speeds

The shape of the cutting tool edge after only four passes at cutting speed of 120 m/min is shown in the Figure 32.There is high adhesion of chips on the rake face of the cutting tool, especially at this high cutting speed, even though the feed rates were low. Figure 32 (b) shows more adverse tool wear when cutting the less porous sample (A) compared to Figure 32 (a) for the more porous sample (B).

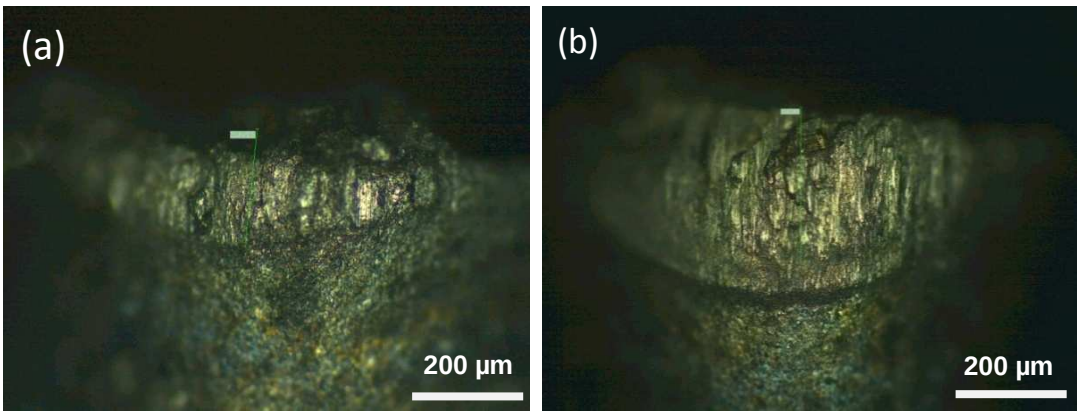

Figure 32 Wear observed on the cutting tool after machining titanium (a) sample B (more porous) (b) sample A (less porous)

For titanium alloy machining, because of the rapid progression of cutting tool wear, it is generally difficult to machine at cutting speeds higher than 60 m/min using an uncoated carbide tool. This limits productivity. This is clearly observed when machining PM titanium. Cutting speed and feed rate are the most important parameters that are usually adjusted when optimizing the machining conditions for titanium. The most deteriorating factor to PM titanium's machinability is cutting speed.

4.6 MACHINABILITY TRIALS: FINAL TESTS (Sample C and D)

The machining specimens (C and D) were machined using similar conditions as used for the pilot test. Before the tests were carried out, about 0.5 mm of the top surface was removed in order to ensure an even surface (trueness), and to remove any form of surface contamination from sintering. (Note, there was no evidence of surface contamination, but this step was taken as a precautionary measure.).

Fourteen passes were taken from each sample at cuttings speeds both of 60 and 90 m/min. About 740 mm^3 material was removed over the fourteen passes, independent of the cutting speed. The cutting tool was examined for wear at the end of two passes over the face of the workpiece. The cutting time (the time taken for one pass of the cutting tool over the workpiece) was recorded as the machining progressed, so as to monitor the time to tool failure. The effect of porosity and cutting speed was evaluated in a similar manner as during the pilot test (Chapter 4.5.2 & 3).

Due to the difficulties encountered when pressing the machining test sample shape, the number of experiments carried out was limited.

4.6.1 FLANK WEAR

For most industrial machining evaluations, flank wear is usually monitored because it affects component accuracy, surface finish and integrity. Using this measure, it is possible to compare the machinability of a material over a range of cutting speeds by assessing the time in minutes it takes to reach a predetermined wear criterion. The average flank wear was used to evaluate the wear rate of the cutting tool during experimentation.

Both samples generated lots of sparks during cutting, similar to the sparks observed in the pilot test. This is as a result of the poor thermal conductivity of the material and the dry cutting condition that was used for the test. Tool wear was focused at the nose and flank of the cutting tool. This form of wear is mostly encountered when machining titanium using an uncoated carbide tool (Ezugwu *et al.*, 2005; Rahman *et al.*, 2006). The wear at the flank of the cutting tool is as a result of dissolution-diffusion and attrition wear, which is common when turning titanium alloys (Ezugwu and Wang, 1997). At the first few passes, there was an initial crater wear on the rake surface, but this gradually disappeared after subsequent cuts in which adhesion of workpiece material to the tool became more dominant. The optical images of the cutting tool wear are shown in Figure 33 for experiments on both sample C and D.

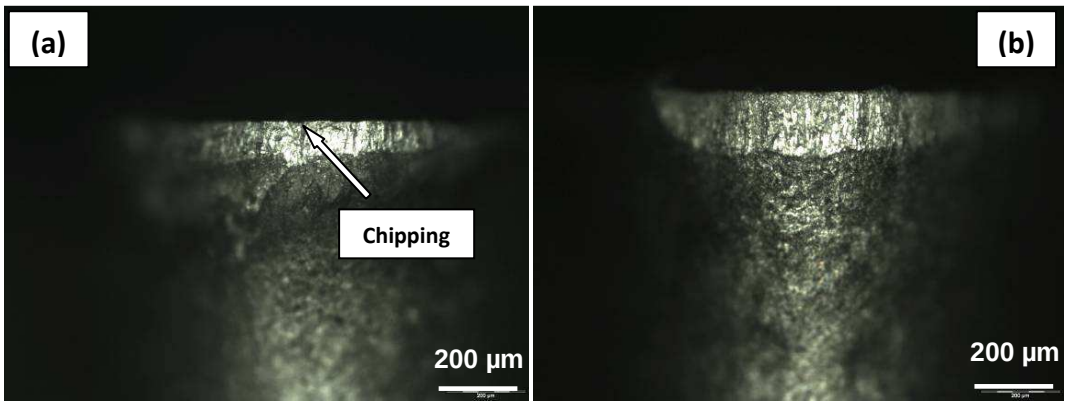

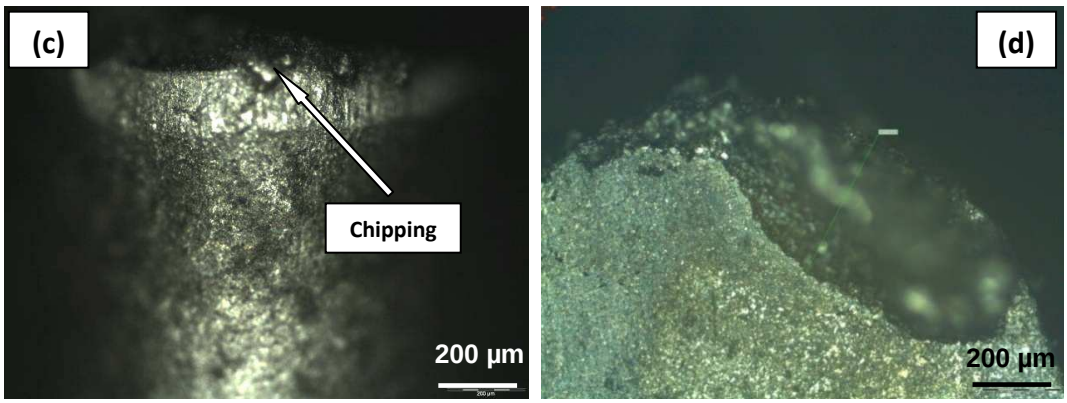

Figure 33 Optical microscope images flank wear of the cutting tool for (a) sample C and (b) sample D, both at a cutting speed of 60 m/min, and (c) flank wear and (d) crater face wear of sample D at a cutting speed of 90 m/min.

4.6.2 INFLUENCE OF CUTTING SPEED

The relationship between the average flank wear and cutting time is shown in Figure 34 for experiments on sample D. For these experiments, face turning was performed over a 60 sec period, with interruptions to measure wear after two passes. Cutting speed shows a significant influence on the cutting tool wear rate during machining titanium alloys. A similar result as that observed during the pilot test was obtained. The machinability is poorer at higher cutting speeds, as shown in the figure; the same level of flank wear was reached at 39 and 57 seconds at cutting speeds of 90 and 60 m/min, respectively. The rapid deformation of the cutting tool edge, coupled with the high heat generated at a high cutting speed, increases the tool wear rate. More sparks were observed at a cutting speed of 90 m/min as compared to 60 m/min. The tool wear rate (the slope of the wear curve) is similar for both cutting speeds.

The images of the cutting tool wear, taken using a light optical microscope at 100x magnification, are shown in Figure 33. In comparing of Figure 33 (b) and (c), there is an increase in the flank wear as the cutting speed increases during machining of Sample D, while there is a noticeable crater wear at the higher cutting speed, as shown in Figure 33 (d). The crater wear is more predominant here. This is expected when machining titanium alloys because the initial cutting is dominated by crater wear but changes to primarily flank wear towards the end of the tool life. At a cutting speed of 90 m/min, the workpiece tends to adhere on the rake face of the tool (this was not as pronounced when cutting at a lower cutting speed). The reason for adhesion is the high temperature in the tool/ chip contact area coupled with the high reactivity of titanium with the cutting tool at elevated temperatures. This mechanism results in crater wear observed (Grzesik *et al.*, 2005).

When machining titanium alloys at higher cutting speeds, it had been reported that the high speed results in rapid chipping of the cutting edge, and plastic deformation or rapid cratering of the cutting edge, leading to the catastrophic failure of the cutting tool. This is due to the temperature generated which tends to be concentrated at the cutting edge closer to the nose of the inserts. Thus, it is recommended the cutting speed used is limited when machining titanium, especially when using an uncoated carbide cutting tool in the dry condition (Che Haron and Jawaid, 2005).

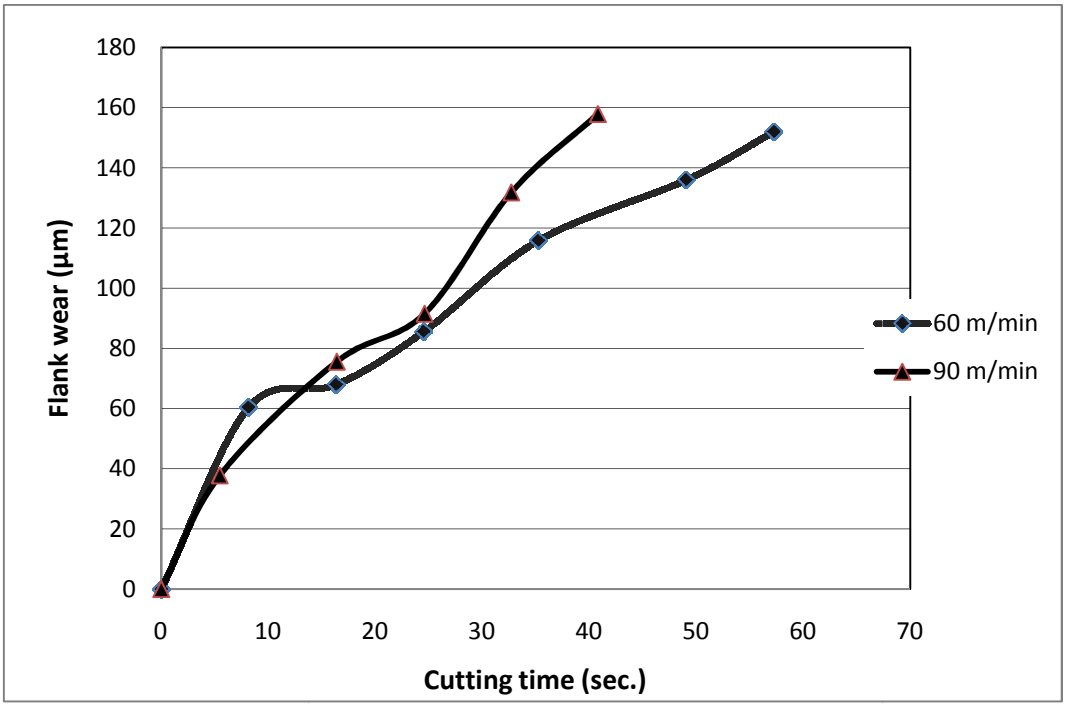

Figure 34 Tool wear curves for machining Sample D at two cuttings speeds (60 m/min and 90 m/min).

4.6.3 INFLUENCE OF POROSITY

The average flank wear with the number of cuts is shown in Figure 35 for both sample C (density 3.82 g/cm^3) and D (density 4.29 g/cm^3). The rate of the flank wear is rapid during the first few cuts; it then becomes fairly constant for a while before becoming more adverse.

Furthermore, tool wear is reduced when cutting the more porous material (sample C) than the denser material (sample D). This confirmed the results obtained from the pilot test (Chapter 4.5.3). The wear rates of both samples were close at the beginning, but diverge with further cutting. Both curves show similar tool wear progression, but with the denser material (sample D) becoming more adverse as cutting progresses.

The average tool flank wear had reached 150 µm in 59 seconds for sample D while, at similar time, it was only 100 µm for sample C, as shown in Figure 36. Again, this confirms that the tool wear is worse for a denser material.

The flank wear rate behaviour is similar to the typical curve for any tool wear, which usually occurs in three stages. The first stage is the primary initial wear stage, characterised by rapid tool wear during the initial cuts. This accelerated wear is due to tool layers that may have been damaged during manufacturing. The next stage is the steady state wear stage, characterised by a linear relationship between tool wear and cutting time; this is the main operating region of the cutting tool. Lastly, the tertiary stage, characterised by accelerated wear, occurs towards the end of the tool life. The accelerated wear is usually caused by high cutting forces, temperatures and severe tool vibrations.

The wear progression curve of both samples (C and D) machined at cutting speed of 60 m/min is shown in Figure 35. A sharp reduction in the tool wear, which occurs at the fourth pass of the cutting tool over the face of the machined samples, is observed. The same phenomenon occurred while machining sample D at cutting speed of 90 m/min, but the drop in the tool wear rate occurred at a much later stage (see Figure 34).

The reduction in the wear progression is due to the porosity gradient in the machining test sample. The middle section is more porous than the top and bottom surfaces of the sample, as indicated in Figure 27. The top surface of the sample is almost fully dense with few pores, while the middle of the sample has quite a number of pores. The denser top surface layer layer experiences a more rapid tool wear rate as compared to the middle of the sample. As material is removed from the top surface of the specimen, the cutting tool is exposed to the more porous middle section of the sample (where there is a drop in the tool wear rate). Progressive tool wear is experienced directly before the tool failure.

Note that the 10 mm section of both samples (C and D) was machined at cutting speed of 60 m/min (see Figure 34, 35 and 36) and the 15 mm section was machined at 90 m/min. Thus the tool passed over a longer cutting length before reaching the centre of the sample for the 15 mm section than the 10 mm section. This explains why the reduction in tool wear occurred at a later stage when machining at 90 m/min, as shown in Figure 34.

Figure 37 shows the relationship between tool wear and the volume of material removed. For the same amount of material removed, the flank wear for the less porous material (sample D) is much greater than the more porous material (sample C).

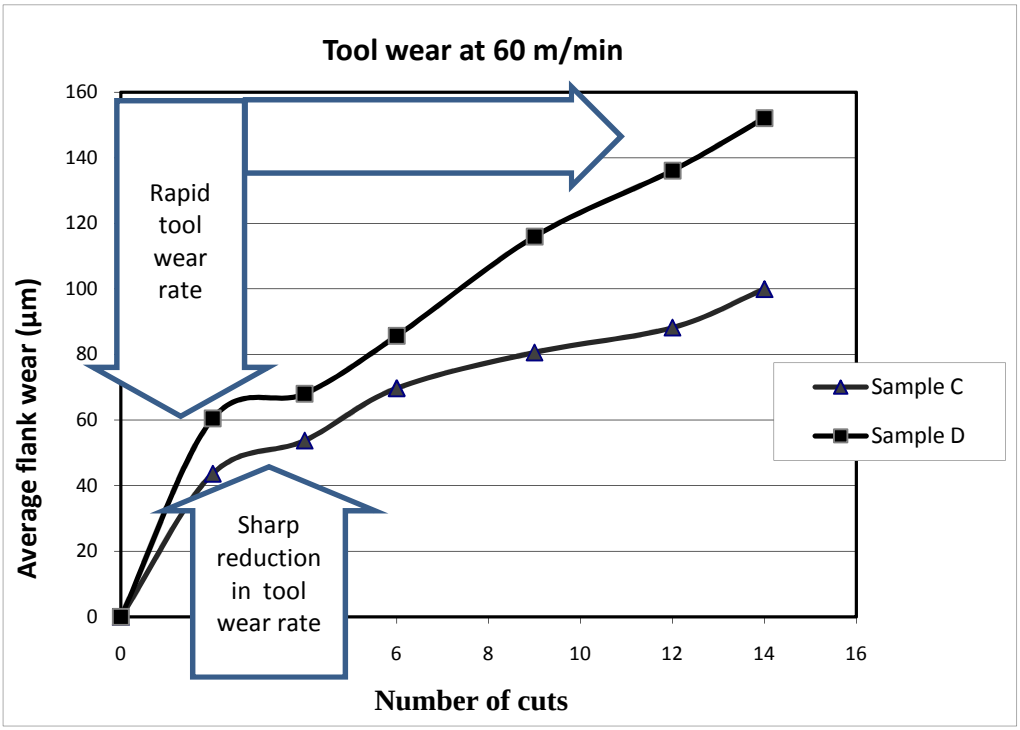

Figure 35 Cutting tool flank wear vs number of cuts (Sample C 3.82 g/cm^3 density, Sample D 4.29 g/cm^3)

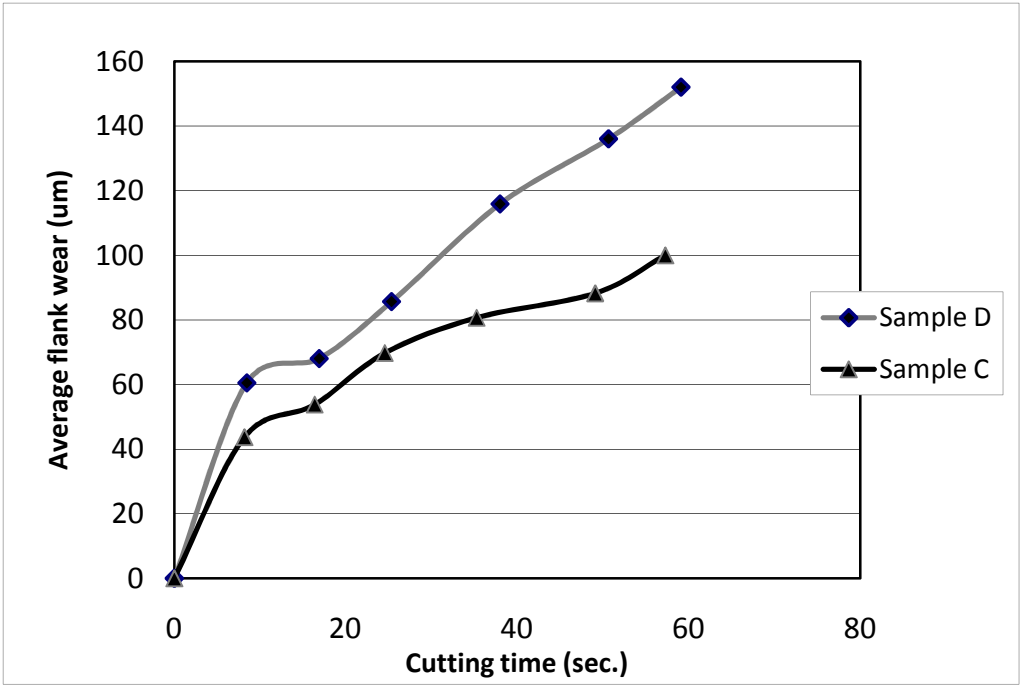

Figure 36 Relationship between the tool wear and cutting time for samples with different porosity (Sample C 3.82 g/cm^3, Sample D 4.29 g/cm^3) at cutting speed of 60 m/min

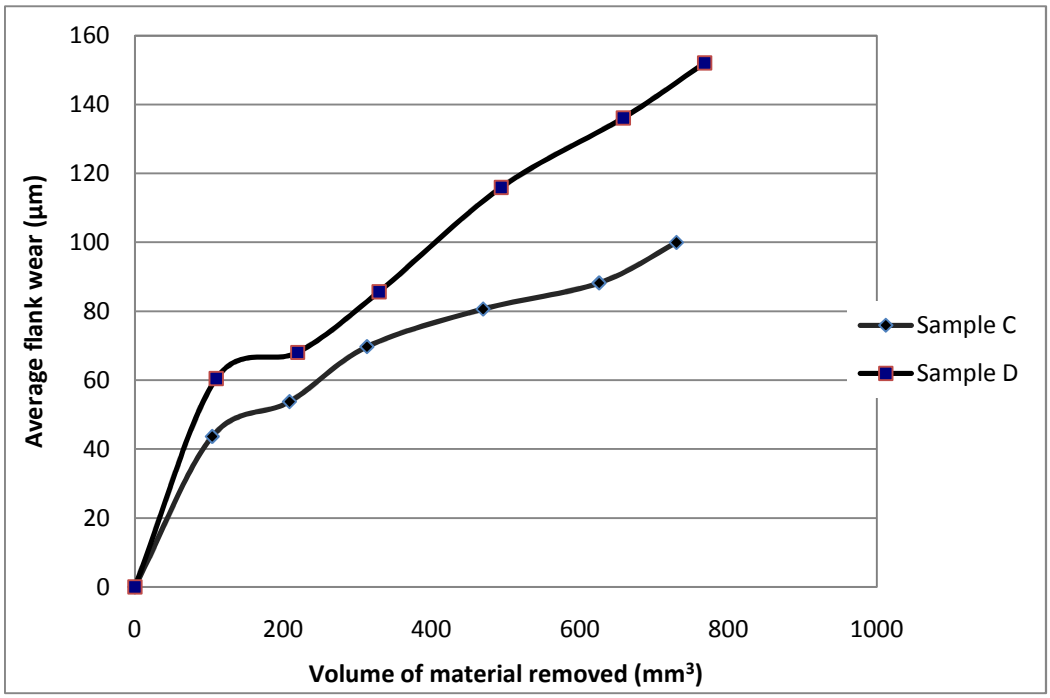

Figure 37 Average flank wear in relationship to the material removal rate at different porosity (Sample C 3.82 g/cm^3, Sample D 4.29 g/cm^3)

The flank wear was examined under the optical microscope to observe and compare the forms of wear associated with samples of different porosity (sample C higher porosity than sample D). Figure 33 (a) and (b) show the images of flank wear of sample C and D, respectively, after machining at a cutting speed of 60 m/min.

As observed in the pilot experiments, the tool wear rate for the sintered titanium decreases as the porosity decreases. Typically, the thermal conductivity of a PM materials increases as its density increases (or as porosity decreases) (German, 2005). This should mean that the heat generated at the tool-workpiece interface is more rapidly dissipated. However, higher porosity also translates to lower material strength for PM materials (German, 2005). This means that the material cuts more easily. These two factors, thermal conductivity and material strength, along with fatigue on the cutting tool which increases with increasing porosity, all influence the machinability of a PM material. Though it was expected that a higher porosity would further increase the rate of wear of the cutting tool, as observed when machining PM steel (Alizadeh, 2008; Salak *et al*., 2006, Capus, 2004; Custon and Simino, 1998, Smith, 1998), this is not so for the PM titanium tested here. The density of the PM steel investigated was between 86-90%, which is similar to what was investigated in this study for PM titanium (between 85-91%). The range of porosity of any PM material determines its machinability (see section 2.4).

The reduction in the cutting tool wear when machining more porous PM titanium can be contributed to the chip breaking. This prevents continuous chip contact on the rake face. Furthermore, the pores in the workpiece dissipate heat easily without transferring it to the tool face.

There is no chemical welding or adhesion of the workpiece material on the rake face of the cutting tool when machining at 60 m/min. Wear on the nose radius shows uniform flank wear, probably because the cutting tool had not yet reached its failure point. The wear of the cutting tool used for machining sample D (Figure 33 (b)) is smooth on the surface but the cutting tool nose used for sample C (Figure 33 (a)) shows some micro-chipping and cracks. These cracks and chipping are created by the large pores within the work piece material (the porosity of sample C is about 15% and sample D is 5%) as the tool moves over the surface during each cutting pass. The cyclic fluctuations, mechanical shocks from the continuous shifting of the cutting edge, in addition to the welding of the material to the cutting edge results in the chipping experienced, as observed during interrupted cutting (Trent, 1991).

4.7 EVALUATION OF SURFACE INTEGRITY

Scanning electron microscopy (SEM) was used to examine the surfaces of the machined samples for surface integrity and defects. The surface integrity can be either influenced by the increase in either cutting speed and, or, the porosity of the PM material. The surface finish of sample B is the best of all the samples machined at a cutting speed of 60 m/min. In addition to this, surface of sample B is better compared to that of sample A when both were machined at 150 m/min. There is a clear indication that the porosity has a more dominant effect on the surface integrity of the machined samples.

From visual examination, the machined surface of sample C (least dense sample) was observed to have large pores on the surface, which can be clearly seen even with the naked eye, which is attributed to the high porous nature of the sample. This phenomenon is not observed with other samples. The pores in the other samples can only be seen under the microscope because of their small size. Under the microscope, the pores in samples A, B and D appeared more evenly dispersed throughout the sample. The level of porosity in samples A, B and D is not as high as that of sample C (<7% compared to approximately 15% for C). This is due to their higher sintered density resulting from the higher compaction pressures used to press these samples. Sample A (sample with highest density) has only a few, smaller pores in its microstructure which can also be seen on its machined surface with the use of the SEM. The machined surfaces of samples D and B had increasing amounts and size of pores compared to sample A.

4.7.1 MACHINED SURFACE TEXTURE

The machined surface was examined for surface texture, waviness, lays and flaws (cracks, nicks, scratches, ridges), and plastic deformation.

Typical machined surfaces of the PM titanium, observed for samples A, B, C and D machined at different cutting speeds, are shown at 50x magnification in the Figure 38. Figure 38 shows the surface of sample A machined at cuttings speeds of both (a) 60 m/min and (b)150 m/min, (c) the surface of sample B machined at 150 m/min, (d) sample C machined at 60 m/min, and sample D machined at (e) 60 and (f) 90 m/min.

All machined surfaces show the cutting lines but some are more pronounced than the others. Sample D shows the best surface while sample C shows the worst. Both are shown after machining at the same cutting speed of 60 m/min. There is presence of waviness on the surface and a rough surface is observed on all samples surfaces. Sample C (Figure 38 (c)) has more of the undulating galloping feature and a more uneven surface.

The surface texture improves as cutting speed increases, but later deteriorates at cutting speeds above 120 m/min. Comparing the surface finish after machining at 60 m/min and 150 m/min, the lower cutting speed showed a poorer surface finish with less defects while there are burrs on the surface of the material machined at 150 m/min. The burrs are due to the high temperature at the chip tool interface which leads to welding of the cutting chips on the tool face which are then transferred on to the workpiece at the next cut.

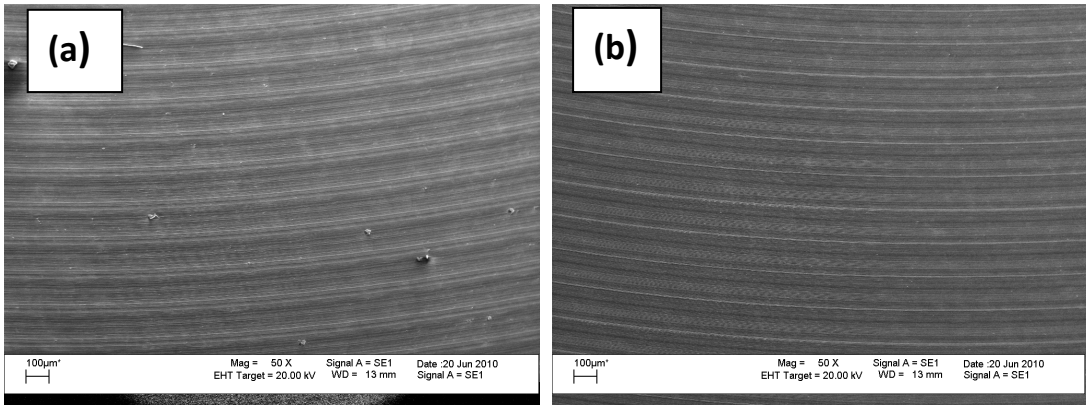

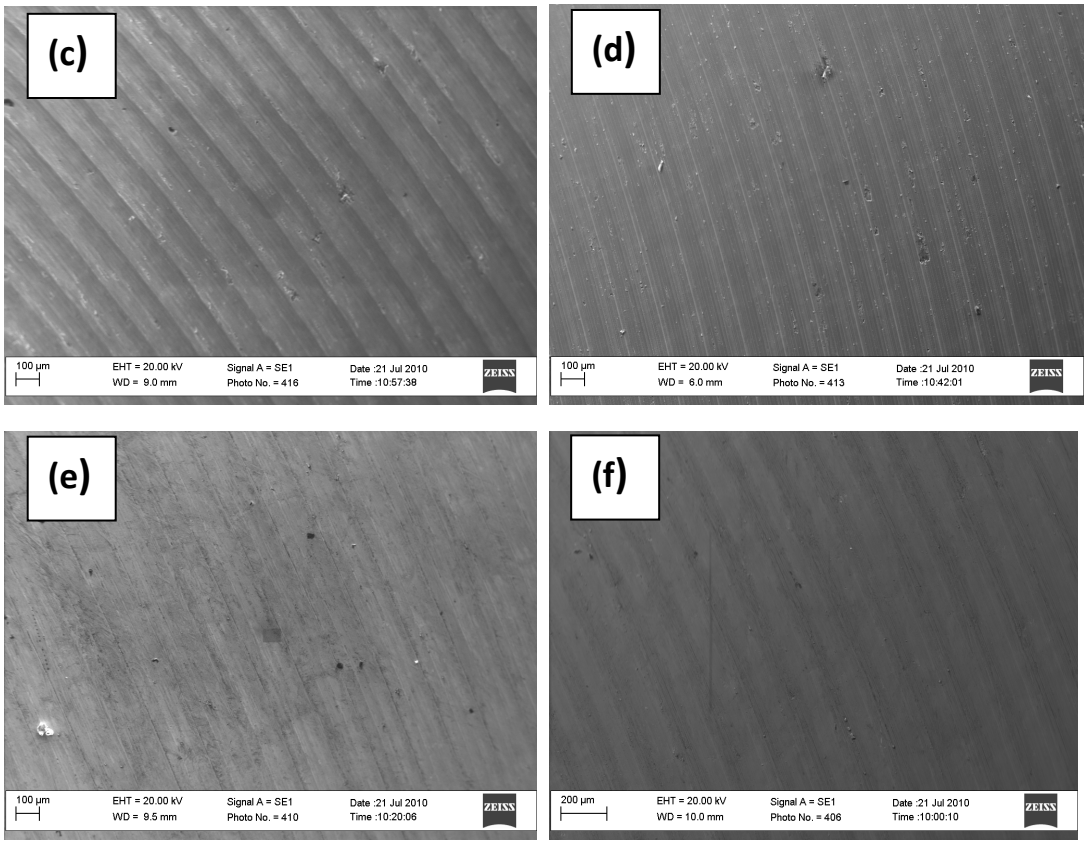

Figure 38 Scanning electron micrograph of machined surfaces at different cutting speeds (a) sample A, 60m/min (b) sample A, 150 m/min, (c) sample B, 150 m/min (d) sample C, 60 m/min (e) sample D, 60 m/min (f) sample D, 90 m/min

Waviness is a component of the surface texture resulting from machining or work deflections, vibration or chatter and is quantified by the number of waves per unit area observed. Waviness can be clearly seen on surfaces cut at 150 m/min (Figure 38 (b) and (c)). Less waviness is observed in sample A (Figures 38 (a) and (b)) compared to sample B (Figure 38 (c)), even at different machining speeds. When machining at high cutting speeds, the temperature at the cutting tool/workpiece interface increases, generating high heat, which causes the chipping on the cutting tool. Machining with a chipped tool results in deeper grooves and more defects on the machined surface. Though the waviness on sample B is more pronounced there are less defects compared to sample A. The higher porosity material show more waviness, but fewer defects. Waviness is more influenced by the porosity in PM machining than by cutting speed.

Sample D, machined at 60 m/min, showed a good surface texture and few pores can be seen in the lines of cut, as seen in Figure 38 (e). Sample C, a higher porosity material also machined at 60 m/min, is however less smooth and contains many intermittent holes, as seen in Figure 38 (d). Large pores are dispersed

throughout the material. They are highly visible even when looking at the surface without using the microscope.

The presence of a white layer (hard surface layer formed along the cutting direction) can be seen on all the machined surfaces as a result of the absence of coolant, but it is more prominent on some surfaces than others. The white layer had been described as brittle and influences mechanical fatigue life, wear resistance and corrosion, and physical properties of engineering materials (Akcan *et al.*, 2002; Aramcharoen and Mativenga, 2008). The formation of a white layer is due to plastic flow, rapid heating, high stress and chemical affinity between the cutting tool and the workpiece (Aramcharoen and Mativenga, 2008). The thickness of the white layer formation increases with increase in cutting speed and porosity. Sample A has the lowest level of white layer. This is probably due to its higher thermal conductivity resulting from its high sintered density (4.41 g/cm^3). Samples C has the most prominent white layer on its surface resulting from its high porosity (Figure 38(c)). Figure 39 shows the presence of white lines on the machined surface. No chemical analysis of the white layer was performed

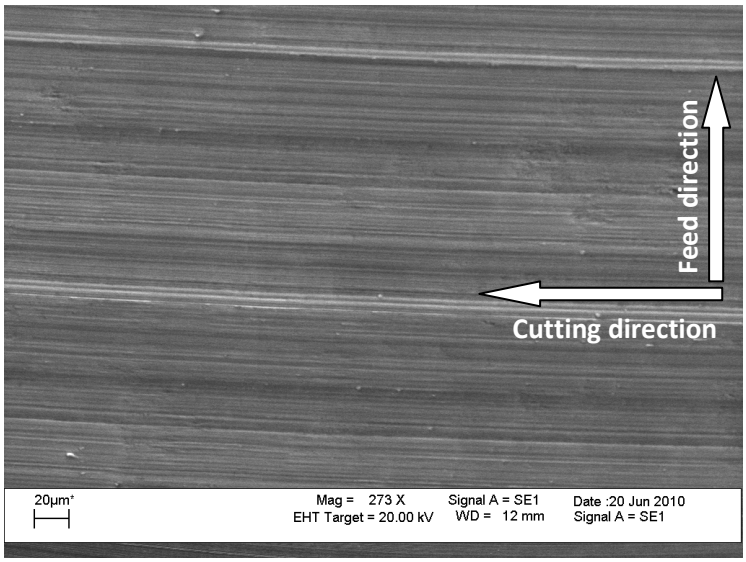

Figure 39 Typical whitelayer on machined surface (sample C)

4.7.2 LAY

The lay can be described as the direction of predominant surface pattern. All the surfaces formed after machining were examined using the SEM to reveal the pattern of cut. The surfaces show similar lay pattern. The lay of the machined surface that is produced by the cutting tool after examination is in a circular curved pattern, perpendicular to the feed direction. This type of pattern is a common phenomenon in many turning and milling operations, and is dependent

on the feed direction and machining operation. The lay pattern is shown in the Figure 39.

4.7.3 DEFECTS/DAMAGES

From examination of the machined surfaces, several types of defects were clearly observed and identified.

Feed marks (marks left on the surface, which is a natural defect) are clearly visible on all the machined surfaces. This is attributed to the feeding and is a natural feature created during machining. The most significant factor in creating feed marks on the machined surface is the progression of the flank wear. The severity of the cutting condition also affects the formation of feed marks. Machining conditions that produce more uniform flank wear on the cutting tool, as in case of machining sample D at a cutting speed of 60 m/min, do not produce deep feed marks (see Figure 38 (e) and (f)). In comparison, the feed marks created on the surface of sample C while machining at same cutting speed, are deeper and more prominent (see Figure 38 (d)). The wear pattern of the cutting tool used for this machining test shows cracks. A tool with high wear creates deeper feed marks (grooves) on the machined surfaces. This is particularly evident in samples A and B (see Figures 38 (b) and (c)) which had even more pronounced feed marks because of the heavy tool wear when both were machined at cutting speeds of 150 m/min.

Other defects observed on the machined surfaces were microchips and debris. Microchips or debris as large as 8 µm are deposited on the machined surfaces of samples A and B, and smaller debris up to 4 µm were observed on samples C and D. The presence of more debris on the machined surfaces of samples A and B is attributed to the severe cutting condition (high cutting speed of 150 m/min) and to the presence of porosity. The amount of debris is more pronounced in sample C than D, in other words for increasing porosity level, even though both were cut using the same conditions. Figure 40 shows tears and deposition of debris on sample C machined surface.

.

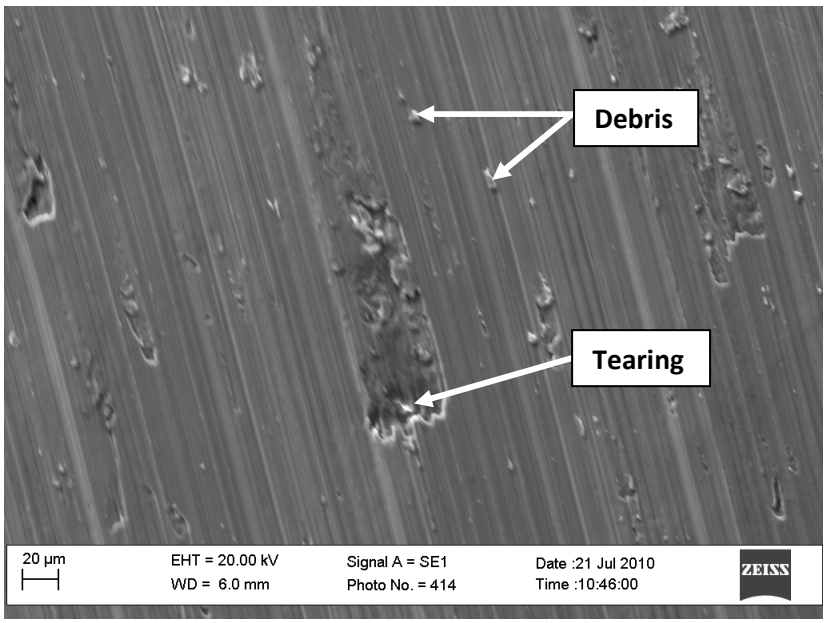

Figure 40 Micro chips, debris and tears produced by the cutting tool on sample C

Tears and laps are defects that are mostly associated with built up edges of the cutting tool. In machining CP titanium, built up edges are not typically observed (Trent, 1991), which supports the results observed in this study. However, in the case of PM materials, some tearing is expected to be observed on the surface, most especially where there are pores. As observed randomly on the surfaces of the machined samples. The edge of the cutting tool catches the edges of the pores and tears the material. At the same time, pieces of the cutting tool are peeled off by the pores. These pieces create potential sites for tearing on surfaces where there are no pores. The material that is removed from the cutting tool is harder than the workpiece and slides between the machined surface and the cutting tool, scratching and tearing the surface as it is dragged along. This effect is shown in Figure 40. Plastic deformation and tearing is increased for the more porous material, as in case of sample C, as compared to the more dense material, sample D. However, in sample A, due to the inhomogeneous flow of the powder during compaction, there are some areas that are more porous than others, most especially the centre of the sample, thus there are more defects at the centre than the outer edge of the machined sample.

The surface finish of the machined surfaces is deteriorated due to chipping at the cutting edge, caused by the high heat generated during machining. The high temperatures cause increased surface roughness and severe microstructure alterations (Che Haron and Jawiad, 2005). When machining titanium, because of its poor machinability, the surface is easily damaged. In addition, the adhesion

and chemical reaction between the tool and the workpiece during machining promotes poor surface finish (Jaffery and Matinvenga, 2009).

4.8 HARDNESS

Table 9 shows the sintered and machined surface hardness of the tested samples using the Rockwell hardness test. The percentage increase in the hardness of the samples after machining is also shown in the table. The increase in the hardness is due to the deformation of the subsurface area of the machined surface causing work hardening of the surface. The level of porosity reduces the surface hardening effect, as is observed for sample C. For both samples (A and D), there is an increase in the machined surface hardness irrespective of the porosity and the cutting speeds. The percentage increase for the more porous sample (C) is, however, less compared to the values obtained for the less porous sample (D). This may emanate from the high temperatures experienced during the chip formation while machining sample D, thus the surface hardens more (in terms of percentage increase) than the surface of sample C. However, there is a small reduction in the hardness of sample D when there is an increase in the cutting speed from 60 m/min to 90 m/min.

Both work hardening and thermal softening usually take place when a workpiece material is subjected to the high cutting pressures and temperatures generated during dry cutting, thus affecting the behaviour of the material. The effect of ageing on the microhardness, as a result of high temperature associated with machining titanium, alters the microstructure of the material when machining dry, thus softening its sub-surface (Ginting A. and Nouari M., 2009).

Table 9 Hardness HRC of samples of sintered and machined surface at relative cutting speeds

	Hardness, HRC		
Samples	**C**	**D**	
sintered surface	52.5	21.4	21.4
machined surface	70	63	56.8
Increase (%)	33	194	165
Cutting speed	60 m/min	60 m/min	90 m/min

4.9 EVALUATION OF CHIP FORMATION

The morphology of the chips formed during turning operations is mostly dependent on the cutting conditions and the workpiece material (Salak *et al*., 2006).

Figure 41 show the shape of the chips formed during the machining tests on CP titanium PM. Figure 42 shows a magnified image of a typical chip at 100x. The chips are serrated, especially those formed at moderate and high cutting speeds. The chips also show rough and smooth areas as a result of fractures along and across the line of flow. All the chips formed in a saw tooth shape, a typical shape formed by machining titanium and its alloys.

Titanium chips are usually formed by an adiabatic or catastrophic thermoplastic shear (Machado and Wallbank, 1990). The chip formation for titanium is explained by the characteristics of its segmentation. The rate of decrease in strength that results from the local increase in temperature (thermal softening) equals or exceeds the rate of increase in strength due to strain hardening in the primary shear zone. Shear occurs on a particular shear plane when the stress built up by the relative tool motion exceeds the yield strength of the material. This energy associated with the deformation is converted to thermal energy and because of titanium's low thermal conductivity, large temperature rises occurs. This in-turn causes local thermal softening and thus the strain continues in the same plane instead of moving to a new plane in the colder material. As deformation proceeds, the deformation shear plane rotates, thus becoming larger, until the increased force due to this rotation exceeds the force needed to plastically deform the colder material or a more favourable plane. This results in a cyclic process, producing a saw–tooth chip form termed as 'catastrophic thermoplastic shear' (Machado and Wallbank, 1990)

At a cutting speed of 60 m/min, the chips formed were long, continuous and greyish in colour (same as the workpiece material) but segmented uniformly. At a cutting speed of 90 m/min, similar chips are formed, but they are slightly discoloured (brownish) and curly. The length of the chips formed at a cutting speed of 90 m/min is shorter than those formed at 60 m/min. At speeds above 90 m/min, the chips formed are brownish, burnt, and serrated. This discolouration occurs a few seconds after leaving the tool contact area. These changes in colour are caused by the formation of thin layer of oxide on the titanium surface indicating the high temperature of the chip. The chips are, however, very brittle. The level of serration of the chips is very pronounced at high cutting speeds due to the high temperature in the cutting zone. These chips showed signs of burning because titanium is highly flammable at these high temperatures. This is observed during the cutting operation, and it is most visible when machining dry.

The length of the chips becomes shorter as the cutting speed is increase further and the chips observed are very thin, which can be as a result of the small contact area with the cutting tool.

Chips formed during machining PM materials are expected to be relatively short, thin and discontinuous, due to the discontinuous nature of the porous material and the lower mechanical properties (Salak *et al.,* 2006). In the case of the tests performed here, the high density materials produced long, continuous chips, indicating that high density PM material is more similar to wrought material.

The chips that were formed from the less dense parts (sample C) are continuous, short spirals, and slightly brown, because of oxidation at the high temperatures. The chips are brittle and also thicker compared to those of the higher dense part that was machined, this can be as a result of the weakness of the material as a result of its porosity as shown in Figure 41 (c).

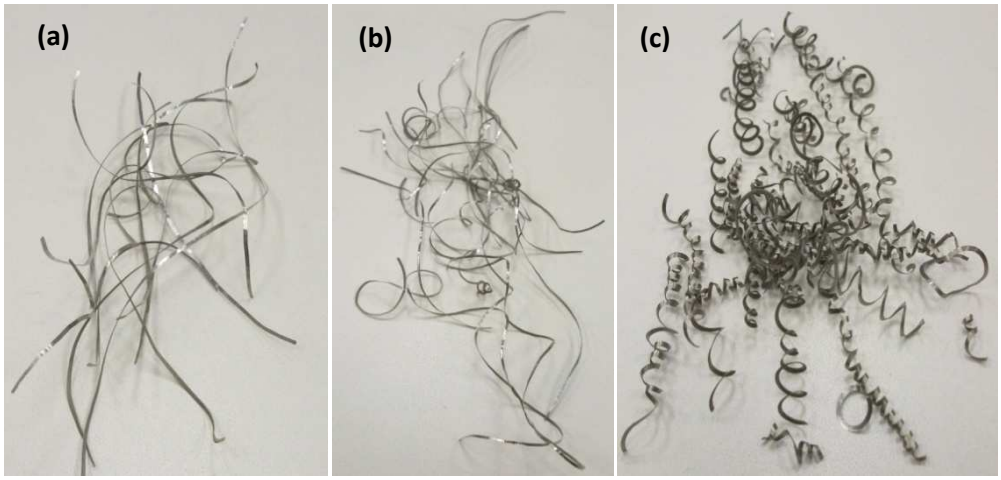

Figure 41 Chip shapes formed during machining (a) sample D, 60 m/min (b) sample D, 90 m/min and (c) sample C, 60 m/min

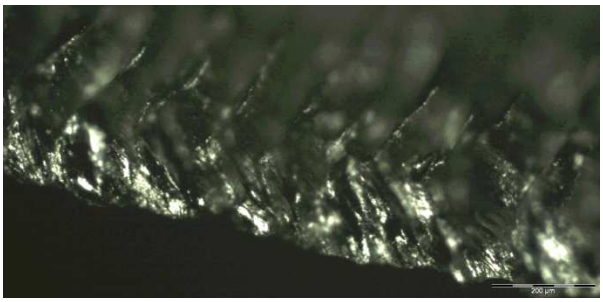

Figure 42 Optical microscopy image (100x magnification) of serrated chip formed during machining

Figure 43 shows the shapes of the segmentation formed on the chips when machining the PM samples under various cutting conditions, as indicated. The

chip obtained from sample D is segmented and continuous as indicated in Figure 43 (f).

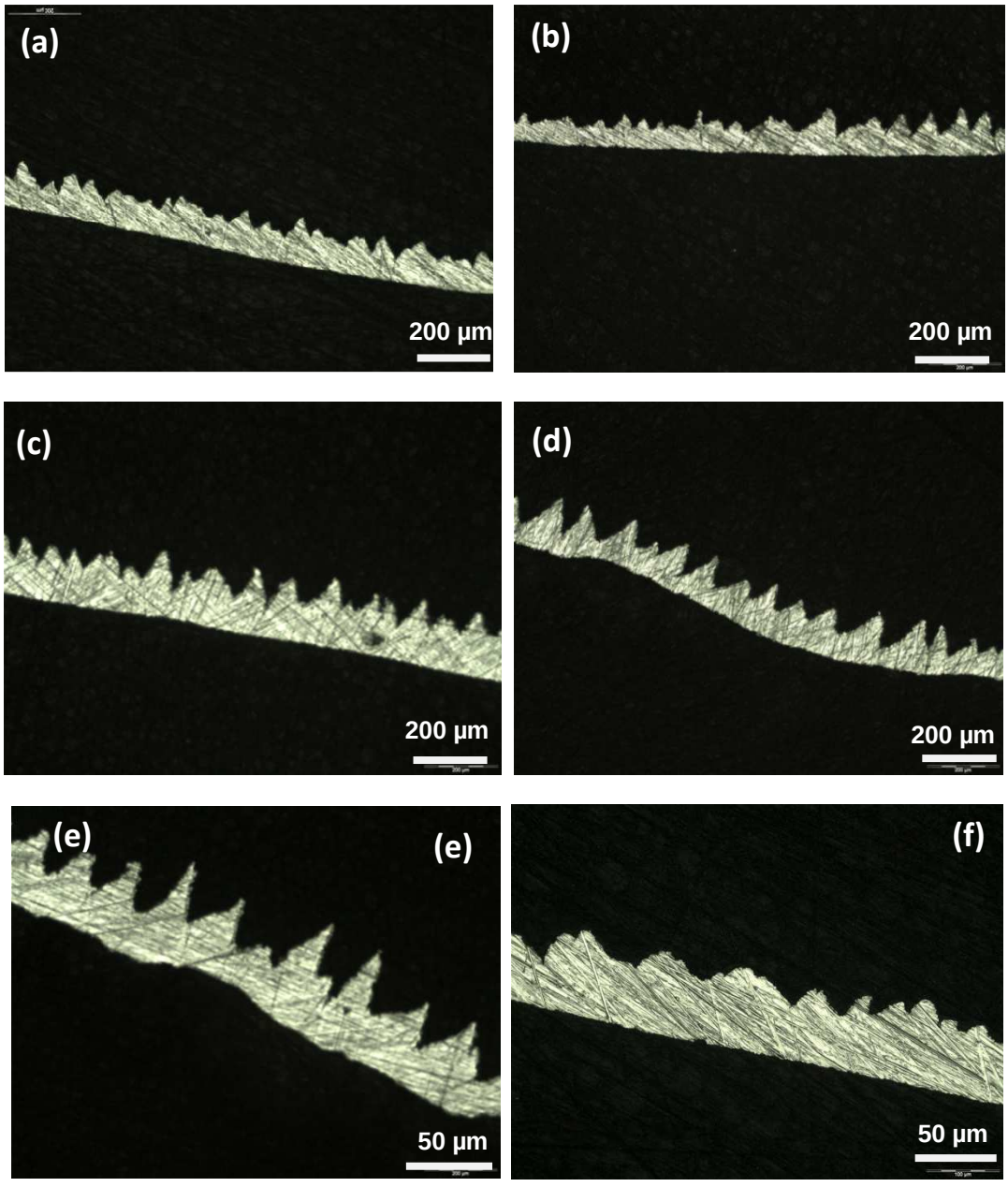

Figure 43 Chip obtained after machining the samples at different cutting speeds (a) sample A at 60 m/min, (b) sample A at 90 m/min, (c) sample A at 120 m/min, (d) sample A at 150 m/min, (e) sample C at 60 m/min, (f) sample D at 60 m/min

The chips formed are segmented and continuous when machining at a lower cutting speeds, as shown in Figure 43 (a), while at higher cutting speeds, the chips are serrated, as shown in Figure 43 (e).

The average chip height varies from 100 - 150 µm (upper points of the saw) to 45 -55 µm (lower points of the saw) for most of the chips formed. At lower cutting speeds, the variations between the peaks and the grooves are not as large as when the materials are machined at higher cutting speeds.

The chips formed by more porous titanium samples are shorter and curl into a helix which can be easily cleared from around the tool. This is as a result of the pores in the samples acting as a mechanical modifier or chip breaker. The modification of the chip is similar to when there are grooves in the tool rake face.

The results obtained from these experiments were compared to the results obtained by Hong *et al.* (2001) for dry cutting of wrought titanium alloy with a similar WC-Co unalloyed grade of carbide cutting tool. Their investigation was carried out at cutting speed of 90 m/min; for the same feed rate of 0.15 mm/ rev, the cutting time for wrought titanium alloys was about 150 seconds. In comparison, it took only 38 seconds (about 3.5 times less) for PM titanium to reach the same flank wear. The result of the tests clearly confirm that wrought titanium has a better machinability, even though the rate of tool wear for a titanium alloy is usually more when compared to CP titanium, because of its lower thermal conductivity.

It has been observed that the thermal conductivity of CP titanium at high pressure differs from that at atmospheric pressure; a higher pressure lowers the thermal conductivity of the material, thus deteriorating its machinability. At active cutting zones, there is a higher pressure associated with the workpiece and tool in contact, making it difficult to dissipate the heat generated during machining (Abdel-Aal *et al.,* 2009). In addition to this, the tool life can also be high when the porosity of the material is either very high or very low, with a high tool failure at an intermediate density (German, 2005). Again, this is attributed to high thermal conductivity at low porosity, which aids machinability, compared to low stress at high porosity, which also aids machinability. At intermediate porosity levels, neither benefit of these extremes is present, resulting in high tool failure.

The result obtained here for PM titanium, showed better machinability for a more porous sintered part. This is attributed to the decrease in the average shear stress in the cutting zone, thus there is an increase in machinability as the porosity increases.

There appears to be no consensus on the effect of porosity on the machinability of sintered materials. Abduljabbar (1982) observed improved mapchinability with a decrease in porosity when studying the machinability of sintered 316L stainless steel. While, the study on the machinability of sintered 304 stainless steel (70 -

90% dense) by Agapiu *et al.* (1989) found that the tool wear was more rapid for a more porous material than for a denser material.

CONCLUSION AND RECOMMENDATIONS

5.1 CONCLUSION

The study presents the investigation of the machinability of sintered CP titanium powder. Initial compressibility studies indicate that the CP sponge fine titanium powder used is suitable for compaction. However, the compressibility of the powder is influenced by the compact shape. While a small compact (10 mm diameter x 10 mm high cylinder) compacts well using only die-wall lubrication, a larger compact such as the test sample shape does not compact well. Careful design of the tooling to assist in powder flow and part ejection is needed for more complex shapes.

Although the tooling was modified and a lubricant was mixed with the powder to improve compaction, evidence of delamination during ejection was still visible, although reduced, and the sharp corners of the part still crumbled. The poor compaction described is attributed to the powder particle size distribution. The powder used had a maximum particle size of approximately 75 μm. This did not adversely affect the compaction of small samples (10 mm diameter by 10 mm high), however, it was found to be too small for a larger compact shape (>20mm diameter, >20mm high). A smaller particle size translates to a higher surface area and therefore increased interparticle friction. This negatively affects the compressibility of powders.

Sintering of the titanium powder compacts was successfully performed in vacuum. Increasing sintering time (from 1 hr to 2 hrs) at temperature, 1200°C, results in a marginal increase in sintered density. The sintered density of the compacts varies from the outer edge to the core. This can be attributed to the uneven density distribution in the green part.

The face turning method is easy to perform and provides a simple means for evaluating the turning process in relation to the tool material, geometry and cutting condition. This method was used in this study for the evaluation of the machininability of sintered titanium.

The tool wear rate during machining of PM CP titanium is poor as compared to the tool wear rate experienced when machining wrought titanium alloys. This result supports published literature on the machinability of sintered PM material. The magnitude of the tool wear increases with increase in cutting speed but decreases with an increase in the porosity of the material, thus machinability is better when machining a more porous part. This result was also observed during machining of sintered 316L stainless steel, but was contrary to the machining of sintered 304L stainless steel. Porosity has a dual effect on the machinability of

sintered materials; it decreases the thermal conductivity of the material, which negatively affects machinability, while simultaneously it decreases the strength of the material, which affects machinability in a positive manner. For the porosity levels investigated in this study, 5% versus 15%, machinability improved with increased porosity. This indicates that the effect of weakening the material is more pronounced than the effect of decreasing the thermal conductivity of the material.

The chip formed when machining is serrated and thin in all cases but at a higher cutting speed, it is brownish because of oxidation. The chips are shorter and curled into a helix when machining a more porous material because the pores interrupt the cutting path and act as chip-breakers.

The denser part shows a better surface texture and fewer defects during dry machining as compared to the porous material.

The deformation and work hardening caused by the turning the PM material subjected to high cutting pressures and temperatures increased the apparent hardness of the machined surface; the surface hardening effect reduces with increase in level of porosity.

In general, the dry cutting condition is not suitable for machining of PM titanium alloys due to the heavy tool wear rate and the poor surface condition, especially at high cutting speeds. However, it serves as a good benchmark for comparing the machinability of different sintered materials.

5.2 RECOMMENDATIONS

It is recommended for machining trials to be carried out on samples compacted using a powder with a larger mean particle size distribution, in the range of 75-150 µm, to better understand its influence in machinability of sintered titanium.

Evaluation of the machinability of sintered α-β titanium alloys will be very useful since this material is mostly used for aerospace application**.**

Improved cutting tool wear may be achieved by means of lubrication during machining. However, the use of conventional lubricants, that can infiltrate pores in the sintered microstructure during machining, may affect the mechanical properties of the part produced and should be investigated.

Cryogenic machining has proved to be useful for improvement in the tool life during machining of wrought titanium alloys and should be investigated for sintered titanium. The use of argon gas coolant for cryogenic machining could be investigated. However, the use of liquid nitrogen and compressed air (which is mostly nitrogen) as coolant are not recommended for titanium machining due to the reactivity (nitriding behaviour) of titanium at high temperatures.

REFERENCES

Abdel-Aal, H.A., Nouari M. and El Mansor M. 2009, *Influence of thermal conductivity on wear when machining titanium alloys,* Tribology International, pp. 359- 372.

Abduljabbar, A.W., 1982, The effect of porosity and metal cutting variables on the machinability of powder metallurgy-316L stainless steel and FCo508 copper-steel, Masters Thesis, University of Wisconsin-Madison, W. I.

Agapiu, J. S., Halldin G. W. and Devries M. F., 1989, Effect of porosity on the machinability of P/M 304L stainless steel, *International Journal of Powder Metallurgy*, Vol. 25, pp. 127-139.

Akcan, S., Shah, I. S., Moylan, S. P., Chandrasekar, S., Chhabra, P. N. and Yang, H.T. Y., 2002, Formation of white layers in steels by machining and their characteristics, *Metallurgical and Materials transaction A,* Vol. 33 (4), pp. 1245-1254.

Alizadeh, E., 2008, Factors influencing the machinability of sintered steels, *Powder Metallurgy and Metal Ceramics*, Vol. 47, pp. 304 - 315

Allen, T., 1990, *Particle size measurements*, 4th edition Chapman and Hall.

Alman, D. E., and Hawk, J. A., 1999, The abrasive wear of sintered titanium matrix-ceramic particle reinforced composite. *Wear,* Vol. 225-229 (1), pp. 629-639.

Andersson, O., and Benner, A., 2001, Machinability of Green Powder Metallurgy Part 2, *Proceedings* of *the International Conference on* Powder Metallurgy and Particulate Materials, Metal Powder Industries Federation, Princeton, NJ, Vol. 6, pp.16–28.

Angelo, P. C. and Subramanian, R., 2008, *Powder Metallurgy, Science, Technology and Applications*, PHI Learning –Private Limited, Connaught Circus, New Delhi, India. pp 87 – 125.

Aramcharoen, A. and Mativenga, P. N., 2008, White layer and hardening effects in hard turning of H13 tool steel with CrTiAlN and CrTiAlN/MoST- coated carbide tools, *International Journal of Advanced Manufacturing Technology,* Vol. 36 (7-8), pp. 650-657.

Astana, R., Kumar, A. and Dahotre, N., 2006, *Material Science in manufacturing*, Elsevier USA, pp. 172-179.

Awopetu, O.O., Dahunsi, O.A., and Aderoba, A.A., 2005, Selection of cutting tools for turning α- titanium alloy Bt5, pp. 196-200 Available: http://www.journal.au.edu/au_techno/2005/apr05/vol8no4_abstract06.pdf

ASM Metals Handbook-Desk Edition, 1985, ASM International, pp. 27–29.

Bäker, M., 2003, The influence of plastic properties on chip formation, *International Journal of Computational Material Science and Surface Engineering*, Vol. 28, pp. 556–562.

Balkrishna, R., and Shinm, Y.C., 2002, A study on the high speed face milling of Ti-6Al-4V alloy, *Proceedings of 2002 ASME International Mechanical Engineering Congress and Exposition*, New Orleans, pp. 277–286.

Barksdale, J., 1968, "Titanium". In Clifford A. Hampel (editor). *The Encyclopedia of the Chemical Elements*. New York: Reinhold Book Corporation, pp. 732–738.

Barnett-Ritcey, D.D., 2004, High speed milling of titanium and Gamma-titanium aluminide: An experimental investigation, Ph.D, thesis, Mc-Master University, Canada.

Benner, A., and Beiss, P., 2000, Drilling and Tapping of Warm Compacted PM Steel, *Proceedings of Euro PM 2000 Conference on Material and Processing Trends for PM Components in Transportation*, Munich, pp. 101–109.

Bhattacharyya, A., 1998, *Metal cutting theory and practice*, New Central Book Agency, Calcutta.

Callister, Jr., W. D., 2003, *Material Science and Engineering – An Introduction*, 6th Edition, John Wiley and Sons Inc., pp. 264-382.

Capus, J., 2004, Machining PM parts, does 'X factor' holds key to success?, *Metal powder report*, Vol. 59 (11), pp. 24- 28.

Capus, J.M, 2005, More roads point to cheaper titanium powder, *Metal Powder Report*, Vol. 60, pp. 22-23.

Causton, R. J. and Cimino, T., 1998, Machinability of P/M steels, *Powder Metal Technologies and Applications*, ASM Handbook, Vol. 7, pp. 671–680.

Chandler, H.E., 1998, *Machining of reactive metals*, Metals Handbook volume 16: machining, pp. 844-857.

Che Haron, C. H. and Jawaid, A., 2005, The effect of machining on surface intergrity of titanium alloy Ti-6Al-4V, *Journal of Materials Processing Technology,* Vol. 166, pp. 188-192.

Chilli factor prolongs cutting tool life in sinter-hard working, 2008, Metal Powder Report, Vol. 63(3), pp. 24-37.

Cordellier, S. and Didiot, B., 2004, *L'état du Monde 2005; annuaire économique géopolitique mondial.* Paris: La Découverte.

Cimino, T.M., and Luk, S.H., 1995, Machinability Evaluation of Selected Green Strength P/M Materials, *Proceedings* of *the International Conference on* Powder Metallurgy and Particulate Materials, Metal Powder Industries Federation, Princeton, NJ, Vol. 8, pp. 129–148.

Cubberly, W. H. and Bakerjian R., 1989, *DESK EDITION: Tool and manufacturing engineers handbook*, SME.

Dabhade, V. V., Rama Mohun, T. R., Ramakrishan, P., 2007, Initial sintering kinetics of attrition milled nanocrystalline titanium powder, *Material Science and Engineering A,* Vol. 452 - 453 , pp. 386 – 394.

Daymi, A., Boujelbene, M., Ben Salem, S., Hadj Sassi, B., Torboty, S., 2009, Effect of the cutting speed on the chip morphology and the cutting forces, *Archives of Computational Material Science and Surface Engineering,* Vol. 1 (2), pp. 77-83.

Deura, T. N., Wakimo, M., Matsunga, T., Suzuki, R. O., and Ono, K., 1998, Titanium powder Production by TiCl4 Gas injection into Magnesium through molten salts, *Metallurgy and Materials Transactions B*, Vol. 29 (6), pp. 1167.

Donachie Jr., M. J., 2000, *Titanium. A Technical Guide*, 2nd edn, ASM International, Metal Park OH, pp. 13-24.

Eylon, D., Froes, F. H., and Abkowitz, S., 1998, *Titanium Powder Metallurgy Alloys and Composites,* ASM Handbook Volume 07: Powder Metal Technologies and Applications, pp. 874-883.

Ezugwu, E. O., and Wang, Z.M., 1997, Titanium alloys and their machinability a review, *Journal Material, Process Technology*, Vol. 68 (3), pp. 262–274.

Ezugwu, E.O., 2004, High speed machining of aero-engine alloys, Journal *of Brazillian Society of Mechanical Science and Engineering*, Vol. 1, pp. 1-11.

Ezugwu, E.O., 2005, Key improvements in the machining of difficult-to-cut aerospace superalloys, *International Journal of Machine Tools and Manufacture*, Vol. 45 (12-13), pp. 1353–1367.

Ezugwu, E. O., Da Silva, R. B., Bonney, J. and Machado, A. R. 2005. Evaluation of the performance of CBN tools when turning Ti-6Al-4V alloy with high pressure coolant supplies, *International Journal of Machine Tools and Manufacture*, Vol. 45 (9), pp. 1009-1014.

Ezugwu, E. O., 2007, Improvements in the machining of aero-engine alloys using self-propelled rotary tooling technique, *Journal of Materials Processing Technology*, Vol. 185(1-3), pp. 60-70.

Ezugwu, E. O., Bonney, J., Da Silva, R. B., Cakir, O., 2007, Surface intergrity of finished turned Ti-6Al-4V alloy with PCD tool using conventional and high pressure coolant, *International Journal of Machine Tools and Manufacture*, Vol. 46(6), pp. 884-891.

Froes, F. H., 2000, "Developments in Titanium P/M", *Metal Powder Report*, Vol. 55, pp. 12- 17.

Froes, F. H., 2000, The titanium image: Facing the realities of life, Journal of the Minerals Metals and Materials Society, Vol. 52(5), p. 12.

Froes F. H., Mashl, S. J., Hebeisen, J.C., Moxson, V. S., and Duz, V. A. , 2004, The technologies of titanium powder metallurgy, *Journal of the Minerals Metals and Materials Society*, Vol. 56(11), pp. 46-49.

Froes, F. H., Ashraf, M. I., and Derek, F., 2007, Cost Affordable Titanium: The component fabrication perspective, *Journal of the Minerals Metals and Materials Society*, Vol. 59(6), pp. 28-31.

Gente, A., Hoffmeister H.W., 2001, Chip formation in machining Ti6Al4V at extremely high cutting speeds, *Annals of CIRP*, Vol. 50, pp. 49–52.

German, R.M., 1994, *Powder metallurgy science*, 2nd ed., Metal Powders Industries Federation, Princeton, pp. 290- 298.

German, R.M., 2005, *Powder metallurgy and particulate Materials Processing*, Metal Powder Industries Federation, New Jersey, USA

German, R. M., and Park S. J., 2008, *Mathematical relations in particulate materials processing: ceramics, powder metals, cermets, carbides, hard materials, and minerals*, Wiley-Interscience, USA, p. 301.

Giting, A. and Nouari, M., 2009, Surface intergrity of dry machined titanium alloys, *International Journal of Machine Tools and Manufacturing*, Vol. 49(3-4), pp. 325-332.

Graham, D., 1998, Machining PM parts, *Manufacturing Engineering.*

Grzesik, W. Krol, S. Čížek, Lubomír, Hubáčková, Jiřina, 2005, *Machining titanium and its alloys : state-of-the-art*, Sborník vědeckých prací Vysoké školy báňské - Technické univerzity Ostrava, Vol. 48, pp. 89-95.

Hayes, F. H. et al., 1984, Advances in Titanium Extraction Metallurgy, *Journal of Manufacturing*, Vol. 36 pp. 70 – 75.

Hooven, III, W. T., St. Pierre, J. and Sanderow, H., 1993, Commercial practice. *In* Fabian, R. (eds.), *Vacuum technology practical heat treating and Brazing.* Materials Park, OH, ASM International, pp. 178.

Hong, S. and Ding, Y., 2001, Cooling approaches and cutting temperatures in cryogenic machining of Ti-6Al-4V, *International Journal of Machine Tools and Manufacturing*, Vol. 41(10), pp. 1417-1437.

Hong, S.Y., Ding, Y., and Jeong, W., 2001, Friction and cutting forces in cryogenic machining of Ti-6Al-4V, *International Journal of Machine Tools Manufacturing*, Vol. 41, pp. 2271–2285.

Ibrahim, G.A., Che Haron C.H., and Ghani J.A., 2009, The Effect of Dry Machining on surface Intergrity of Titanium Alloy Ti-6Al-4V Eli, *Journal of applied Sciences,* Vol. 9 (1), pp.121-127.

International Titanium Powder homepage, [S.a.]. [Online]. Available: http://www.itponline.com/index_files/aboutITP.htm [14 October 2010]

Jaffery, S. I. and Mativenga, P. T, 2009, Assessment of the machinability of Ti-6Al-4V alloy using wear map approach, *The International Journal of Advanced Manufacturing Technology*, Vol. 40(7-8), pp. 687-696.

Jones, P.E., and Eylon, D., 1999, Effects of conventional machining on high cycle fatigue behaviour of intermetallic alloy Ti-47Al-2Nb-2Cr, *Journal of Material Science and Engineering A*, Vol. 263(2), pp. 296–304.

Joubert, H. J, 2008, Investigation of lubrication strategies in Ti6Al4V milling operations, Masters thesis, Stellenbosch University.

Kikuchi, M. et al., 2003, Grindability of cast Ti-Cu alloys, *Journal of Dental Materials*, Vol. 19, pp. 375-381.

Kikuchi, M., 2009, The use of cutting temperature to evaluate the machinability of titaium alloys, *Acta Biomaterialia*, Vol. 5(2), pp. 770-775.

Kitagawa, T., Kubo, A. and Maekawa, K., 1997, Temperature and wear of cutting tools in High-speed machining of Inconel 718 and Ti6Al4V2Sn, *Wear*, Vol. 202(2), pp. 142-148.

Klar, E. and Prasan K. S., 2007, *Powder metallurgy stainless steels: Processing, microstructures, and properties*, ASM international, OH, USA.

Kuttolamadom, M. A., Jones, J. J., Mears, M. L., Kurfess, T., Choragadi, A., 2010, Investigations of the machining of titanium components for light weight vehicles, *Conference paper of SAE 2010 world congress and exhibition, April 2010, Detroit MI, USA*, Paper number 2010-01-0022.

Laubscher, R. F., Van Trotsenburg, S., 2010, The effect of high speed machining on the surface integrity of certain titanium alloys, *Proceedings of the 2010 International Conference on Competitive Manufacturing (COMA '10)*, Stellenbosch, 3 – 5 February 2010, pp. 185–190, GCCE, Stellenbosch.

Lutjering, G., and James C., 2003, *Titanium: History of titanium*, Williams Springer, pp. 2-5.

Machado, A. R., and Wallbank J., 1990, Machining of titanium and its alloys-a review, *Proceedings Institution of Mechanical Engineers, Journal of Engineering Manufacturing*, Vol. 204, pp. 53–60.

Madan, D. S., 1995, Advances of Powder Metallurgy and Particulate Materials, *International Journal of Powder Metallurgy*, Vol. 1, pp. 55–67.

Molinari, A., Musquar, C., and Sutter, G., 2002, Adiabatic shear banding in high speed machining of Ti-6Al-4V: experiments and modelling, *International Journal of Plasticity*, Vol. 18, pp. 443–459.

Moll, J. H., 2000, Utilization of Gas-Atomized Titanium and Titanium-Aluminide Powder, *Journal of the Minerals Metals and Materials Society*, Vol. 52(5), pp. 32-35.

Moxson, V., Senkov O., and Froes F. H., 2000, Innovations in titanium powder processing, *Journal of Metallurgy*, Vol. 52(5), pp. 24-26.

Nabhani, F., 2001, Wear mechanisms of ultra-hard cutting tools materials, *Journal of Materials Processing Technology*, Vol. 115(3), pp. 402-413.

Naboychenko S., and Dowson, G., 2009, *Hand book of Non ferrous Metal powders; Technologies and Applications*, Elsevier London, pp. 14-20.

Norgate, T. E., and Wellwood, G., 2006, The potential Applications for titanium metal powder and their life cycle implants, *Journal of the Minerals Metals and Materials Society*, Vol. 58(9), 58-63.

Norihiko, N., 2002, High-speed machining of titanium alloy, *Journal of Mechanical Engineering*, pp. 109–114.

Oled, D., Stanislav, N., Eylon, D. Froes, F. H., and Abkowitz, S., 1998, *Titanium Powder Metallurgy Alloys and Composites*, ASTM Handbook Volume 07 Powder Metal technologies and applications, pp. 874-883.

Panigrahi, B. B., Godkhindi, M. M., Das, K., Mukunda, P. G., and Ramakrishnan, P., 2005, Sintering kinetics of micrometric titanium powder, *Journal of Material Science and Engineering A*, Vol. 396 (1-2), pp. 255– 262.

Poulachon, G., and Moisan, A, 2000, Cutting mechanisms and metallurgical aspects, *Transactions ASME Journal of Manufacturing Science and Engineering*, Vol. 122, pp. 406-412.

Powder Metallurgy design guide book, 1995, 2nd Edition, MPIF Princeton, USA.

Rahman, M., Wong, Y.S., and Zareena, A.R., 2003, Machininability of titanium alloys, *JSME international*, Vol. 46, pp. 107–115.

Rahman, M., Wang Z., and Wong Y., 2006, A Review on High Speed Machining of titanium Alloys, *JSME International*, Vol. 49(1), pp. 11-20.

Ramstedt, M., Andersson, O., Vidarsson, H., and Hu, B., 2001, Machinability of Green Powder Metallurgy Part 1, *Proceedings* of *the International Conference on* Powder Metallurgy and Particulate Materials, Metal Powder Industries Federation, Princeton, NJ, Vol. 12, pp. 151–162.

Rajiv A., Ashok K., and Narendra B. D., 2006, *Materials Processing and Manufacturing Science*, Powder Metallurgy, USA, Elsevier, pp. 172-207.

Robert-Perron, E., Blais, C., Thomas Y., Pelletier, S. and Dionne, M., 2005, An integrated approach to the chracterisation of powder metallurgy component performance during green machining, *Metallugical and Materials Transaction A*, Vol. 402 (1-2), pp. 325-334.

Robert-Perron, E., Blais, C., Pelletier S. and Thomas Y., 2007a, Machinability of green powder metallurgy components: Part 1. Characterisation of influence of tool wear, *Metallugical and Materials Transaction A*, Vol. 38(6), pp. 1330-1336.

Robert-Perron, E., Blais, C., Pelletier S. and Thomas Y., 2007b, Machinability of green powder metallurgy components: Part 2. Sintered properties of components

machined in green state, *Metallugical and Materials Transaction A*, Vol. 38(6), pp. 1337-1342.

Robertson, I. M, and Schaffer, G. B., 2009, Some effects of particle size on the sintering of titanium and master sintering curve model, *Metallurgical and Materials Transaction A,* Vol. 40 (8), pp. 1968 – 1979.

Sandvik coromant, 2008, Application Guide: Titanium machining, Sweden.

Salak, A., Vasilko, K., Selecka, M. and Danninger, H., 2006, New short time face turning method for testing the machinability of PM steels, *Journal of Materials Processing Technology*, Vol 176(1-3), pp. 62–69.

Schwarzkopf P., 1947, *Powder Metallurgy, Its physics and Production*, Macmillan Company, New York.

Seong, S., Younossi, O. and Goldsmith, B. W., 2009, *Titanium: Industrial base, price trends and technology initiatives*, The RAND Corporation, Santa Monica, California, USA.

Sheikh-Ahmad, J., and Balley, J.A., 1997, *Flow* instability in the orthogonal machining of CP titanium, *Journal of Manufacturing Science and Engineering*, Vol. 119, pp. 307–312.

Shivpuri, R., Hua, J., Mittal, P., and Srivastava, A.K., 2002, Microstructure mechanics interactions in modeling chip segmentation during titanium machining, *Annals of CIRP*, Vol. 51, pp. 71–74.

Smith T. H., 1998, Getting the Measure of PM Machinability, *Metal Powder Report*, Vol. 53(5), pp.31-35.

St-Laurent, S., and Chagnon, F.,1997, Behaviour of metal powder during cold and warm compaction, *Proceedings* of *the International Conference on* Powder Metallurgy and Particulate Materials, Metal Powder Industries Federation, Princeton, NJ, Vol. 3, pp. 20-27.

Sun, S., Brandt, M., and Dargusch, M.S., 2009, Characteristics of cutting forces and chip formation in machining of titanium alloys, *International Journal of Machine tools and Manufacture*, Vol. 49, pp. 561-568.

Taylor, J., 1962, The tool wear-time relationship in metal cutting, *International Journal of Machine tools and Manufacture*, Vol. 2, 119-152.

Ten Haaf, P.,Mielnik, K. and Lauwwers B, 2008, Development of HSC strategies and tool geometries for the efficient machining of Ti6Al4V. *Proceedings of the*

3rd International CIRP High Performance Cutting Conference, University College Dublin (UCD) Belfield Campus, 2008, pp. 753-761, Dublin.

Timet (Titanium Metals Corporation USA.), 1997, *Corrosion resistance of titanium*, [Online] Available: http://www.timet.com/coresistframe.html [accessed on February 8, 2010]

Kobelco, Characteristics *of titanium*, [S.a.]. [Online] Available: http://www.kobelco.co.jp/english/titan/characteristic/index.html [accessed on March 4, 2010]

TITAL GmbH, 2010, *Titanium investment casting save cost and resources*, [Online] Available: [http://www.aerospacetechnology.com/contractors/sub_contract/tital/press18.html [accessed on May 2, 2010]

Tremblay, L., Danaher, J.E., Chagnon, F., and Thomas,Y., 2002, Development of Enhanced Green Strength Lubricating Systems for Green Machining, *Proceedings* of *the International Conference on* Powder Metallurgy and Particulate Materials, Metal Powder Industries Federation, Princeton, NJ, Vol.12, pp. 123–137.

Trent, E. M., 1991, *Metal Cutting.* 3rd. Oxford : Butterworth-Heinemann Ltd, pp. 237 - 240.

Watson, D., Bayha T., Hofman T., and Festeau G., 2007, Titanium takes off: The art and science of milling titanium to make aerospace parts, *Cutting Tool Engineering Magazine*, Vol. 59, pp. 36-43.

Yang, X., and Liu, C.R., 1999, Machining titanium and its alloys, *Machining Science Technology* Vol. 3(1), pp. 107–139.

Yang, X., Liu C.R., and Grandt, A.F., 2002, An experimental study on fatigue life variance, residual stress variance, and their correlation of face turned and ground Ti 6Al-4V, *Journal of Manufacturing Science and Engineering*, Vol. 124, pp. 809–818.

APPENDIX A: TOOLING DESIGN

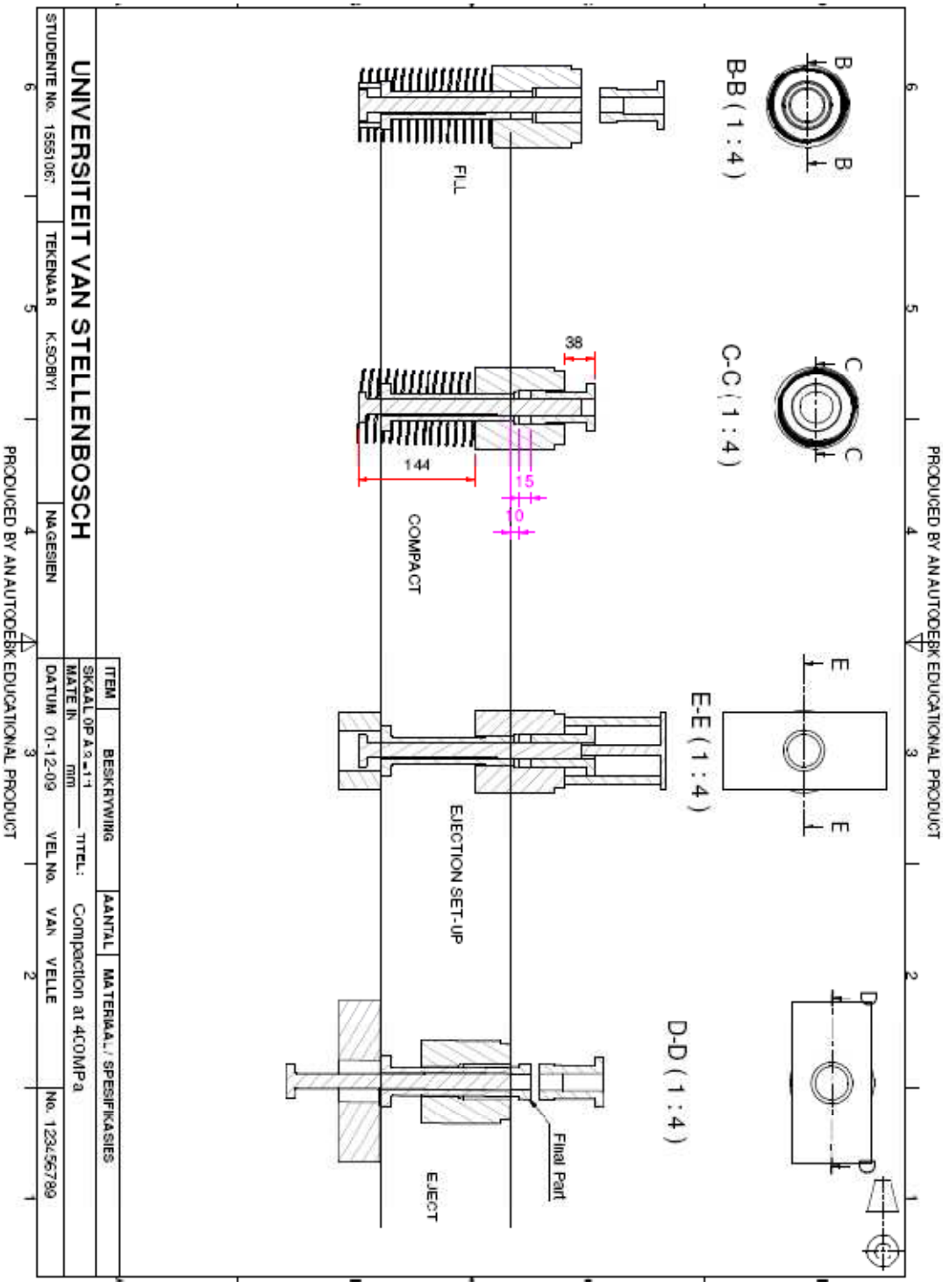

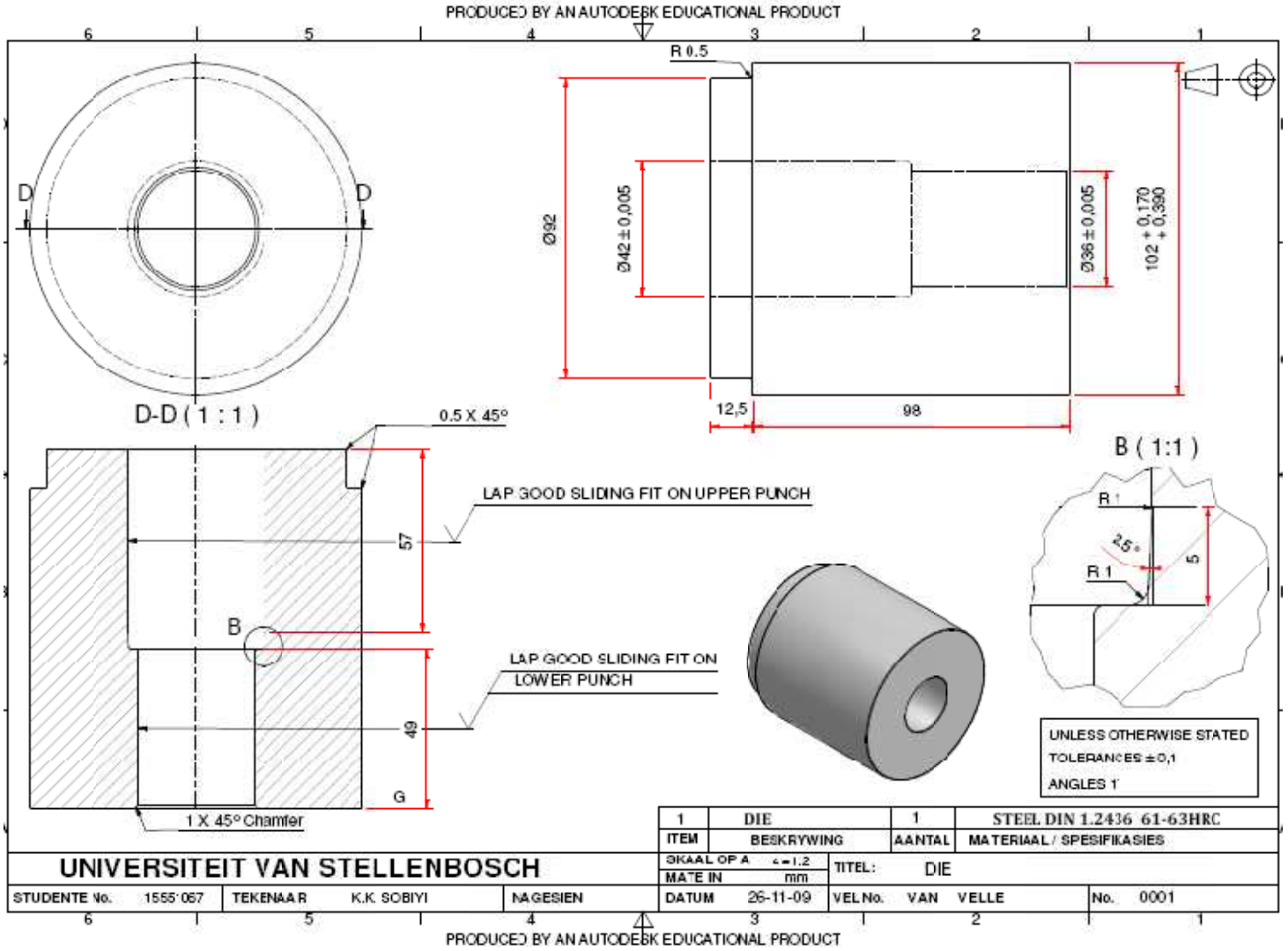
PRODUCED BY AN AUTODESK EDUCATIONAL PRODUCT
D
D
D-D (1 : 1)
R 0.5
Ø92
Ø42 ± 0,005
Ø36 ± 0,005
102 + 0,170
+ 0,390
12,5
98
0.5 X 45°
LAP GOOD SLIDING FIT ON UPPER PUNCH
57
B
LAP GOOD SLIDING FIT ON
LOWER PUNCH
49
G
1 X 45° Chamfer
B (1:1)
R 1
25°
5
R 1
UNLESS OTHERWISE STATED
TOLERANCES ±0,1
ANGLES 1°
1 DIE 1 STEEL DIN 1.2436 61-63HRC
ITEM BESKRYWING AANTAL MATERIAAL / SPESIFIKASIES
UNIVERSITEIT VAN STELLENBOSCH
SKAAL OP A4 1:2
MAATE IN mm
TITEL: DIE
STUDENTE No. 1555067 TEKENAAR K.K. SOBIYI NAGESIEN
DATUM 26-11-09 VELNo. VAN VELLE No. 0001
PRODUCED BY AN AUTODESK EDUCATIONAL PRODUCT

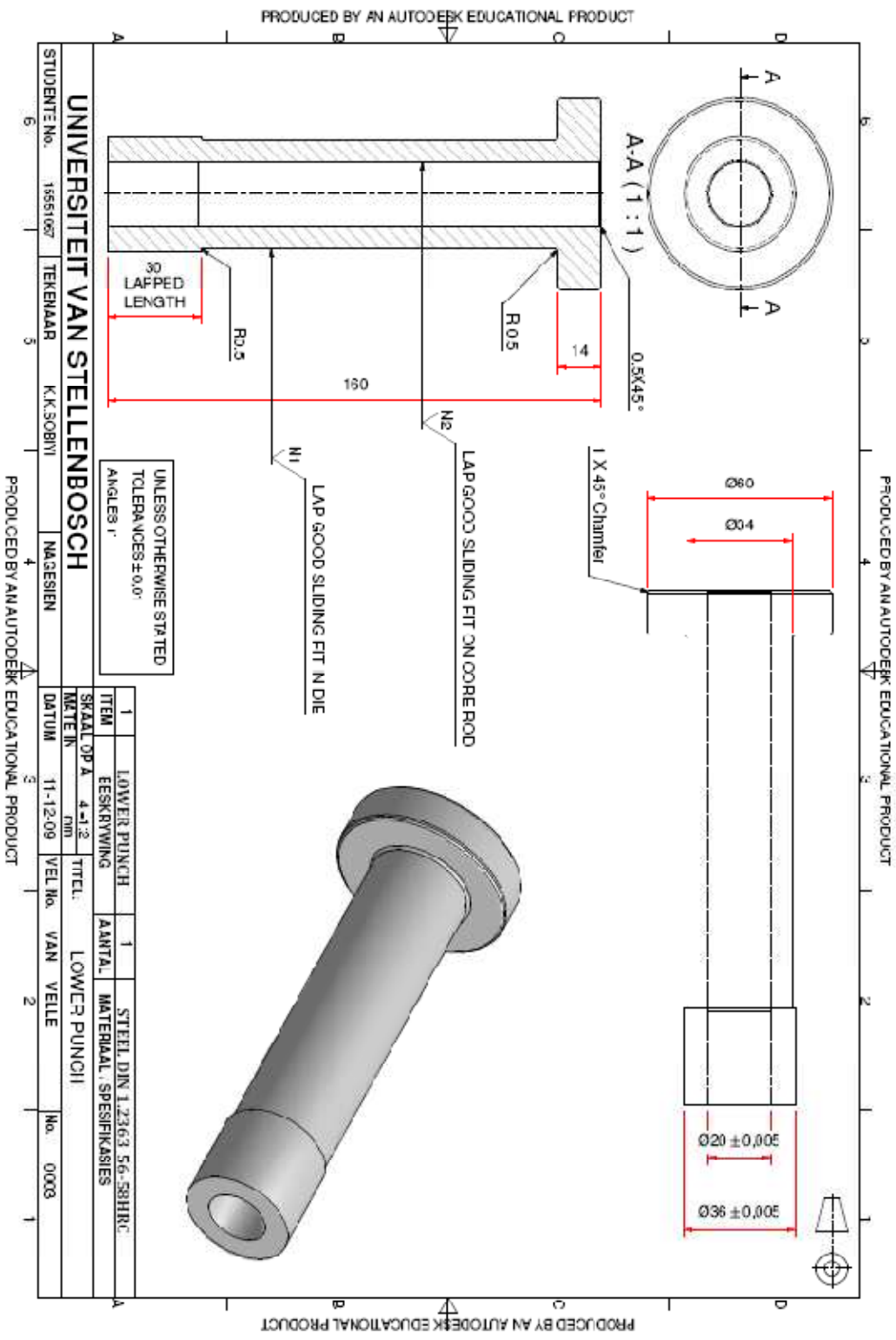
PRODUCED BY AN AUTODESK EDUCATIONAL PRODUCT
A-A (1 : 1)
30
LAPPED
LENGTH
R0.5
R0.5
14
160
0.5X45°
1 X 45° Chamfer
Ø60
Ø34
Ø20 ±0,005
Ø36 ±0,005
N2
LAP GOOD SLIDING FIT ON CORE ROD
N1
LAP GOOD SLIDING FIT IN DIE
UNLESS OTHERWISE STATED
TOLERANCES ± 0,0°
ANGLES 1°
UNIVERSITEIT VAN STELLENBOSCH
STUDENT No. 15551057
TEKENAAR K.K.SOBIYI
NAGESIEN
DATUM 11-12-09
SKAAL OP A 4 - 1:2
MATE IN mm
TITEL: LOWER PUNCH
VEL No. VAN VELLE
No. 0003
ITEM 1 LOWER PUNCH 1 STEEL DIN 1.2363 56-58HRC
BESKRYWING AANTAL MATERIAAL SPESIFIKASIES

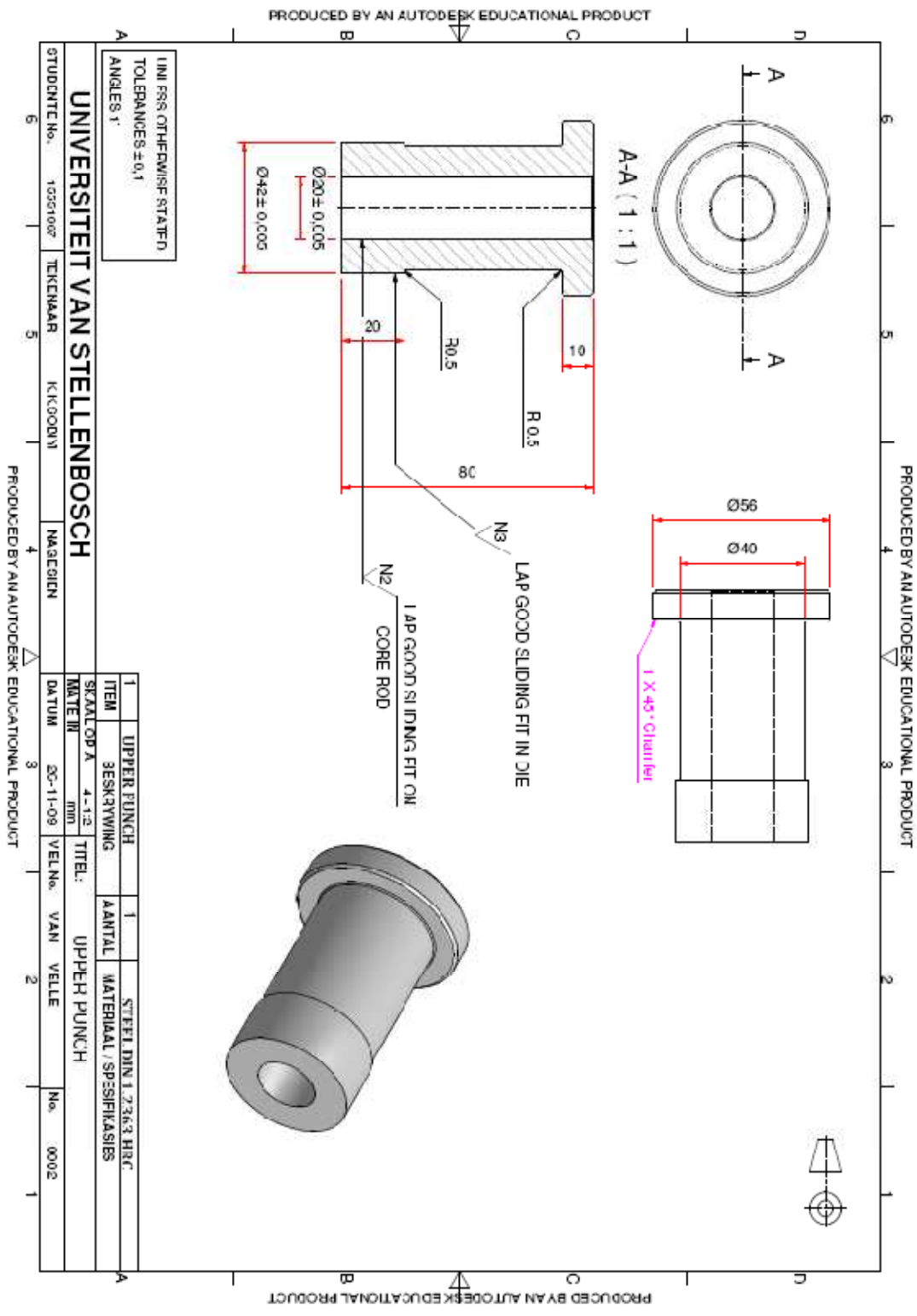
PRODUCED BY AN AUTODESK EDUCATIONAL PRODUCT
A-A (1 : 1)
Ø20± 0,005
Ø42± 0,005
20
R0.5
R 0.5
10
80
Ø56
Ø40
1 X 45° Chamfer
N3
LAP GOOD SLIDING FIT IN DIE
N2
LAP GOOD SLIDING FIT ON CORE ROD
UNIVERSITEIT VAN STELLENBOSCH
UPPER PUNCH
STEEL DIN 1.2363 HRC
STUDENTE No. 13551007
TEKENAAR KKLOOSM
NAGESIEN
DATUM 25-11-09
SKAAL OP A4 1:2
MATE IN mm
TITEL: UPPER PUNCH
VELNo. 0002
ITEM 1 UPPER PUNCH
AANTAL 1
MATERIAAL / SPESIFIKASIES STEEL DIN 1.2363 HRC
UNLESS OTHERWISE STATED
TOLERANCES ±0,1
ANGLES 1°

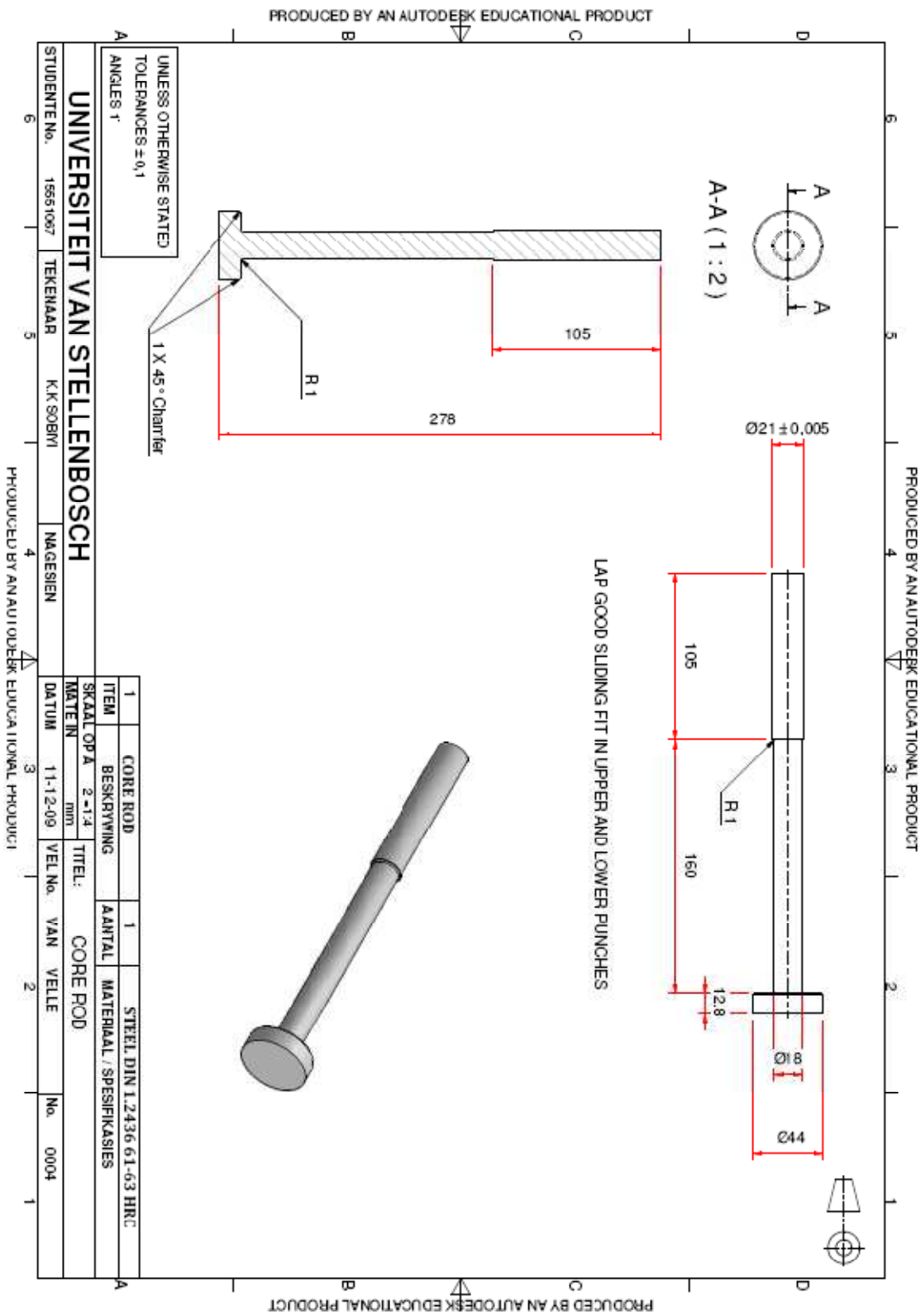
PRODUCED BY AN AUTODESK EDUCATIONAL PRODUCT
UNLESS OTHERWISE STATED
TOLERANCES ± 0,1
ANGLES 1°
A-A (1 : 2)
105
R1
278
1 X 45° Chamfer
Ø21 ± 0,005
105
R1
160
12,8
Ø18
Ø44
LAP GOOD SLIDING FIT IN UPPER AND LOWER PUNCHES
UNIVERSITEIT VAN STELLENBOSCH
STUDENTE No. 15551067
TEKENAAR K.K SOBYI
NAGESIEN
DATUM 11-12-09
SKAAL OP A2 - 1:4
MATE IN mm
TITEL: CORE ROD
VEL No.
VAN
VELLE
No. 0004
ITEM 1
BESKRYWING CORE ROD
AANTAL 1
MATERIAAL / SPESIFIKASIES STEEL DIN 1.2436 61-63 HRC

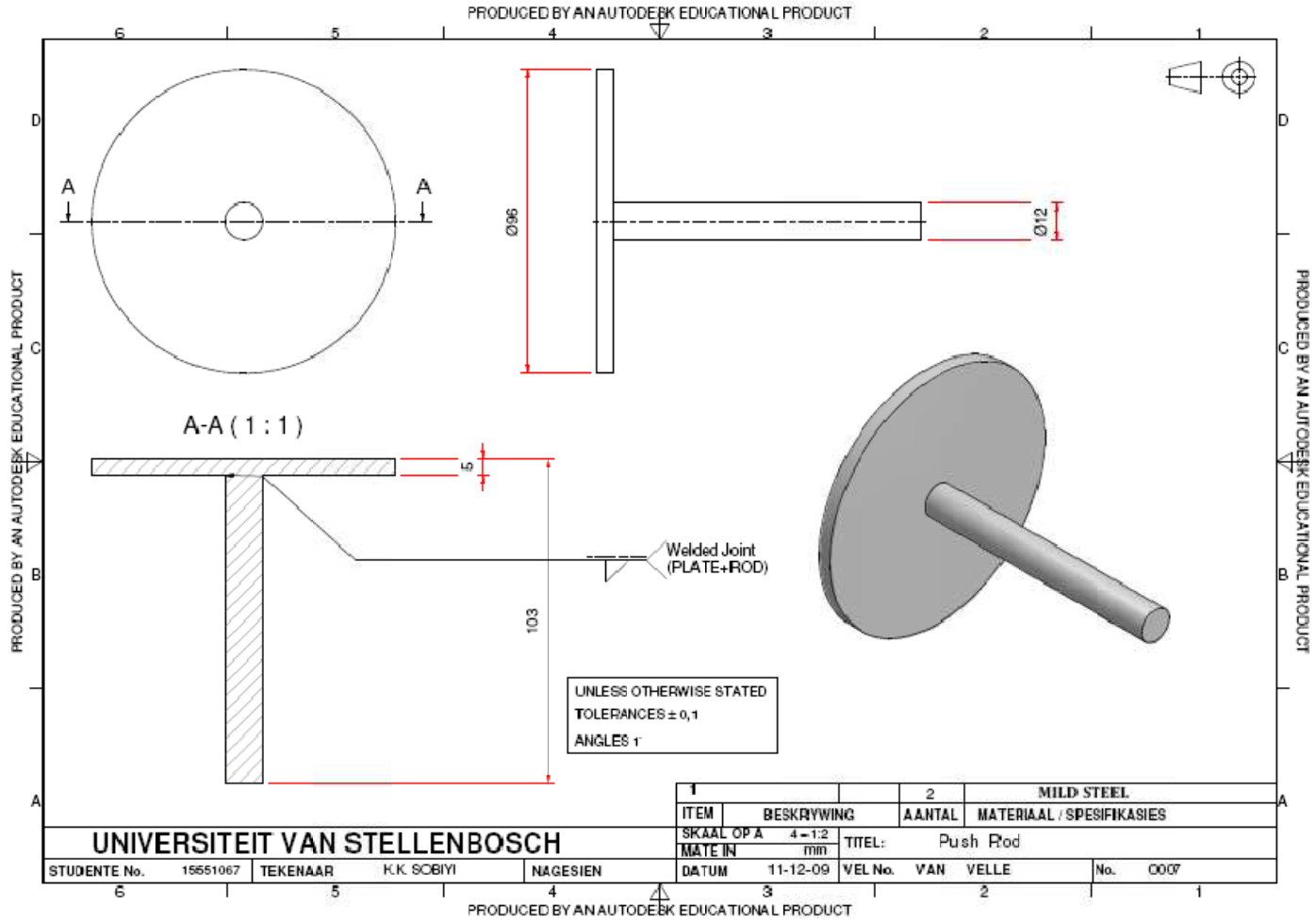
PRODUCED BY AN AUTODESK EDUCATIONAL PRODUCT
A
A
Ø96
Ø12
A-A (1 : 1)
5
Welded Joint
(PLATE+ROD)
103
UNLESS OTHERWISE STATED
TOLERANCES ± 0,1
ANGLES 1°
1
2
MILD STEEL
ITEM
BESKRYWING
AANTAL
MATERIAAL / SPESIFIKASIES
UNIVERSITEIT VAN STELLENBOSCH
SKAAL OP A 4 - 1:2
MATE IN mm
TITEL: Push Rod
STUDENTE No. 15551067
TEKENAAR K.K. SOBIYI
NAGESIEN
DATUM 11-12-09
VEL No. VAN VELLE
No. 0007

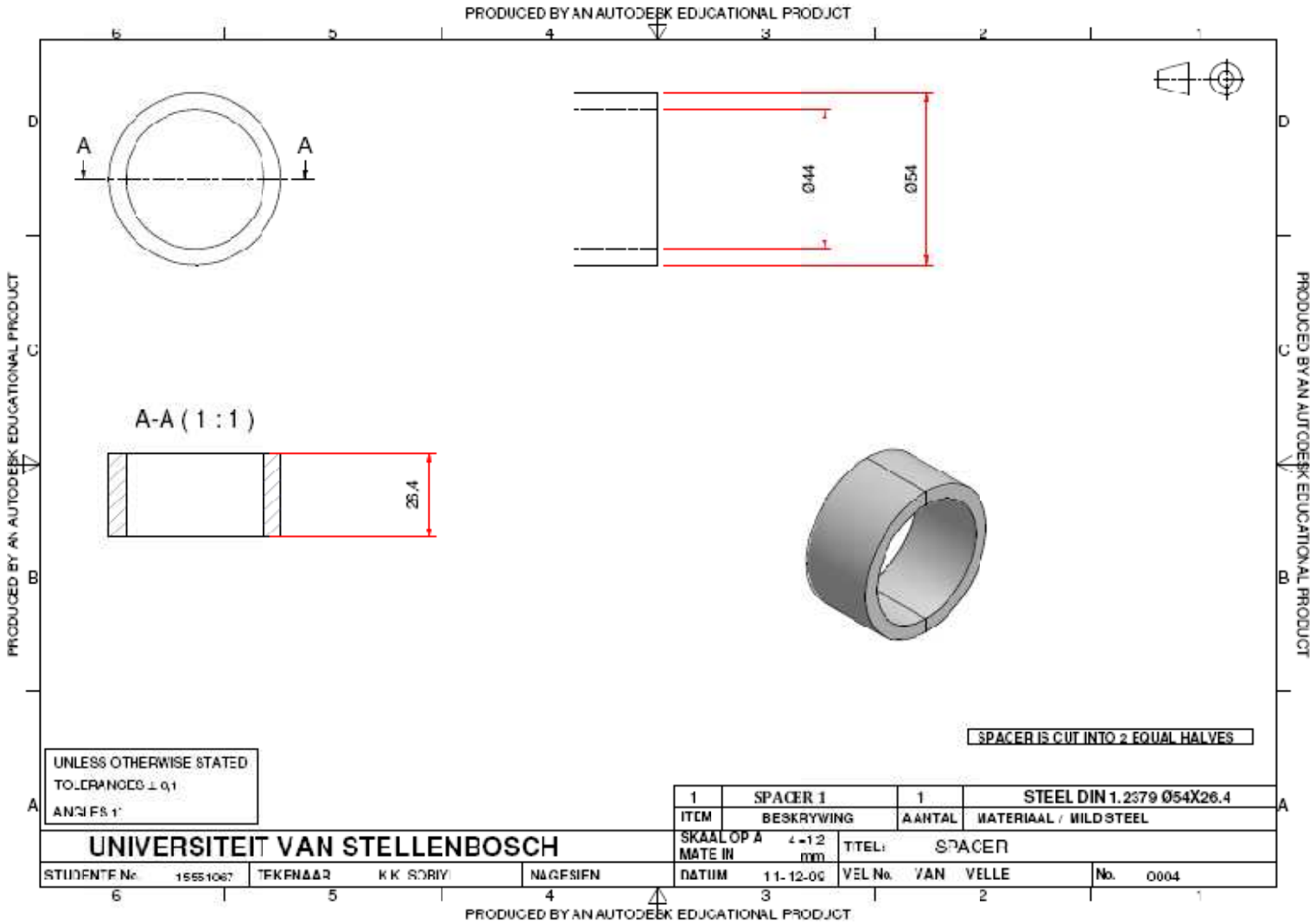
PRODUCED BY AN AUTODESK EDUCATIONAL PRODUCT
A
A
Ø44
Ø54
A-A (1 : 1)
26.4
SPACER IS CUT INTO 2 EQUAL HALVES
UNLESS OTHERWISE STATED
TOLERANCES ± 0,1
ANGLES 1°
1 SPACER 1 1 STEEL DIN 1.2379 Ø54X26.4
ITEM BESKRYWING AANTAL MATERIAAL / MILD STEEL
UNIVERSITEIT VAN STELLENBOSCH
SKAAL OP A4 MATE IN 1:2 mm
TITEL: SPACER
STUDENTE No 15551067 TEKENAAR K K SORIY NAGESIEN
DATUM 11-12-09
VEL No. VAN VELLE No. 0004
PRODUCED BY AN AUTODESK EDUCATIONAL PRODUCT

APENDIX B: G96 CODES

G 96 codes for machining trials

G 96	S1170	T0606	M04	M09
E 22	X 0	Z-5S6	I-1000	K-1000
E 50	S 1072	F 0.15		
G 00	X 70	Z 5		
E 01	X 0	F 0.15		
E 00	X 150	Z 150		
M 05	M 09			
M 30				

APPENDIX C: COMPRESSIBILITY AND SINTERING DATA

Compressibility studies showing green, sintered densities, shrinkages (radial and axial) and densification ratios at different sintering times

Pressure	Mass original	Mass final	Diameter green(cm)	Length green(cm)	Density green	Dt (cm)	Dc	Db	Lf	D avg	ΔL axial	ΔL radial	Cal density	Measured density	densification ratio	shrinkage	Sintering time
400	2.47	2.48	1.008	0.99	3.13	0.938	0.894	0.94	0.887	0.924	10.4%	8.3%	4.17	4.34	0.72	10.4%	2hrs
450	2.61	2.62	1.008	1.02	3.21	0.942	0.898	0.944	0.923	0.928	9.5%	7.9%	4.20	4.36	0.74	9.7%	2hrs
500	2.77	2.78	1.008	1.07	3.24	0.946	0.91	0.946	0.976	0.934	8.8%	7.3%	4.16	4.34	0.75	9.2%	1hr
400	2.47	2.47	1.008	0.99	3.13	0.942	0.9	0.944	0.891	0.929	10.0%	7.9%	4.09	4.33	0.72	10.3%	1hr
600	3	3.01	1.008	1.105	3.40	0.95	0.92	0.948	1.023	0.939	7.4%	6.8%	4.25	4.48	0.76	8.8%	2hrs
350	3	3.01	1.008	1.236	3.04	0.93	0.89	0.934	1.112	0.918	10.0%	8.9%	4.09	4.23	0.72	10.4%	1hr
450	2.83	2.84	1.008	1.108	3.20	0.944	0.902	0.948	1.015	0.931	8.4%	7.6%	4.11	4.23	0.76	8.9%	1hr
500	2.01	2.01	1.008	0.76	3.31	0.934	0.922	0.934	0.688	0.93	9.5%	7.7%	4.30	4.46	0.74	9.4%	2hrs

Experimental determination of Die fill height

Pressure	Density	CR	h_f 10mm	h_f 15mm	Total fill	Total height	Die Length	Core rod
350	3.059475	2.859	28.59323	42.88984	71.483	121.48307	151.4831	126.4831
400	3.169914	2.963	29.62536	44.43804	74.063	124.0634	154.0634	129.0634
500	3.314432	3.098	30.976	46.464	77.44	127.43999	157.44	132.44
600	3.449409	3.224	32.23746	48.35619	80.594	130.59366	160.5937	135.5937